



University
of Glasgow

Heiserich, Lisa (2011) *HIF prolyl hydroxylase-3 regulates actin polymerisation and hypoxia-induced motility and invasion*. PhD thesis.

<http://theses.gla.ac.uk/2421/>

Copyright and moral rights for this thesis are retained by the author

A copy can be downloaded for personal non-commercial research or study, without prior permission or charge

This thesis cannot be reproduced or quoted extensively from without first obtaining permission in writing from the Author

The content must not be changed in any way or sold commercially in any format or medium without the formal permission of the Author

When referring to this work, full bibliographic details including the author, title, awarding institution and date of the thesis must be given

**HIF Prolyl Hydroxylase-3 regulates actin
polymerisation and hypoxia-induced motility and
invasion**

Lisa Heiserich

December 2010

This thesis is submitted to the University of Glasgow towards the
degree of Doctor of Philosophy

Beatson Institute for Cancer Research
Garscube Estate
Switchback Road
Glasgow, G61 1BD

Faculty of Medicine
University of Glasgow

Abstract

Limited oxygen availability (hypoxia) influences cell migration and invasion, but the underlying mechanisms are poorly understood. Much of the cellular response to hypoxia is regulated by a family of Hypoxia Inducible Factor (HIF) prolyl hydroxylases (PHD1-3), each of which is thought to regulate specific pathways. Their activity is dependent on the availability of oxygen and α -ketoglutarate but despite intensive studies their activity *in vivo* and their substrates are poorly defined.

In this study we performed a quantitative proteomic screen to identify new substrates of PHDs. Co-immunoprecipitations using FLAG-tagged PHDs were performed under hypoxia to trap the enzyme-substrate interactions, and binding partners were identified by mass spectrometry. Actin was identified to interact with PHD3 specifically under hypoxia. Subsequently two defined prolyl residues in β -actin were shown to be hydroxylated. Hypoxia-induced rearrangement of the actin cytoskeleton was shown to be dependent on PHD3 activity as a knockdown of PHD3 was sufficient to increase the intracellular G- to F-actin ratio. An increase in cell migration and invasion was also found to be dependent on PHD3 activity. Mutation of both hydroxylated prolyl residues led to a similar phenotype regarding actin rearrangement and cell migration. Using constantly active HIF-mutants, we could show that these PHD3-dependent pathways are independent of HIF.

All together, this study shows a pro-invasive pathway linking HIF-independent oxygen-sensing pathways and actin signalling. However, the mechanism of how hypoxia-induced actin rearrangement leads to increased migration and invasion remains to be elucidated.

Table of Contents

Abstract	2
Table of Contents	3
List of Tables	5
List of Figures	6
Acknowledgement	8
Author's Declaration	9
Abbreviations	10
Chapter 1 – Introduction	11
1 Introduction	12
1.1 <i>Tumorigenesis and hypoxia</i>	12
1.2 <i>Superfamily of Fe(II)- and α-ketoglutarate-dependent dioxygenases</i>	14
1.2.1 HIF-prolyl hydroxylases (PHD)	15
1.2.1.1 Enzyme structure and reaction mechanism	16
1.2.1.2 Intracellular localisation and abundance	18
1.2.1.3 Substrate specificity of PHDs	19
1.2.1.4 Functions of PHD isoforms.....	19
1.3 <i>Hypoxia-induced metastasis</i>	22
1.3.1 Modes of invasion.....	24
1.3.2 Actin-based cell migration	24
1.3.3 Higher order actin organisation and its regulation	29
1.3.4 Actin isoforms	31
1.4 <i>Hypoxia and glucose metabolism</i>	31
1.5 <i>Quantitative proteomics (SILAC)</i>	34
1.6 <i>Aims</i>	35
Chapter 2 – Material and methods	36
2 Material and methods	37
2.1 <i>Materials</i>	37
2.1.1 General reagents.....	37
2.1.2 General buffers and solutions.....	38
2.2 <i>Methods</i>	39
2.2.1 DNA techniques.....	39
2.2.1.1 Cloning of PHD-FLAG plasmids	39
2.2.1.2 Site directed mutagenesis	41
2.2.1.3 Transformation of DH5 α bacteria	41
2.2.1.4 Agarose gel	42
2.2.2 Cell lines and growth conditions	42
2.2.3 Freezing and thawing of cells	42
2.2.4 Transfection using lipofectamine 2000	43
2.2.5 Drugs and treatment of cells with these drugs.....	43
2.2.6 Preparation of lysates	44
2.2.7 SDS-PAGE	44
2.2.8 Immunoblotting	45
2.2.9 Immunoprecipitations	46
2.2.9.1 Dynabeads	46
2.2.9.2 FLAG-sepharose	47
2.2.9.3 GFP-agarose.....	48
2.2.10 SILAC	48

2.2.11	Hydroxylation of actin	50
2.2.12	Immunostaining	50
2.2.13	Quantification of filamentous actin.....	51
2.2.14	Wound healing scratch assay.....	52
2.2.15	Inverse invasion assay	52
2.2.16	Statistical analysis	53
Chapter 3 – Quantitative proteomic screen		54
3	Quantitative proteomic screen to identity new targets of PHDs	55
3.1	<i>Introduction</i>	55
3.2	<i>Results</i>	55
3.2.1	PHD substrates can be trapped on the enzyme under hypoxia.....	55
3.2.2	Incorporation of heavy amino acids in HCT116 cells.....	58
3.2.3	SILAC screen	59
3.2.4	Assessment of the hypoxic response in HCT116 cells	61
3.2.4.1	Results for PHD3.....	62
3.2.4.2	Results for PHD1.....	65
3.2.4.3	Results for PHD2.....	70
3.3	<i>Conclusions</i>	74
Chapter 4 – Validation of potential substrates		76
4	Validation of potential PHD substrates	77
4.1	<i>Introduction</i>	77
4.2	<i>Results</i>	78
4.2.1	Validation of potential PHD targets.....	78
4.2.1.1	Interaction of PHDs and specific metabolic enzymes.....	78
4.2.1.2	Binding of actin and PHDs	82
4.2.1.3	Binding to PHD3 under different oxygen conditions	84
4.2.2	Actin as PHD3 substrate	86
4.2.3	Co-localisation of actin and PHD3	88
4.3	<i>Conclusions</i>	96
Chapter 5 – Biological role of actin hydroxylation.....		99
5	The biological role of actin hydroxylation	100
5.1	<i>Introduction</i>	100
5.2	<i>Results</i>	100
5.2.1	Loss of PHD3 activity leads to rearrangement of the actin cytoskeleton.....	100
5.2.2	Loss of PHD3 activity leads to increased migration and invasion..	109
5.2.3	Mutation of Pro70 and Pro322 effects the actin cytoskeleton and cell migration.....	117
5.2.4	Effect of HIF1 α and HIF2 α on the actin cytoskeleton and cell migration.....	121
5.3	<i>Conclusions</i>	124
Chapter 6 – General summary and outlook.....		126
6	General summary and outlook	127
References		133

List of Tables

Table 2.1: General reagents and kits.....	37
Table 2.2: General buffers and solution	38
Table 2.3: PCR conditions	39
Table 2.4: Primer sequences.....	40
Table 2.5: RNA interference and oligonucleotide sequences.....	43
Table 2.6: Antisera	45
Table 2.7: Secondary antibodies	46
Table 3.1: SILAC analysis of samples overexpressing PHD3-FLAG.....	64
Table 3.2: SILAC analysis of samples overexpressing PHD1-FLAG.....	67
Table 3.3: SILAC analysis of samples overexpressing PHD2-FLAG.....	72

List of Figures

Figure 1.1: Processes that are influenced by hypoxia [12]	13
Figure 1.2: Regulation of HIF-1 α stability by oxygen-sensitive proline hydroxylation [23].	15
Figure 1.3: Reaction mechanism of prolyl hydroxylation [31]	17
Figure 1.4: Key steps in metastasis.	23
Figure 1.5: The structures of an actin monomer and actin filament.....	25
Figure 1.6: Dendritic Nucleation/Array Treadmilling Model for Protrusion of the Leading Edge	27
Figure 1.7: The dramatic effects of Rac, Rho, and Cdc42 on actin organisation in fibroblasts.....	30
Figure 1.8: Overview over the reaction involved in glycolysis [102]	32
Figure 1.9: Reaction catalysed by lactate dehydrogenase	33
Figure 3.1: Binding conditions that stabilise the enzyme-substrate (PHD-HIF1 α) complex	57
Figure 3.2: Check incorporation of amino acids	58
Figure 3.3: Scheme of the quantitative proteomic screen (SILAC).	60
Figure 3.4: Assessment of the hypoxic response in HCT116 cells	61
Figure 3.5: Testing the conditions for the large-scale co-immunoprecipitation using FLAG-tagged PHD3.....	62
Figure 3.6: SILAC analysis of immunoprecipitations of PHD3-FLAG.....	63
Figure 3.7: SILAC analysis of immunoprecipitations of PHD1-FLAG.....	66
Figure 3.8: SILAC analysis of immunoprecipitations of PHD2-FLAG.....	71
Figure 4.1: Validation of binding between PHD1 and lactate dehydrogenase, triosephosphate isomerase and fructose-bisphosphate aldolase.....	79
Figure 4.2: Validation of binding between PHD2 or PHD3 and lactate dehydrogenase, triosephosphate isomerase and fructose-bisphosphate aldolase.....	81
Figure 4.3: Validation of interaction between PHDs and actin in HCT116 cells ..	82
Figure 4.4: Validation of interaction between PHDs and actin in U2OS cells	83
Figure 4.5: Validation of specific binding of PHD3 and actin under hypoxia.....	84
Figure 4.6: Validation of specific binding of PHD3 and actin under hypoxia.....	85
Figure 4.7: β -actin is hydroxylated at two specific proline residues (Pro70 and Pro322)	87
Figure 4.8: Colocalisation of PHDs and phalloidin-stained actin cytoskeleton ...	89
Figure 4.9: Colocalisation of PHDs and GFP-actin	91
Figure 4.10: Actin rearrangement under different oxygen conditions when PHD3 is overexpressed	93
Figure 4.11: Binding of actin and PHD3 after treatment with actin drugs	95
Figure 5.1: Rearrangement of the actin cytoskeleton following inhibition of PHDs	101
Figure 5.2: Rearrangement of the actin cytoskeleton is dependent on PHD3 activity.	103
Figure 5.3: Actin rearrangement in A375 cells is dependent on PHD activity. .	105
Figure 5.4: Actin rearrangement in A375 cells is dependent on PHD3 activity.	107
Figure 5.5: Actin organisation in A375-derived knock down cells	108
Figure 5.6: Cell migration is dependent on PHD activity.....	110
Figure 5.7: Cell migration is dependent on PHD3 activity	111

Figure 5.8: Dependency of cell migration on ability of actin to polymerise	112
Figure 5.9: Distance and velocity analysis of A375 cells in wound healing scratch assays	114
Figure 5.10: Distance and velocity analysis of A375-derived PHD1-2 knockdown cells in wound healing scratch assays	115
Figure 5.11: Invasion of A375 cells and derived shPHD3 stable clones into matrigel	116
Figure 5.12: Immunoblot analysis confirming the knockdown of endogenous actin and expression of wildtype GFP-actin and its mutants	118
Figure 5.13: Pro70 and Pro322 of β -actin regulate the state of actin	119
Figure 5.14: Pro70 and Pro322 of β -actin regulate cell migration.....	120
Figure 5.15: Effect of HIF1 α and HIF2 α on actin cytoskeleton.....	122
Figure 5.16: Effect of HIF triple mutants on cell migration	123
Figure 6.1: Working model of how PHD3 regulates the actin cytoskeleton (as described in the text).....	128

Acknowledgement

First, I would like to thank my supervisor Eyal Gottlieb, for all the advice and support during my time in his lab. I am very grateful to my advisors Walter Kolch and Jim Norman for their help and guidance throughout my PhD. I also wish to thank Laura Machesky who always took the time to discuss my project.

I would especially like to thank Richard Unwin and Willy Bienvenut, without them I could not have done the mass spec part of my project, and to Patrick Caswell for all his help with the invasion assays. I am grateful to the Beatson Institute and Cancer Research UK for funding this project.

A big hug and thank you goes to the past and present members of R12 - the past 4 years would not have been the same without you. I had the chance to meet and work with wonderful people at the Beatson, who made this a memorable and enjoyable time, and I am grateful for their friendship.

Special thanks to all the people back home, especially to my family who always believed in me.

Ich möchte diese Arbeit meiner Familie widmen, die immer für mich da sind und immer an mich geglaubt haben.

Author's Declaration

I hereby declare that this thesis represents my own work unless otherwise stated. No part of this work has been submitted for consideration as part of any other degree.

Lisa Heiserich

Abbreviations

ADP	Adenosine Diphosphate
Asp	Asparagine
ATP	Adenosine Triphosphate
BSA	Bovine Serum Albumine
cDNA	DNA complementary to mRNA
CO ₂	Carbondioxide
Cyt D	Cytochalasin D
DMEM	Dulbecco's Modified Eagles Medium
DMOG	Dimethylloxaloylglycine
DMSO	Dimethylsulfoxide
DNA	Deoxyribose Nucleic Acid
ECL	Enhanced Chemiluminescence
ECM	Extracellular Matrix
EDTA	Ethylene Diamine Tetraacetic Acid
ER	Endoplasmic Reticulum
FBS	Fetal Bovine Serum
GFP	Green Fluorescent Protein
HIF	Hypoxia Inducible Factor
HRE	Hypoxia Responsive Element
HRP	Horseradish Peroxidase
IgG	Immunoglobulin G
IP	Immunoprecipitation
kDa	Kilodalton
Lat A	Latrunculin A
LB	Luria-Bertani Medium
LC	Liquid Chromatography
MS	Mass Spectrometry
NLS	Nuclear Localisation Signal
PBS	Phosphate Buffered Saline
PCR	Polymerase Chain Reaction
PHD	Prolyl Hydroxylase Domain Protein
Pi	Inorganic Phosphate
Pro	Proline
pVHL	Von Hippel-Lindau protein
RPMI	Roswell Park Memorial Institute medium
SDS	Sodium Dodecyl Sulfate
SDS-PAGE	SDS-Polyacrylamide Gel Electrophoresis
SEM	Standard Error of the Mean
shRNA	short hairpin RNA
SILAC	Stable Isotope Labelling by Amino Acids in Cell Culture
siRNA	Short Interfering RNA
T α KG	3-Trifluoromethylbenzyl- α -ketoglutarate
TCA	Tricarboxylic Acid
3'UTR	3'Untranslated Region
Wt	Wildtype

Chapter 1 – Introduction

1 Introduction

1.1 Tumorigenesis and hypoxia

Cancer is thought to be one of the most frequent diseases in the developed world with an estimated one in three persons affected by it [1]. Tumorigenesis is a multistep process, in which cancer cells accumulate genetic alterations in pathways that control cell growth and proliferation leading to a selective growth advantage. Six essential alterations were originally described to contribute to tumour formation. These hallmarks of cancer were described as self-sufficiency in growth signals, insensitivity to growth-inhibitory signals, evasion of programmed cell death, limitless replicative potential, sustained angiogenesis and tissue invasion and metastasis [2]. Recently, additional hallmarks of cancer were proposed to include evasion of immune surveillance as well as several stress phenotypes including metabolic, proteotoxic, mitotic, oxidative and DNA damage stress [3, 4]. Metabolic stress is induced by high glucose uptake and elevated rates of glycolysis which is used as main source of energy production in tumours. An imbalance in the stoichiometry of protein complex subunits as well as improper folding of proteins lead to activation of the heat shock response in tumours which is evidence of proteotoxic stress. Chromosome mis-segregation and chromosome instability are linked to mitotic stress whereas the elevated levels of reactive oxygen species (ROS) that are highly reactive and contribute to DNA damage lead to oxidative stress in tumours. Rapidly growing tumours can outgrow their vascular system leading to low oxygen (hypoxia), low pH and nutrient starvation within these tumours (for reviews: [5-9]). Oxygen is only able to diffuse 100-180 μm from the nearest capillary to cells before it is fully metabolised. Therefore many solid tumours contain areas of hypoxia compared to the surrounding normal tissue. Hypoxia provides a strong selective pro-tumorigenic pressure and hypoxic tumours are often found to be more aggressive and metastatic. As shown in Figure 1.1 cells adapt to the hypoxic microenvironment by inducing adaptive mechanisms that influence processes involved in regulating the above named hallmarks of cancer either directly or indirectly as various transcription factors were shown to be hypoxia-responsive [10, 11]. For example, hypoxia influences pathways involved in angiogenesis, glucose metabolism, cell proliferation and survival as well as migration. The

master transcriptional regulator of hypoxia- inducible genes is the heterodimeric transcription factor, Hypoxia Inducible Factor (HIF). HIF is composed of an oxygen regulated α -subunit and an oxygen-insensitive β -subunit.

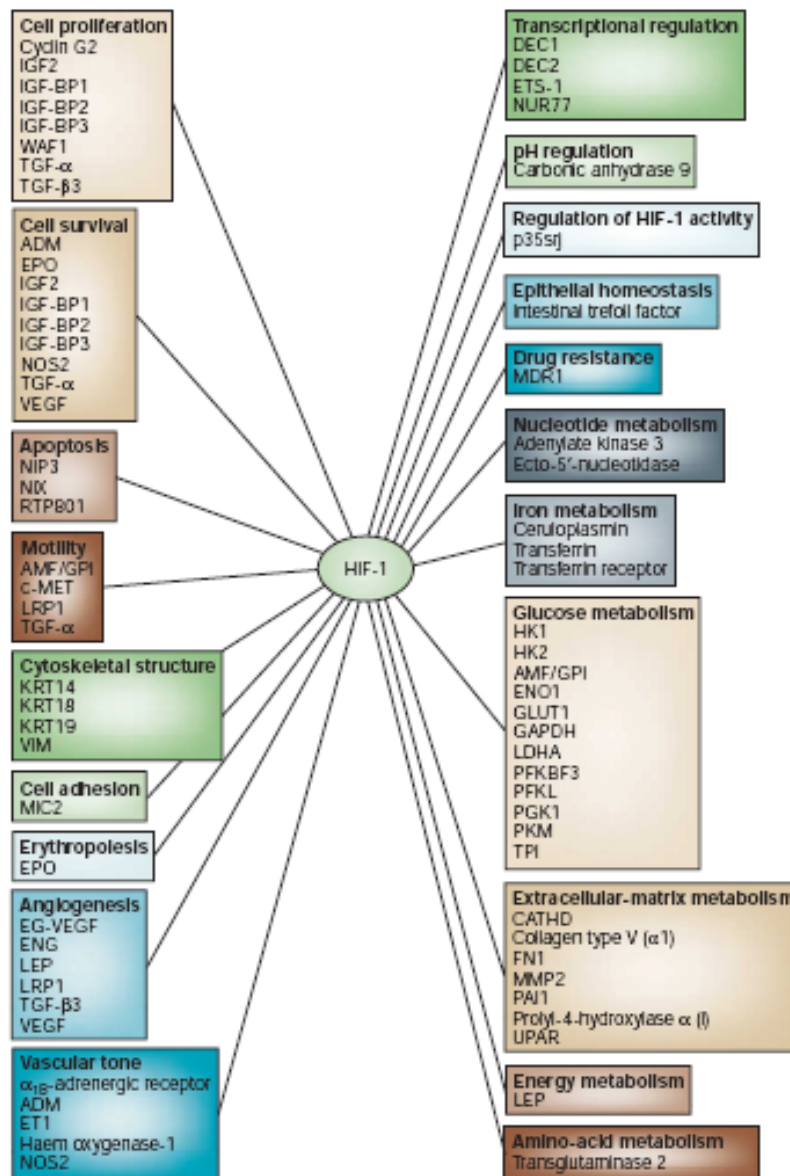


Figure 1.1: Processes that are influenced by hypoxia [12]

Genes that are transcriptionally activated by HIF-1. Genes that are involved in many processes are transcriptionally activated by HIF-1. ADM, adrenomedullin; ALDA, aldolase A; ALDC, aldolase C; AMF, autocrine motility factor; CATHD, cathepsin D; EG-VEGF, endocrine gland-derived VEGF; ENG, endoglin; ET1, endothelin-1; ENO1, enolase 1; EPO, erythropoietin; FN1, fibronectin 1; GLUT1, glucose transporter 1; GLUT3, glucose transporter 3; GAPDH, glyceraldehyde-3-P-dehydrogenase; HK1, hexokinase 1; HK2, hexokinase 2; IGF2, insulin-like growth-factor 2; IGF-BP1, IGF-factor-binding-protein 1; IGF-BP2, IGF-factor-binding-protein 2; IGF-BP3, IGF-factor-binding-protein 3; KRT14, keratin 14; KRT18, keratin 18; KRT19, keratin 19; LDHA, lactate dehydrogenase A; LEP, leptin; LRP1, LDL-receptor-related protein 1; MDR1, multidrug resistance 1; MMP2, matrix metalloproteinase 2; NOS2, nitric oxide synthase 2; PFKBF3, 6-phosphofructo-2-kinase/fructose-2,6-bisphosphatase-3; PFKL, phosphofructokinase L; PGK 1, phosphoglycerate kinase 1; PAI1, plasminogen-activator inhibitor 1; PKM, pyruvate kinase M; TGF- α , transforming growth factor- α ; TGF- β 3, transforming growth factor- β 3; TPI, triosephosphate isomerase; VEGF, vascular endothelial growth factor; UPAR, urokinase plasminogen activator receptor; VEGFR2, VEGF receptor-2; VIM, vimentin.

Tumour hypoxia is often correlated with tumour aggressiveness and resistance to radio- and chemotherapies [13, 14]. It is therefore important to understand hypoxic signalling to improve treatments and patient survival. Several types of tumours were identified with loss of function mutations in several genes involved in oxygen-sensing pathways, which helped to improve our understanding of oxygen sensing pathways. These tumours include: Loss of function mutations of the E3-ligase pVHL found in clear cell renal carcinomas as well as mutations in succinate dehydrogenase (SDH) and fumarate hydrolase (FH) leading to inhibition of HIF prolyl hydroxylase (PHD) activity in paragangliomas, pheochromocytomas, leiomyomas and renal cell cancer. Recently it was shown that nuclear localisation of PHD2 can increase anchorage-independent growth of cancer cells [15] whereas mutations in PHD2 were linked to paragangliomas suggesting that PHD2 may act as tumour suppressor [16, 17]. A better understanding of the mechanisms leading to formation of these tumours will help to design better treatments.

1.2 Superfamily of Fe(II)- and α -ketoglutarate-dependent dioxygenases

The cellular response to hypoxia is mostly mediated by Hypoxia Inducible Factor (HIF) prolyl hydroxylases (PHD), which belong to a superfamily of Fe(II)- and α -ketoglutarate-dependent dioxygenases. PHDs catalyse the hydroxylation of specific prolyl residues in an oxygen-dependent fashion but retain low affinity to oxygen making them good oxygen sensors. This is a unique function of PHDs as activity of other prolyl hydroxylases such as collagen prolyl-4-hydroxylases is preserved under hypoxia [18]. Hydroxylation of proline residues is a well known posttranscriptional modification of a number of secreted proteins such as collagen become enzymatically hydroxylated at prolyl residues in the endoplasmic reticulum. Hydroxylation of collagen is important for the stability of collagen fibres (for reviews: [19, 20]). However cellular oxygen sensing is the first example that protein hydroxylation is used in intracellular signalling.

1.2.1 HIF-prolyl hydroxylases (PHD)

Mammalian PHDs were originally identified as homologues of the *Caenorhabditis elegans* (*c.elegans*) gene product *egl-9* [21, 22]. In *c. elegans* *egl-9* acts as prolyl hydroxylase that targets HIF1 α for degradation via the pVHL- ubiquitin-proteasome pathway (Figure 1.2) [22].

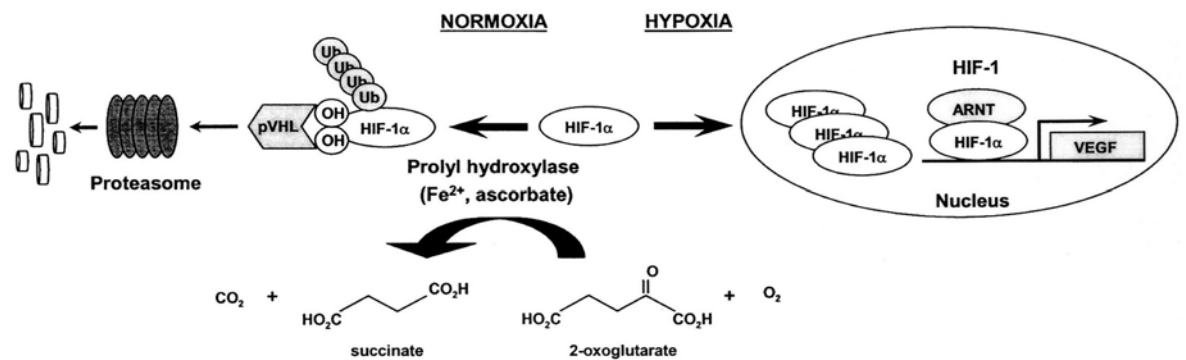


Figure 1.2: Regulation of HIF-1 α stability by oxygen-sensitive proline hydroxylation [23]. Under normal oxygen concentrations, HIF-1 α is hydroxylated at Pro⁴⁰² and Pro⁵⁶⁴ by HIF prolyl hydroxylases. The reaction requires O₂ and iron(II) and utilizes peptidyl proline and α -ketoglutarate as co-substrates; ascorbate is a cofactor needed for maximal activity. Hydroxyproline, succinate, and CO₂ are produced. Proline hydroxylation of HIF-1 α increases its affinity for pVHL, which targets HIF-1 α for ubiquitination and degradation. Under hypoxic conditions, prolyl hydroxylase activity decreases and non-hydroxylated HIF-1 α is free to accumulate in the nucleus where it associates with the HIF β -subunit to activate transcription of target genes.

The name of the protein *egl-9* derives from an egg laying defective phenotype in *c. elegans*. As these hydroxylases seemed to be a conserved gene family among species, human homologues were identified by sequence homology using a candidate gene approach and subsequently via biochemical purification of hydroxylase activity [18, 22, 24]. Only a single member of this family was found in *c. elegans* whereas three paralogous transcripts could be identified in human. The three mammalian isoforms were identified by different groups and are therefore known by different nomenclatures PHD1/2/3, EglN2/1/3 or HPH3/2/1 respectively [18, 21, 22, 24]. All three PHDs have a conserved genomic structure

with five coding exons. The translated proteins contain a conserved C-terminal region responsible for their hydroxylase activity and highly variable N-termini. PHD2 seems to be the ancestral form of the protein [21]. PHDs show a 42-59% sequence similarity to each other [18, 22, 24] and have different sizes: PHD1 is 43.6 kDa, PHD2 46 kDa whereas PHD3 is much smaller with 27.3 kDa. Later, a fourth human prolyl-4-hydroxylase was identified in a database search [25, 26]. The sequence of this hydroxylase is more closely related to collagen hydroxylases than PHDs, but its activity seemed to decrease under hypoxia. It was found to be a transmembrane protein localised in the ER membrane with its catalytic site inside the lumen. However not much is known about its function and we will only refer to PHD1-3 in the following sections.

1.2.1.1 Enzyme structure and reaction mechanism

X-ray crystallographic analysis from different dioxygenases gave an insight into their structure and function [27]. Recently, the catalytic domain of PHD2 was crystallised as a homotrimer in complex with an inhibitor or in a complex with a peptide of the HIF1 degradation domain [28, 29]. Dioxygenases consist of a core of eight β - strands that are folded into a β -barrel jelly roll motif. The enzymes show a highly conserved two-histidine, one-carboxylate motif to coordinate Fe(II) binding at the catalytic site.

PHDs as well as dioxygenases in general use α - ketoglutarate and molecular oxygen as co-substrates and require Fe(II) and ascorbate for their activity. Dioxygenases seem to work by a common mechanism as was shown for the asparaginyl hydroxylase FIH (Figure 1.3): The binding of the protein substrate, α - ketoglutarate and molecular oxygen is followed by oxidative decarboxylation of α -ketoglutarate and splitting of molecular oxygen to give succinate and CO₂ as well as a hydroxyprolyl residue [30]. The binding of α - ketoglutarate and the prime protein substrate is reversible.

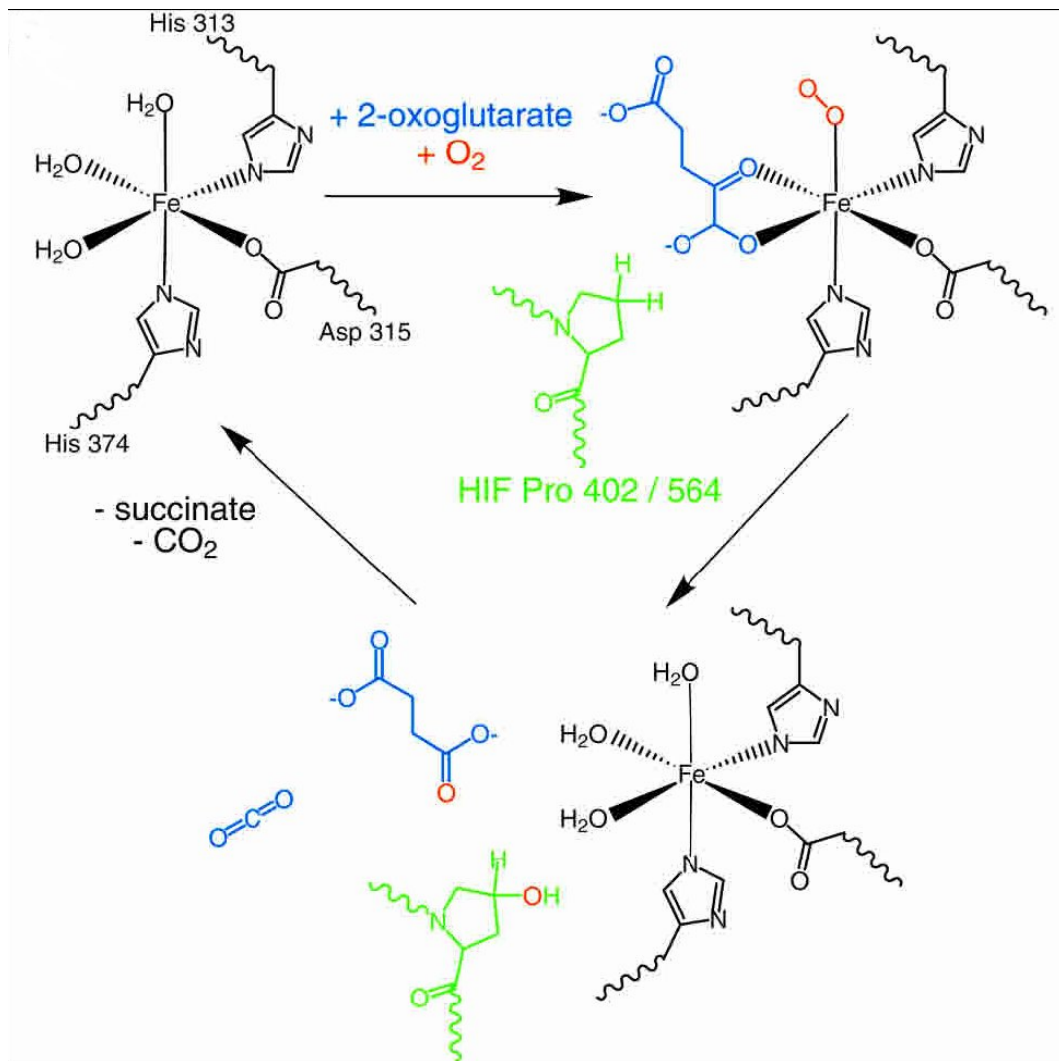


Figure 1.3: Reaction mechanism of prolyl hydroxylation [31]

As the activity of PHDs is mainly regulated by oxygen supply with their k_M for oxygen near physiological oxygen levels, PHDs are thought to function as molecular oxygen sensors [22, 32]. However, other factors such as availability of α -ketoglutarate also influence their activity. Reduction in hydroxylase activity was detected when oxygen concentration was reduced from 20% to 10% and progressive inhibition was observed at lower oxygen tensions [22]. TCA cycle intermediates such as succinate and fumarate were shown to inhibit PHD activity [33, 34]. However elevated levels of α -ketoglutarate can overcome the inhibition of PHD activity by succinate and fumarate as well as by hypoxia [35, 36]. Therefore the intracellular ratio of α -ketoglutarate to succinate, meaning the ratio of co-substrate to product, is important for PHD activity. Hypoxia mimetics such as desferroxamine or divalent metals such as Co^{2+} , Mn^{2+} or Zn^{2+}

can block enzyme activity by blocking iron availability. Ascorbate appears to be important for enzyme activity, however its role is not quite clear [37].

1.2.1.2 Intracellular localisation and abundance

PHD isoforms are ubiquitously expressed but expression levels vary between the isoforms and between different cell types [38, 39]. PHD2 is widely expressed in all cell types, PHD1 levels are high in testis whereas PHD3 is most abundant in the heart. Under hypoxia, levels of PHD2 and PHD3 are upregulated whereas PHD1 levels are independent of ambient oxygen concentrations [40, 41]. Subsequently PHD2 as well as PHD3 were shown to be upregulated in a HIF-dependent manner as their promoters were shown to include hypoxia-response elements (HRE) [42, 43]. This upregulation in PHD2 and PHD3 was suggested to be an important feedback mechanism for reoxygenation [44]. However, the intracellular abundance of PHD1 and PHD3 was shown to be dependent on other factors apart from oxygen levels adding to the complexity of regulating PHDs levels and activity. PHD1 and 3 were shown to be targeted for proteasomal degradation by the E3 ubiquitin ligases Siah2 [45]. Siah2 is upregulated under hypoxia inducing degradation of PHD1 and 3 under these conditions.

PHDs show distinct intracellular localisation: PHD1 localises predominantly to the nucleus, PHD2 to the cytoplasm whereas PHD3 is evenly distributed between both compartments [40]. This localisation is not influenced by the oxygen supply. Localisation is determined by the presence of a nuclear localisation signal (NLS) in PHD1, or a region responsible for nuclear export in PHD2 [46]. Importins α/β are involved in regulating the localisation of PHD1. PHD2 is able to shuttle between the nucleus and the cytoplasm using the CRM1 export receptor and an unknown import receptor but it is thought to be actively excluded from the nucleus leading to its cytoplasmic localisation [46, 47]. Recently, PHDs were suggested to form larger protein complexes as they were shown to interact with scaffolding proteins. PHD3 was shown to interact with the chaperonin TRiC which is thought to play a role in formation of multiprotein complexes [48] as well as with the WD-repeat protein Morg1 which can act as a molecular scaffold [49]. PHD3 was also suggested to be able to form homo- and heteromultimers with other PHDs especially under hypoxia which affects their activity and susceptibility to Siah2-dependent degradation [50]. The protein OS-9 was shown

to interact with HIF1 α as well as PHD2 and PHD3 [51]. The formation of this ternary complex promotes hydroxylation of HIF and ultimately regulates HIF levels. Larger complexes seem to be involved in these pathways however the functions of these interactions remain unclear.

1.2.1.3 Substrate specificity of PHDs

PHDs seem to show different substrate specificities, but it is unknown how the different isoforms distinguish between substrates [52]. A conserved LXXLAP motif is thought to be the substrate binding motif for prolyl hydroxylases in general but mutations in all positions can be tolerated apart from the proline that is hydroxylated [22, 53, 54]. Apart from this core binding motif, distal residues from the hydroxylation site such as a leucine ten residues downstream of the hydroxylated prolyl residue seem to be important for substrate binding and to be involved in the recruitment of the hydroxylase [55, 56]. Acidic residues are found in the vicinity of the hydroxylacceptor proline and they seem to be involved in substrate binding as well [57]. These residues are either found N- terminal or C- terminal to the hydroxyproline. Recently, a region relatively far from the catalytic site on PHDs was shown to be important for substrate preference [58]. This region shows moderate conservation among the family members which could account for target preferences [29, 59]. In general, substrate specificity seems to be provided by multiple interactions and a rigid consensus sequence might be absent.

1.2.1.4 Functions of PHD isoforms

Distinct functions have been described for each of the PHD isoforms: the best studied example is their role in the degradation of the oxygen regulated α -subunit of the heterodimeric transcription factor, HIF. HIF is composed of an oxygen-regulated α -subunit and an oxygen-insensitive β -subunit and is the master transcriptional regulator of hypoxia- inducible genes (for reviews: [30, 31, 37, 60-62]). Proteasomal degradation of the α -subunit is dependent on the hydroxylation of two specific prolyl residues [63, 64]. Hydroxylation of these prolyl residues promotes binding to pVHL, the substrate recognition unit of an E3 ubiquitin-ligase complex, and its subsequent degradation by the ubiquitin-proteasome pathway leading to low steady state levels of HIF α under normoxia.

Non-hydroxylated HIF is not recognized by the pVHL complex leading to its accumulation under low oxygen conditions and its subsequent translocation into the nucleus. In the nucleus HIF α dimerizes with the β -subunit and then binds to hypoxia- response elements (HRE) within the promoters of its target genes. Although HIF1 α is stabilised within minutes after exposure to hypoxia, most of the cellular response to HIF is determined by transcription. PHD2 plays a non-redundant role in this pathway as loss of PHD2 activity is sufficient to stabilise HIF1 α under normoxia [65]. PHD1 and PHD3 have little or no effect on the stability of HIF1 α .

Beside their importance in regulating HIF levels, PHDs have been shown to be involved in other pathways: Loss of PHD2 in tumours leads to increase in nuclear factor kappa B (NF κ B) activity, subsequently to an increase interleukin-8 (IL-8) and angiogenin and ultimately to an increase in blood vessels. Therefore PHD2 influences tumour angiogenesis in a NF- κ B-dependent manner [66]. PHD2 also associates with the tumour suppressor protein inhibitor of growth family member 4 (ING4) regulating HIF activity [67]. ING4 does not seem to be a substrate of PHD2 as the interaction does not seem to be affected by hydroxylase activity or affect HIF stability but rather be involved in recruitment of transcriptional repressors. In a yeast two-hybrid screens PHD2 was identified to interact with the peptidyl prolyl *cis/trans* isomerase FK506-binding protein 38 (FKBP38), which seems to be involved in PHD2 protein regulation [68], and the melanoma antigen 11 (MAGEA11) leading to inhibition of PHD activity [69]. PHD3 is involved in neuronal cell death following the withdrawal of neuronal growth factor (NGF) [70]. It was shown to act downstream of c-Jun in this pathway and upstream of the motor protein kinesin KIF1B β through an HIF-independent pathway [71]. During skeletal muscle differentiation PHD3 interacts with and stabilises myogenin [72]. The interaction is thought to prevent myogenin from ubiquitination and degradation via the ubiquitin-proteasome system. The underlying pathway was later shown to be HIF-independent but PHD3 appears regulate NF- κ B [73]. In a yeast two-hybrid system the activating transcription factor-4 (ATF4) was identified as a new interaction partner of PHD3 which regulates ATF4 stability [74]. Under hypoxia PHD3 forms a complex with PRP19, a multifunctional protein playing a role in splicing, ubiquitination and cell growth, under hypoxia inhibiting cell death during the hypoxic response [75].

Although a role of PHD3 has been described in these different pathways, PHD3 substrates remain elusive. However, recently PHD3 was shown to hydroxylate the β 2-adrenergic receptor [76]. Hydroxylation of the receptor led to its degradation via the ubiquitin-proteasome system. PHD1 was shown to inhibit I κ B-kinase β (IKK β) influencing NF κ B activity [77]. NF κ B is activated under hypoxia through a PHD1-dependent pathway that involves increased expression and activation of IKK β leading to phosphorylation-dependent degradation of I κ B α and liberation of NF κ B. The pathway appears to be dependent on a prolyl residue located in a LXXLAP motif in IKK β . Loss of PHD1 leads to neuroprotection against cell death following oxidative stress using HIF-independent pathways [78] and to protection of skeletal muscles and hepatocytes against ischemia/reperfusion injury through metabolic regulation [79, 80]. Furthermore, PHD1 controls cyclin D1 levels in estrogen-dependent tumorigenesis [81]. Inactivation of PHD1 decreased cyclin D1 levels suppressing mammary gland proliferation in a HIF-independent manner. Regulation appears to be on the transcriptional level of cyclin D1. PHD1 and PHD2 are able to interact with and regulate the large subunit of RNA Polymerase II [82]. A region in the large subunit of RNA polymerase II (Rpb1) was identified to have sequence and structural similarity with the HIF1 α -domain that binds pVHL. Binding of Rpb1 to pVHL appeared to be hydroxylation dependent [83].

Confirming differential functions of each of the PHD isoforms different phenotypes were observed in PHD knockout mice. Underlining the importance of PHD2 in development PHD2^{-/-} mice showed embryonic lethality whereas PHD1^{-/-} and PHD3^{-/-} mice were viable. PHD2^{-/-} embryos died between days E12.5 and E14.5 with severe defects in heart and placenta [84]. PHD3^{-/-} mice showed a phenotype in the sympatho-adrenal system. PHD3 was shown to have an important role in regulating the development of the sympatho-adrenal system in a partially HIF2 α -dependent manner [85, 86]. PHD3 appears to increase NGF-dependent neurite growth though less functional. As mentioned above PHD1^{-/-} mice revealed the involvement of PHD1 in metabolic regulation in skeletal muscles and hepatocytes [79, 80]. Loss of PHD1 lowers oxygen consumption in skeletal muscles by shifting to a more anaerobic metabolism. Loss of PHD1 was associated with an increase in concentration of the nuclear receptor peroxisome proliferators-activated receptor (Ppar α) leading to increase in pyruvate

dehydrogenase kinase 1 and 4 (PDK) gene transcription. PDKs negatively regulate the pyruvate dehydrogenase complex restricting the entry of glycolytic intermediates into the tricarboxylic acid cycle (TCA) cycle. Loss of PHD1 impairs oxidative muscle performance but provides protection against ischemia through reducing oxidative stress. Some of these functions appear to be HIF-independent but substrates of PHDs in these pathways have so far proved difficult to identify and are therefore mostly unknown.

1.3 Hypoxia-induced metastasis

Hypoxic tumours show an increased potential to form metastases. Numerous theories exist to explain metastasis, however most agree that it is a multifaceted process requiring modifications of the tumour cells and their microenvironment. Many aspects of metastasis are not fully understood, especially when and how cells move away from the primary tumour and how efficient these cells can proliferate at distant sites. However, it is known that metastasis involves some distinct processes such as local invasion of cells leading to intravasation into the lymphatic or vascular system, extravasation into distant organs and survival and proliferation at the distant site (Figure 1.4) [87].

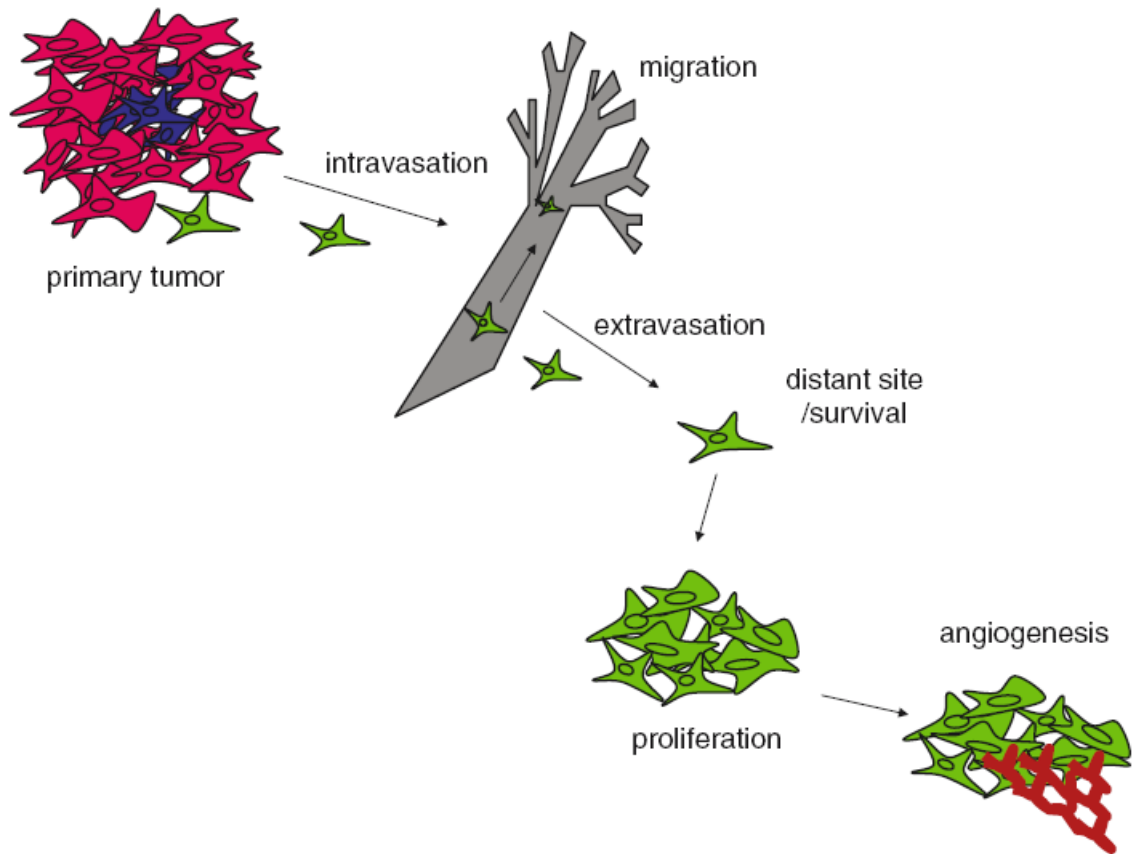


Figure 1.4: Key steps in metastasis.

In order to metastasise, a malignant cell must dissociate from the primary tumor and intravasate into the vascular or lymphatic systems by degrading and migrating through the basement membrane and extracellular matrix. Once in the lymph or the blood streams, this cell must evade the host immune system, migrate and home into its target site, and extravasate out of the circulation. The cell must overcome both anchorage-dependent growth and the ability to senesce at this distant site, while proliferating and inducing angiogenesis to nourish its own growth [88].

In order to be able to break away from the primary tumour cellular behaviour has to be altered resulting in changed adhesive properties, change in polarity, activation of motility and resistance to anoikis [89]. Some of these processes can be influenced by hypoxia. A number of proteins involved in progression of metastasis were shown to be HIF-target genes (Figure 1.1) such as vimentin, fibronectin, matrix metalloproteinase 2 (MMP2), urokinase plasminogen activator receptor (uPAR), receptor kinase c-Met and the cytokine receptor CXCR4 [90]. These proteins play a part in different phases of the metastatic progression. For example, expression of CXCR4 is suggested to be important for homing at distant sites, connective tissue growth factor (CTGF) promotes anchorage-independent cell growth and uPAR is involved in degradation of various proteins

in the extracellular matrix (ECM) [88, 91]. Another protein involved in changes in the ECM, namely lysyl oxidase (LOX), was found to be regulated in a HIF-dependent fashion [92]. LOX is important for crosslinking collagen and elastin in the extracellular matrix. Increased LOX expression was linked to changes in the actin cytoskeleton as well as regulation of focal adhesions. Upregulation of c-Met leads to sensitizing cells to its ligand hepatocyte growth factor (HGF). HGF-induced Met activation switches on an invasive programme that promotes extracellular matrix degradation, activates cell dissociation and cell migration [93]. One hallmark of invasion is the loss of cell-cell contacts, which is usually marked by loss of E-cadherin. Expression of E-cadherin and HIF were shown to be mutually exclusive [94]. Furthermore, hypoxia induces the expression of integrin $\beta 1$ (ITGB1) promoting wound healing in the intestinal submucosa [95] whereas it suppresses expression of $\alpha 5$ integrin inducing anoikis resistance and anchorage-independent growth [96].

1.3.1 Modes of invasion

In order to metastasise to distal sites, tumour cells have to invade into surrounding tissues of the primary tumour. Single cells are able to invade in different modes, either in a mesenchymal (elongated) or in an amoeboid (rounded) pattern [97, 98]. Mesenchymal motility is linked to an elongated cell shape. Cells are polarised with an obvious leading edge. Interactions with the extra-cellular matrix (ECM) are regulated by integrins and ECM-degrading proteolytical enzymes are required generating the path for migration. In contrast, amoeboid migration is linked to a characteristic round shape of the cells. Amoeboid cell migration is independent of ECM degradation and cells are able to squeeze through gaps in ECM fibres. Some cell types can use both modes of invasiveness and undergo transitions between them. Changes between modes of invasion rely on the specifics of the microenvironment.

1.3.2 Actin-based cell migration

Cell migration is dependent on specific functions of the actin cytoskeleton. Actin is a nucleotide-binding protein that is found at high intracellular concentrations and is highly conserved between species [99]. The actin cytoskeleton is crucial

for cell shape, stability and internal transport. G-actin molecules, the monomeric form of the protein, are the building blocks for filaments (F-actin) and the actin network. Rearrangement of this actin cytoskeleton is the basis of actin-based motility. Actin-based motility can be classified into the following steps: protrusion, adhesion, retraction and de-adhesion [100, 101]. During protrusion parts of the cell spread out into new areas and new contacts with surrounding areas are built during adhesion. During retraction the cell body is shifted in the direction of the movement followed by loss of contact to surrounding areas (de-adhesion). These processes have to be regulated tightly for efficient cell migration.

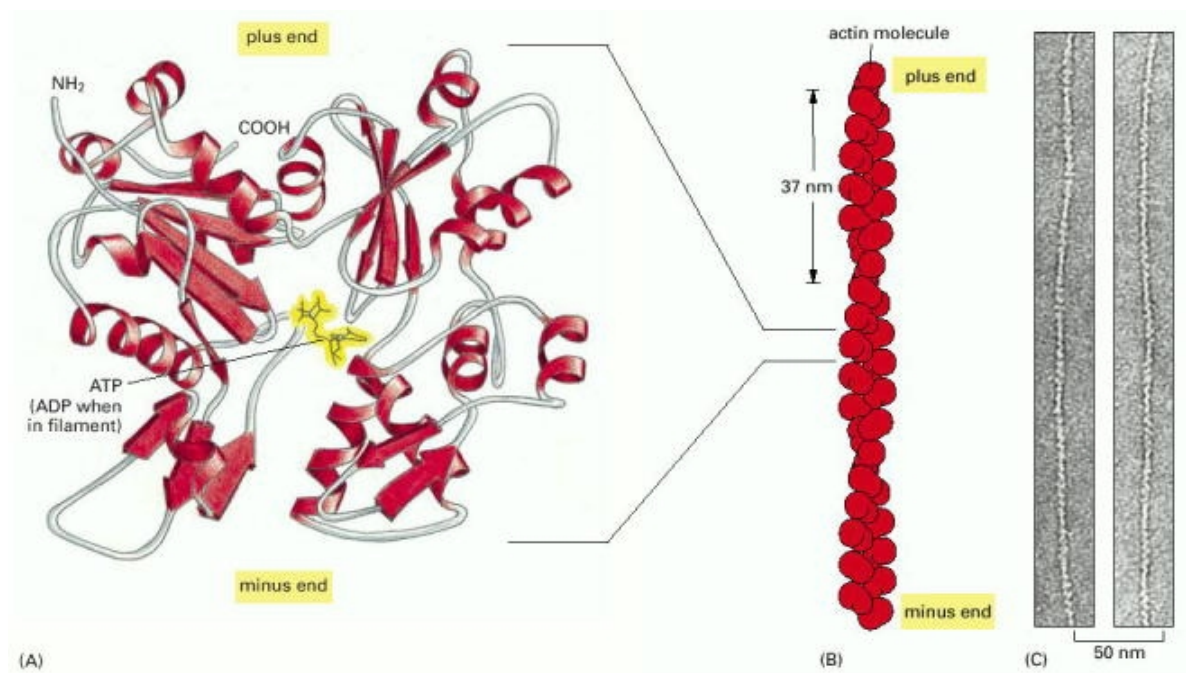


Figure 1.5: The structures of an actin monomer and actin filament

(A) The actin monomer has a nucleotide (either ATP or ADP) bound in a deep cleft in the center of the molecule. (B) Arrangement of monomers in a filament. Although the filament is often described as a single helix of monomers, it can also be thought of as consisting of two protofilaments, held together by lateral contacts, which wind around each other as two parallel strands of a helix, with a twist repeating every 37 nm. All the subunits within the filament have the same orientation. (C) Electron micrographs of negatively stained actin filaments. (C, courtesy of Roger Craig.) [102]

To build up actin filaments from monomers oligomers must be formed first. As actin dimers and trimers are not a stable entity spontaneous assembly of G-actin

into oligomers is not favoured. A nucleation step is needed for this rate-limiting step in the formation of filaments. Different actin nucleators facilitate the formation of actin oligomers. Elongation of these newly formed oligomers is directly dependent on the monomer concentration. Actin monomers consist of 4 structural domains and an ATP binding cleft in the middle. As shown in Figure 1.5 each actin monomer has two distinguishable sites, a plus and a minus end. Actin filaments are organised into double helical polymers of globular subunits arranged head to tail leading to molecular polarity of these filaments.

Actin monomers are added to the (+) end of the filament in an ATP-bound state and released from the (-) end in an ADP-bound state as polymerisation is accompanied by hydrolysis of ATP to ADP+Pi and the subsequent release of the γ -phosphate group. The biochemical differences of ATP bound actin on one end of the filament and ADP bound actin at the other end are crucial for directed polymerisation. The ability to polymerise depends on the concentration of actin monomers. The minimal required concentration of G-actin to drive polymerisation is the critical concentration. Due to the hydrolysis of ATP to ADP within the filament the critical concentration is different between the (+) and the (-) end of the filament leading to higher affinity for ATP-bound actin to the (+) end. As the intracellular concentration ATP-bound actin lies between the critical concentration of the (+) and the (-) end of the filament addition of monomers to the (+) end and depolymerisation at the (-) end is favoured, a process called treadmilling.

In a steady state the overall length of filaments does not change which means that the rates of polymerisation and depolymerisation are equal. Without regulatory proteins treadmilling is slow. More and more regulatory proteins are being discovered leading to the appreciation of the complexity of the intracellular actin machinery. Several core proteins that increase treadmilling were identified: profilin, ADF/cofilin, capping protein (CP), Arp2/3 complex and activators of the Arp2/3 complex (Figure 1.6).

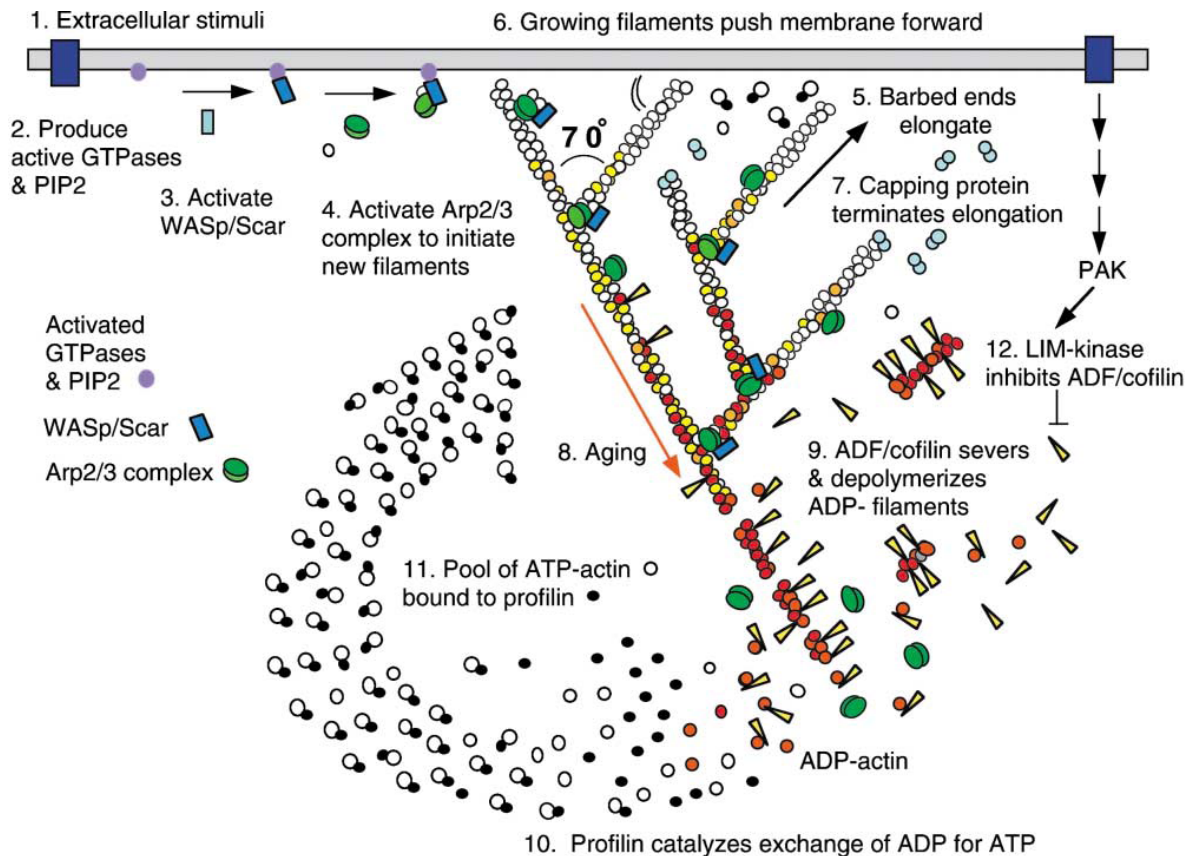


Figure 1.6: Dendritic Nucleation/Array Treadmilling Model for Protrusion of the Leading Edge

(1) Extracellular signals activate receptors. (2) The associated signal transduction pathways produce active Rho-family GTPases and PIP2 that (3) activate WASp/Scar proteins. (4) WASp/Scar proteins bring together Arp2/3 complex and an actin monomer on the side of a pre-existing filament to form a branch. (5) Rapid growth at the (+) end of the new branch (6) pushes the membrane forward. (7) Capping protein terminates growth within a second or two. (8) Filaments age by hydrolysis of ATP bound to each actin subunit (white subunits turn yellow) followed by dissociation of the γ -phosphate (subunits turn red). (9) ADF/cofilin promotes phosphate dissociation, severs ADP-actin filaments and promotes dissociation of ADP-actin from filament ends. (10) Profilin catalyzes the exchange of ADP for ATP (turning the subunits white), returning subunits to (11) the pool of ATP-actin bound to profilin, ready to elongate (+) ends as they become available. (12) Rho-family GTPases also activate PAK and LIM kinase, which phosphorylates ADF/cofilin. This tends to slow down the turnover of the filaments. (Redrawn from a figure in Pollard et al., 2000). Reprinted with permission from the Annual Review of Biophysics and Biomolecular Structure, Volume 29, copyright 2000 by Annual Reviews, www.annualreviews.org. [100]

In a simplified view a pool of unpolymerised actin monomers is important for a quick reaction to external stimuli (for reviews: [100, 103]). A high G-actin concentration allows faster growth of the free actin filaments. Free monomeric actin is mostly bound to profilin or actin sequestering proteins such as thymosin- β 4. Actin monomers bound to profilin are ready for addition to filaments whereas monomers bound to thymosin- β 4 are placed into reserve. Profilin binds to the plus end of the monomer inhibiting spontaneous nucleation and blocking

binding to the (-) end of filaments but ready for addition to a free (+) end. The binding of actin to profilin induces a nucleotide exchange from ADP to ATP whereas thymosin- β 4 slows down the rate of spontaneous ATP hydrolysis. Binding of actin monomers to the (+) end of the filament induces a conformational change in actin reducing its affinity for profilin. Thymosin- β 4 competes with profilin for binding of actin monomers but profilin has a stronger affinity for monomers. Formation of new filaments is induced by external stimuli. These extracellular signals activate members of the WASp/Scar family which in turn stimulate the Arp2/3 complex. Members of the Wiskott-Aldrich syndrome protein (WASP) family are nucleation promoting factors, capable of activating Arp2/3. The Arp2/3 complex is a multiprotein complex of actin related proteins serving as a nucleation factor for actin polymerisation and as (-) end of new filaments. It initiates the formation of new daughter filaments on the side of existing filaments. The Arp2/3 complex is intrinsically inactive and needs to be activated. A stable nucleus for further actin polymerisation is formed when two subunits of the Arp2/3 complex mimicking actin monomers bind one additional actin monomer. New filaments are polymerised rapidly until they are capped by the capping protein (CP), preventing further monomer addition. ATP hydrolysis within the filament and the subsequent dissociation of the γ -phosphate determines the age of the filament and older, ADP-containing parts are favoured to bind ADF/cofilin. Treadmilling is normally limited by the slow dissociation rate of actin monomers from the (-) end of the filament however ADF/cofilin can increase the rate of actin filament by different means. Binding of ADF/cofilin changes the twist of the actin helix inducing a mechanical stress that weakens the contacts between actin subunits in the filaments. This facilitates the dissociation of ADP-actin subunits from the (-) end of the filaments. Binding of ADF/cofilin also induces debranching and severing of the filaments into short segments. Severing is important to increase the concentration of free filament ends and therefore disassembly. Once ADP-bound monomers are released into the cytoplasm profilin competes with ADF/cofilin for binding and subsequently induces a nucleotide exchange, converting monomers back to ATP-actin/profilin. This complex is then ready to be added to new (+) ends. Capping of (+) ends as well as rapid depolymerisation of (-) ends is important to control the concentration of free actin monomers ready for polymerisation. Capping a large fraction of actin filament (+) ends limits the length of filaments and inhibits non-

productive consumption of monomers. Capping protein can be regulated by phosphatidylinositol-4,5-bisphosphate (PIP₂) which is not only able to inhibit the function of CP but also to uncap (+) ends.

1.3.3 Higher order actin organisation and its regulation

Actin filaments can assemble in different higher order patterns within the cell. Different protrusive structures with dense arrays of actin filaments have been described [103-105]. The simplest ones are filopodia, finger-like protrusions containing tight bundles of actin filaments held together by cross-linking proteins with their (+) ends facing the membrane. Lamellipodia are protrusive sheets with a ruffling appearance, containing branched actin filaments. These structures can co-exist at the leading edge. A loose actin meshwork is found in the cell body with apparently randomly organised actin filaments. Within the cell body stress fibres can form [106, 107]. Stress fibres are contractile actomyosin structures found in non-muscle cells, which are arranged in bundles of alternating polarity interspersed with bipolar myosin II filaments and crosslinked with actin-binding proteins such as α -actinin. Association of stress fibres and focal adhesions prevent retraction at the rear of the cell and therefore cell migration. Three categories of stress fibres are found in mammalian cells: ventral stress fibres that are attached to focal adhesions at both ends, dorsal stress fibres that are attached to focal adhesion on one end and traverse arcs of curved bundles that do not associate with focal adhesions. It is currently accepted that an optimal G- to F-actin ratio in the cell is required for efficient cell motility as efficient cell movement requires actin polymerisation, but high levels of stress fibres can oppose cell migration by increasing cell adhesion.

Several external signals can induce rearrangement of the actin cytoskeleton. Signalling pathways seem to converge on Cdc42, Rac and Rho, members of the Rho-family of GTPases. GTPases act as molecular switches controlling cellular processes by cycling between an active, GTP-bound state and an inactive, GDP-bound state. Activation of each of these Rho-GTPases has profound effects on the actin cytoskeleton (Figure 1.7) [101].

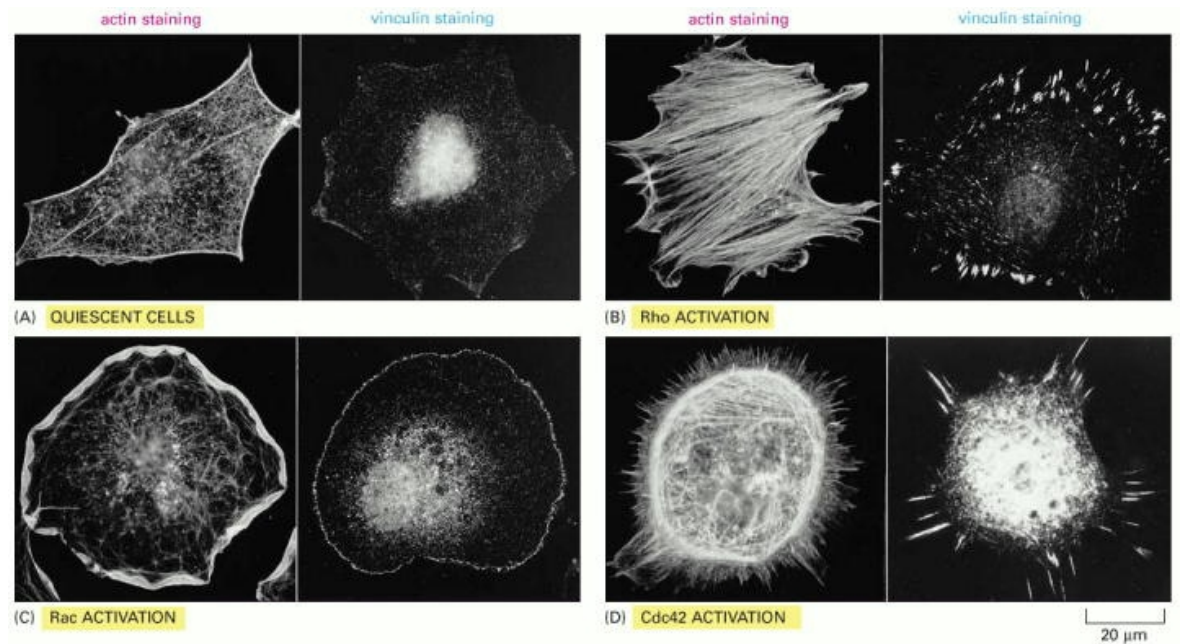


Figure 1.7: The dramatic effects of Rac, Rho, and Cdc42 on actin organisation in fibroblasts
 In each case, the actin filaments have been labelled with fluorescent phalloidin, and focal contacts have been located with an antibody against vinculin. (A) Serum-starved fibroblasts have actin filaments primarily in the cortex, and relatively few focal contacts. (B) Microinjection of a constitutively activated form of Rho causes the rapid assembly of many prominent stress fibers and focal contacts. (C) Microinjection of a constitutively activated form of Rac, a closely related monomeric GTPase, causes the formation of an enormous lamellipodium that extends from the entire circumference of the cell. (D) Microinjection of a constitutively activated form of Cdc42, another Rho family member, causes the protrusion of many long filopodia at the cell periphery that form adhesive contacts with the substratum. The distinct global effects of these three GTPases on the organisation of the actin cytoskeleton are mediated by the actions of dozens of other protein molecules that are regulated by the GTPases. Many of these target proteins resemble the various actin-associated proteins that we have discussed in this chapter. [108]

RhoA promotes the formation of actin stress fibres and focal contacts through phosphorylation of myosin light chain (MLC) and inactivation of the myosin light chain phosphatase. Phosphorylated MLC assembles into filaments and associates with actin filaments to form contractile stress fibres. Rac causes formation of a large lamellipodia and actin ruffles whereas Cdc42 stimulates the formation of filopodia. These effects are mediated by the action of downstream effectors, some of them described in section 1.3.2. These proteins are not only involved in intracellular signalling but can also determine the mode of cell invasion. Mesenchymal motility is mainly driven by Rac and Cdc42 whereas amoeboid migration is linked to a RhoA signalling.

1.3.4 Actin isoforms

Three actin isoforms were identified in vertebrates: α -, β - and γ -actin, which are mostly localised in the cytoplasm. α -actins are mostly found in muscle cells, β - and γ -isoforms in non-muscle cells. β - and γ -actin isoforms vary in only four amino acids in their N-termini and are co-expressed in most tissues although the β -isoform is expressed in excess [109]. β - and γ -actin seem to have distinct functions in the cell however these are not quite clear. Spatial segregation has been observed for the β - and γ -isoforms. β -actin is the main isoform to drive protrusion whereas γ -actin displays a more ubiquitous distribution, often found in perinuclear regions and often incorporated into stress fibres. Enrichment of β -actin to the leading edge may be achieved by preferred interaction with certain actin binding proteins and in part by localisation of its mRNA and its local translation. All actin isoforms are mostly found in the cytoplasm however actin has also been implicated to localise in the nucleus and to play a role in chromatin remodelling, RNA processing, transcription and nucleocytoplasmic transport [110-112]. However the molecular mechanisms by which actin exerts these functions as well as the polymerisation status of nuclear actin remain unclear [113].

1.4 Hypoxia and glucose metabolism

A hallmark of hypoxic tumours is their shift from aerobic to anaerobic metabolism marked by an increase in the rate of glycolysis and lactate production [102]. Glycolysis is the step by step breakdown of one molecule of glucose (consisting of 6 carbon atoms) broken down into two molecules of pyruvate (each containing three carbon atoms). During this process the binding energy of glucose is conserved as metabolic energy in form of ATP molecules. Hypoxic tumours rely on glycolysis followed by lactic acid fermentation as main source of ATP/energy as oxidative phosphorylation is restricted as an energy source due to the lack of oxygen. Metabolic enzymes, such as L-lactate dehydrogenase and fructose-bisphosphate aldolase are upregulated in a HIF-dependent manner making glycolysis in hypoxic tumours more efficient.

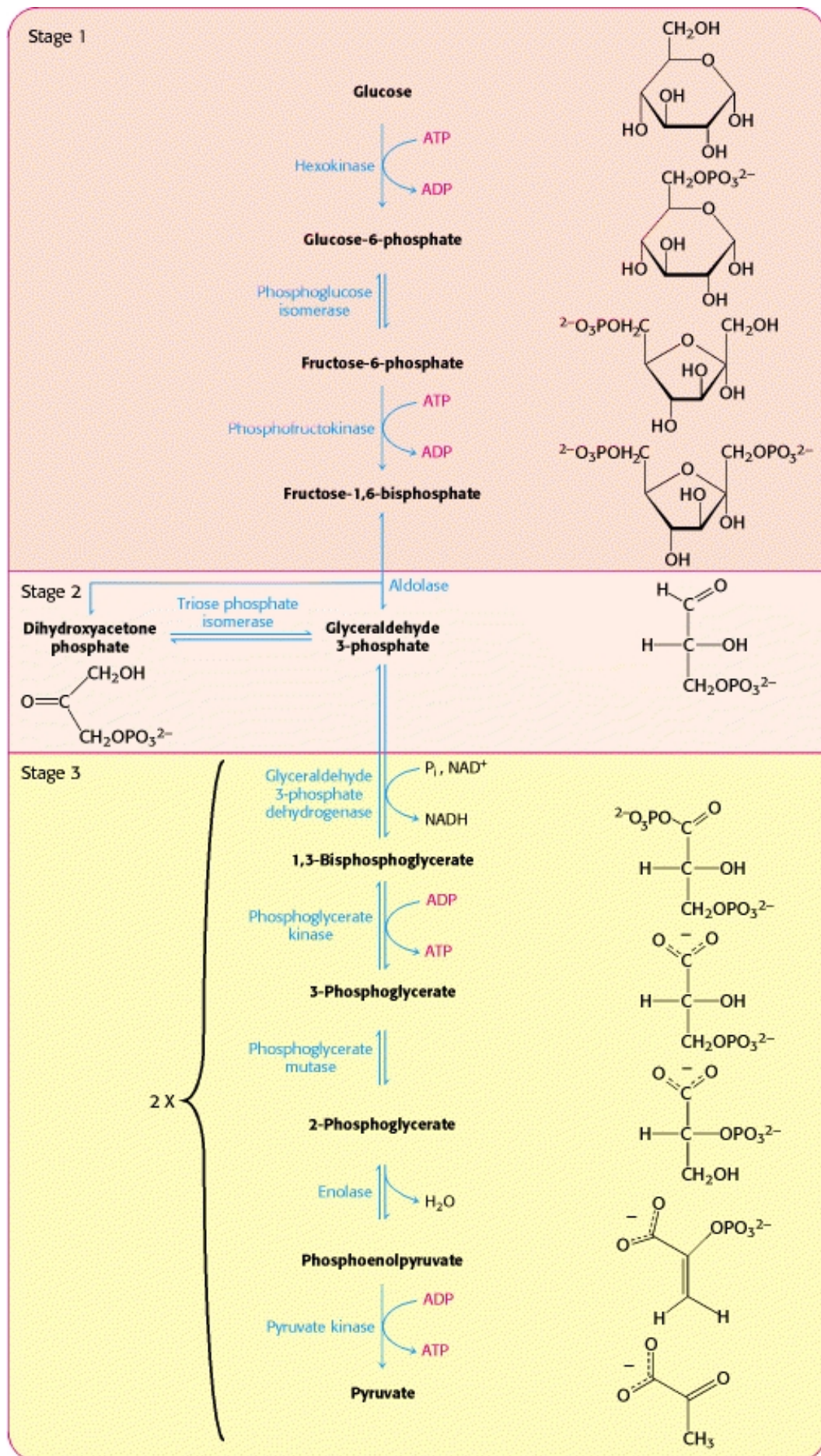


Figure 1.8: Overview over the reaction involved in glycolysis [102]

Figure 1.8 shows an overview over the glycolytic pathway including the reactions that are catalysed by fructose-bisphosphate aldolase and triosephosphate isomerase. Aldolase is the enzyme that catalyses the reaction of cleaving fructose 1,6-bisphosphate into glyceraldehyde 3-phosphate and dihydroxyacetone phosphate, a six-carbon molecule split into two three-carbon molecules. This reaction is reversible in intracellular conditions. The subsequent reaction in the glycolytic pathway is catalysed by triosephosphate isomerase. Glyceraldehyde 3-phosphate and dihydroxyacetone phosphate are isomers that are converted into one another by triose phosphate isomerase. This reaction is reversible but as glyceraldehyde 3-phosphate is removed by subsequent reactions of glycolysis, the reaction tends to produce glyceraldehyde 3-phosphate. By the subsequent reactions of aldolase and triose phosphate isomerase two molecules of glyceraldehyde 3-phosphate are formed from one molecule of fructose 1,6-bisphosphate funneling dihydroxyacetone phosphate into the main glycolytic pathway.

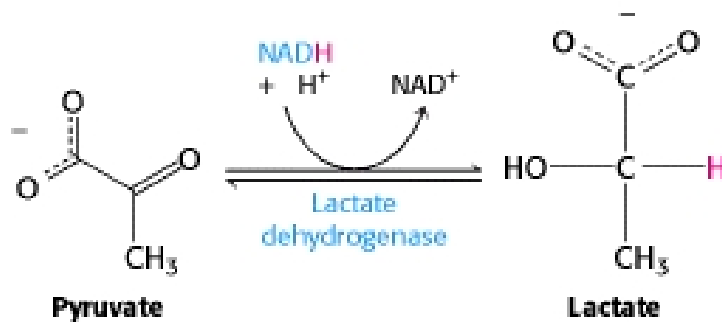


Figure 1.9: Reaction catalysed by lactate dehydrogenase

In the absence of oxygen lactate is formed from the end product of glycolysis, namely pyruvate (Figure 1.9). Lactate dehydrogenase catalyses the reduction of pyruvate to form lactate. This reaction is necessary to regenerate redox balance to keep glycolysis running under hypoxic conditions.

1.5 Quantitative proteomics (SILAC)

With proteomic techniques large numbers of proteins can be analysed, however so far results have mostly been qualitative. In recent years several methods have been established to obtain quantitative information [114]. Mass spectrometric analyses are not quantitative *per se* so quantitative data is mostly obtained by reporting relative changes in protein amounts between two samples. To be able to compare two samples to each other they have to be labelled. Labelling can be introduced at different stages of the workflow with various labelling techniques, using different chemical or metabolic labelling methods. To differentiate between labelled and unlabelled peptides in mass spectra a mass difference of at least 3 Da is favourable. A quantitative approach using metabolic labelling has emerged in recent year. Stable isotope labelling by amino acids in cell culture (SILAC) was first described in 2002 [115]. Metabolic labelling is a non-radioactive approach that substitutes specific standard essential amino acids in the growth medium with an isotopically labelled form of that amino acid so they are incorporated into cellular proteins. Labelling of different essential amino acids with ^{13}C , ^{15}N or ^2H has been described in the literature [116]. SILAC is a straightforward approach that induces a mass shift between peptides pairs in labelled and unlabelled samples but no other chemical changes, so labelled peptides behave the same as their non-labelled counterparts. Cultures are grown for at least 5 doubling times to achieve 100% incorporation of labelled amino acids, including proteins with low turnover. Complete labelling of proteins is important as incomplete labelling makes it difficult to obtain reliable relative comparison. SILAC is a good tool to investigate protein-protein interactions. Often protein interactions are transient, show high background interactions and false-positives in non-quantitative mass spectrometric approaches. It is often a trade-off between sensitivity and specificity. In SILAC however background proteins bind equally leading to a one-to-one ratio between labelled and unlabelled peptides, whereas specific interactions show differential ratios, removing false positive results. There are a few advantages of SILAC labelling over other labelling techniques: less manipulation steps are required in the workflow so limited material can be analysed. The fragmentation patterns of peptides are identical apart from the mass shift.

Furthermore, several peptides from the same protein can be compared, leading to a higher confidence level for ratios identified. However, it has to be kept in mind that peptides are analysed stochastically by the mass spectrometer which means analysis of high abundant proteins is favoured over co-eluting low abundant proteins. Other factors such as accessibility of the protease, solubility of the peptide as well as its ionisation efficiency are important for peptide identification. Identification of single peptides can lead to false positive identification, if they do not show a high sequence score whereas identification of several peptides (ideally covering a wider protein sequence) can give a more reliable ratio. In this study SILAC is used to identify new interaction partners of PHDs.

1.6 Aims

In this project PHDs were investigated to gain a better understanding of intracellular oxygen sensing. As discussed in section 1.2.1.4, each PHD isoform was found to be involved in various different pathways however their substrates are mostly unknown. The aim of this project is to identify new substrates that contribute to PHD-dependent functions. A quantitative proteomic approach was used to identify proteins that interact with PHDs. After identifying potential new substrates, their hydroxylation status was investigated to identify new substrates. Furthermore, the biological function of the identified interaction was investigated in more detail.

Chapter 2 – Material and methods

2 Material and methods

2.1 Materials

2.1.1 General reagents

Unless listed in Table 2.1, reagents were purchased from Sigma.

Table 2.1: General reagents and kits

Reagent	Company
Acrylamide solution - 30% acrylamide, 37.5:1 bis-acrylamide	Severn Biotech Ltd.
Ammonium persulfate (APS)	Fisher Scientific
BSA standard (2 mg/ml)	Pierce
DH5 α competent cells	Invitrogen
DMEM	Invitrogen
Dynabeads M-280 sheep anti-mouse IgG	Invitrogen
Rapid DNA ligation kit	Roche Applied Sciences
ECL Western Blotting Detection reagent	GE Healthcare Life Sciences
Ethanol	Fisher Scientific
FBS	Autogen Bioclear, Harlan
Gel extraction kit	Qiagen
L-glutamine	Invitrogen
Glycine	Fisher Scientific
HyperLadderI DNA marker	Bioline
α -ketoglutarate (T α KG)	Synthesised as described by MacKenzie [35]
KCl	Fisher Scientific
Laemmlli sample buffer 2x	Biorad
Lipofectamine 2000 transfection reagent	Invitrogen
MgCl ₂	Fisher Scientific
Methanol	Fisher Scientific
NaCl	Fisher Scientific
Nitrocellulose membrane 0.22 μ m	Anachem
PCR purification kit	Qiagen
Plasmid purification kit	Qiagen
QuickChange Site-directed Mutagenesis Kit	Stratagene
High-Range molecular weight marker (protein) (RPN 800E)	GE Healthcare Life Sciences
Restriction enzymes	Roche Applied Sciences
RPMI	Invitrogen
SimplyBlue Safe Stain (Coomassie)	Invitrogen
SDS (sodium dodecyl sulphate)	Fisher Scientific
Tris base ultrapure	Melford
Trypsin	Invitrogen
Vectrashield mounting medium	Vector laboratories Inc.

Biorad agarose gel casters, agarose gel tanks, Mini-Protean III Ready Gel System for SDS-PAGE and Western blotting

Invitrogen Novex mini-cell gel tank and NuPage 10% Bis-Tris gels

Biotrace Invivo₂ Hypoxic chamber and Ruskinn gas mixer

Tissue culture reagents Becton Dickson

2.1.2 General buffers and solutions

Table 2.2: General buffers and solution

Solution	Composition
L-Broth (LB) medium	10 g/l Tryptone 5 g/l yeast extract 10 g/l mM NaCl
LB agar plates	LB medium + 15 g/l bacto agar
Tris-acetate-EDTA (TAE)	40 mM Tris-acetate, 1 mM EDTA
Phosphate buffered saline (PBS)	137 mM NaCl 2.7 mM KCl 10 mM Na ₂ HPO ₄ 2 mM KH ₂ PO ₄ , pH 7.4
PBS-T	PBS + 0.05% Tween-20
1x SDS-PAGE running buffer	25 mM Tris 192 mM glycine 0.1% SDS, pH 8.3
1x blotting buffer	25 mM Tris 192 mM glycine 0.01% SDS 20% methanol
Blocking buffer for Western blots	5% milk powder in PBS-T
Stripping buffer for Western blots	0.2 M glycine 1% SDS pH 2.5
RIPA	50 mM Tris-HCl 150 mM NaCl 2 mM EDTA 1% NP-40 0.5% sodium deoxycholate 0.1% SDS
NP-40 lysis buffer (TNN)	50 mM Tris-HCl pH 7.5 150 mM NaCl 5 mM EDTA 0.5% NP-40 protease inhibitor cocktail

Washing buffer for IP	50 mM Tris-HCl pH 7.5 150 mM NaCl 5 mM EDTA 0.25% NP-40
Lysis buffer for actin quantification	20 mM KPO ₄ pH 8 10 mM Pipes pH 8 5 mM EGTA pH 8 2 mM MgCl ₂ 0.1% TritonX-100 3.7% formalin 2 μM Phalloidin-TRITC
Washing buffer for actin quantification	0.1% Saponin 20 mM KPO ₄ pH 8 10 mM Pipes pH 8 5 mM EGTA pH 8 2 mM MgCl ₂

2.2 Methods

2.2.1 DNA techniques

2.2.1.1 Cloning of PHD-FLAG plasmids

To subclone PHD1 or PHD3 into a pCMV-5a vector (Sigma) containing a C-terminal FLAG-tag the following cDNA plasmids were purchased from Invitrogen: IOH13327 containing the cDNA sequence for PHD3 and IOH27186 containing the cDNA sequence for PHD1. A PCR using the primers specified in Table 2.4 was used to introduce HindIII and BamHI or EcoRI and HindIII restriction sites adjacent to the PHD1 or PHD3 coding sequence respectively. The PCR was performed using a BioMix mastermix with 2 μM of each primer and 110 ng template for PHD1 or 130 ng template for PHD3 under the following conditions:

Table 2.3: PCR conditions

Cycles	Temperature	Time
1	94 °C	2 minutes
35	94 °C	30 seconds
	55 °C	40 seconds
	72 °C	3 minutes

The PCR products were run on a 1% agarose gel, the appropriate band was cut out and purified from the gel using QIAquick gel extraction kit (Qiagen). Then 30 μl of the purified PCR products as well as 2 μg of the vector pFLAG-CMV-5a were

digested first with BamHI (Roche) for PHD1 or HindIII (Invitrogen) for PHD3 for 4 hours at 37°C. After a purification step a second digest was set up overnight at 37°C with HindIII for PHD1 or EcoRI (Invitrogen) for PHD3. Afterwards the digested insert was purified again. The digested vector was dephosphorylated using shrimp alkaline phosphatase (Promega) according to the manufacturer's instructions.

Ligations were carried out using Rapid DNA ligation kit (Roche). An approximate 3 fold molar excess of the insert fragment over the vector fragment was used for the ligation reaction. The reaction was incubated at room temperature for 2 hours before 5 µl of the ligation mix were transformed into DH5α bacteria. Clones containing the insert were sequenced (Research services, Beatson Institute) to confirm the correct formation of the fusion protein.

The PHD2-Myc/FLAG plasmid was purchased from Origene. Myc-tagged triple mutant HIF1α (HIF1αTM) and HIF2α (HIF2αTM) constructs were a kind gift from M.C. Simon [117].

Table 2.4: Primer sequences

Name	Experiment	Sequence 5'-3'
PHD1 forward	Cloning of PHD1-FLAG	GCCAAGCTTGCCGCCATGGACAGCCCCTGCCAGCCG
PHD1 reverse	Cloning of PHD1-FLAG	GCCGGATCCGGTGGGCGTAGGCCGGCTGTGAT
PHD3 forward	Cloning of PHD3-FLAG	GCCGAATTCGCCGCCATGCCCTGGGACACATCATG
PHD3 reverse	Cloning of PHD3-FLAG	GCCAAGCTTGTCTTCAGTGAGGGCAGATTC
Actin P70A forward	Site directed mutagenesis of GFP-actin	CTCACCTGAAGTACGCCATCGAGCACGGC
Actin P70A reverse	Site directed mutagenesis of GFP-actin	GCCGTGCTCGATGGCGTACTTCAGGGTGAG
Actin P322A forward	Site directed mutagenesis of GFP-actin	CACTGCCCTGGCAGCCAGCACAATGAAG
Actin P322A reverse	Site directed mutagenesis of GFP-actin	CTTCATTGTGCTGGCTGCCAGGGCAGTG

All primers were purchased from Eurofins MWG.

2.2.1.2 Site directed mutagenesis

The pEGFP- β -actin plasmid was purchased from Clontech. Point mutations were introduced into the plasmid using the site-directed mutagenesis kit from Stratagene following the manufacturer's instructions. Primers were designed including the desired mutation (listed in Table 2.4). A 50 μ l reaction was set up containing 25 ng plasmid DNA, 125 ng of each primer, 1 μ l dNTP mix, 5 μ l 10x reaction buffer and 1 μ l PfuTurbo DNA polymerase. A PCR program with the following parameters was used:

Cycles	Temperature	Time
1	95 °C	3 minutes
16	95 °C	90 seconds
	55 °C	1 minute
	68 °C	12 minutes

The parental DNA was digested by adding the restriction enzyme DpnI (10U/ μ l) to the reaction mix and incubating the mixture for 2 hours at 37 °C. 5 μ l of the reaction was transformed into competent DH5 α cells (see section 2.2.1.3). Sequences were verified by sequencing (Research services, Beatson Institute for Cancer Research).

2.2.1.3 Transformation of DH5 α bacteria

50 μ l DH5 α competent cells were thawed on ice. 5 μ l DNA was added and cells were incubated on ice for 15-30 minutes. After a heat shock of 40 seconds at 42 °C cells were incubated on ice for further 2 minutes. 250-500 μ l LB medium were added and cells were incubated for 30 minutes at 37 °C shaking at 220 rpm. Cells were then plated onto agar plates containing the relevant antibiotic and grown overnight at 37 °C. Single colonies were inoculated in LB medium containing the relevant antibiotic and grown overnight at 37 °C for DNA purification. Small scale or large scale plasmid DNA preparations were performed using Qiagen kits following the manufacturer's instructions.

2.2.1.4 Agarose gel

1% (w/v) agarose was boiled in 1x TAE buffer. Before solidification 1 µg/ µl ethidiumbromide was added and the gel was allowed to solidify in the gel chamber. DNA samples were diluted in 10x loading buffer containing glycerol and bromphenol blue. Samples were then separated at 100V in 1x TAE running buffer. DNA was visualised by a UV transilluminator. Specific bands could be cut out and extracted from the gel using the Qiagen gel extraction kit according to the manufacturer's instructions.

2.2.2 Cell lines and growth conditions

The human colon carcinoma cell line HCT116 was cultured in RPMI medium (Invitrogen) supplemented with 10% FBS (Harlan) and 2 mM L-glutamine (Invitrogen). The serum was heat-inactivated at 55°C for 45 minutes prior to use. The renal clear cell carcinoma cell line RCC4, the melanoma cell line A375 and the osteosarcoma cell line U2OS were cultured in DMEM medium (Invitrogen) supplemented with 10% FBS and 2 mM L-glutamine. Cells were maintained in a humidified incubator at 37°C in 5% CO₂. For routine culturing cells were incubated with trypsin solution (0.25% Trypsin in PBS-EDTA) and then plated at a density as needed for culturing or transfection.

For the SILAC screen the SILACTM Protein Identification (ID) and Quantitation Kit from Invitrogen was used (Catalog No.: MS10031 using RPMI-Flex plus ¹³C₆-labelled arginine: Catalog No.: MS10011). Cells were grown in heavy and light medium until 100% incorporation of labelled amino acids was achieved.

2.2.3 Freezing and thawing of cells

Cells were harvested and re-suspended in 90% FCS supplemented with 10% DMSO. Cells were frozen overnight at -80°C in a cryo freezing container (Nalgen) before they were placed in a liquid nitrogen tank. When taken out of the nitrogen tank cells were thawed rapidly at 37°C. Cells were added to pre-warmed medium, then were centrifuged at 1000 rpm for 4 minutes to remove the DMSO and finally re-suspended in fresh medium for culturing. All cells were regularly tested for mycoplasma contamination (Research Services, Beatson Institute).

2.2.4 Transfection using lipofectamine 2000

Cells were transfected with Lipofectamine 2000 transfection reagent (Invitrogen) according to manufacturer's instructions. Cells were plated the day before transfection to allow them to adhere overnight. 4-5 hours after the transfection mix was added to the cells the medium was replaced with fresh medium. Depending on the assay cells were analysed 24-48 hours after transfection. The following constructs were used for the knock down of specific genes:

Table 2.5: RNA interference and oligonucleotide sequences

Name	Target gene	Sense sequence	Company
shPHD1 (22327)	PHD1	CCGGACTGGGACGTTAAGGTGCATG CTCGAG CATGCACCTTAACGTCCCAGTTTTT	OpenBiosystems
shPHD2 (1043)	PHD2	CCGGGACGACCTGATACGCCACTGT CTCGAG ACAGTGGCGTATCAGGTCGTCTTTTT	OpenBiosystems
shPHD3 (1048)	PHD3	CCGGCACCTGCATCTACTATCTGAA CTCGAGTTCAGATAGTAGATGCAGGTGTTTTT	OpenBiosystems
shControl		CCTAAGGTTAAGTCGCCCTCG CTCTGAG CGAGGGCGACTTAACCTTAGG	Addgene
siActin (5)	actin	CUAUGACUUAGUUGCGUUAAdTdT	Sigma
siActin (7)	actin	CCUGUACACUGACUUGAGAdTdT	Sigma
Non-targeting siRNA pool		Pool of non-targeting siRNAs	Dharmacon

The generation of A375 stable knockdown cell lines was described previously by [118].

2.2.5 Drugs and treatment of cells with these drugs

After transfection cells were incubated for 24 hours before they were subjected to either normoxia (21% oxygen) or hypoxia (1% oxygen) for another 24 hours. Hypoxia was achieved using a humidified Invivo₂ 500 hypoxic chamber (Biotrace, Bridgend, UK) and Ruskin hypoxic gas mixer at 37 °C with 1% O₂, 5% CO₂ and 94% N₂ unless otherwise specified. Hypoxia was defined as 24 hours to equilibrate the sample including all buffers and plastic dishes to hypoxic conditions. Normoxic cells could then be treated for 3 hours with 1 mM Dimethylxaloylglycine (DMOG), a non-cleavable α -ketoglutarate analog, whereas hypoxic cells could be treated for 1 hour with 1mM α -ketoglutarate trifluoromethyl benzyl ester

(TαKG), a cell-permeable α-ketoglutarate derivative which can re-activate prolyl hydroxylases under hypoxia.

The actin drugs Latrunculin A (Sigma) and Cytochalasin D (Sigma) were used to disrupt the actin cytoskeleton. Latrunculins are toxins isolated from the red sea sponge *Negombata magnifica*. Latrunculin binds to actin monomers in a 1:1 stoichiometry so they are unable to polymerise [119, 120]. Cytochalasins are extracted from *zygosporin mansonii*. They bind to the (+) end of actin filaments and prevent monomer addition [121]. This leads to depolymerisation of actin filaments by cellular mechanisms. Cells were treated with 300 nM Latrunculin A or 10µg/ml Cytochalasin D for 15 minutes.

2.2.6 Preparation of lysates

Treated or untreated cells were washed twice with cold PBS (on ice) and lysed in RIPA or TNN buffer containing protease inhibitors (Sigma). Hypoxic cells were lysed in hypoxic RIPA or TNN buffer in the hypoxic chamber. Cells were taken out of the hypoxic chamber after lysis and placed on ice immediately. Cell extracts were incubated on ice for 20 minutes before they were centrifuged at 12,000 x g for 10 minutes at 4°C to remove debris. Supernatants were transferred to fresh tubes. The protein concentration of cell extracts was measured by using Bradford reagent (Sigma) according to the manufacturer's instructions. BSA dilutions ranging from 0.08 mg/ml up to 2 mg/ml were used as standards. 10 µl of the standards as well as of a 1:10 dilution of the cell extracts were analysed in a 96well plate by adding 200 µl Bradford reagent. After an incubation of 5 minutes the plate was analysed at 595 nm using a Spectra Max plus plate reader (Molecular devices).

2.2.7 SDS-PAGE

Proteins samples were resolved on SDS-PAGE. Denaturing polyacrylamide gels of 10% or 12% acrylamide were cast using a mini-Protean gel caster (Biorad). Gels were overlaid with water and allowed to set until polymerised. Excess water was removed and a 5% stacking gel was poured on top of the resolving gel. Protein samples were loaded onto the gel with a prestained protein marker next to them

(GE Healthcare) and run in 1x SDS-PAGE running buffer through the stacking gel at 80 V before separating the samples at 120 V.

Protein samples used for proteomics were run on 10% precast NuPage gels (Invitrogen) in 1x MOPS SDS running buffer at 150 V. Proteins on NuPage gels were visualised by Coomassie staining. The staining was carried out according to manufacturer's instructions.

2.2.8 Immunoblotting

After electrophoresis proteins were transferred from the gel onto a nitrocellulose membrane (0.22 μm , Anachem) in 1x SDS-PAGE blotting buffer using a wet transfer system (Biorad). Proteins were transferred at 200 mA per gel for 2 hours in ice cold buffer. The membrane was blocked in 5% milk (Marvel) in PBS-T for non-specific binding at room temperature for 30-60 minutes. Then the membrane was washed in PBS-T and incubated with the primary antibody for 2 hours at room temperature or over night at 4°C (for antibody dilutions see Table 2.6). Following 3 washes in PBS-T for 5-10 minutes, the blots were incubated with the appropriate horseradish peroxidase-conjugated secondary antibody at room temperature for 30-60 minutes (for antibody-dilutions see Table 2.7). After 3 more washes with PBS-T for 5-10 minutes proteins were visualized by Enhanced Chemiluminescent Reagents (ECL, GE Healthcare) and exposure to Fuji X-Ray films.

To reprobe the membrane with another primary antibody, membranes were incubated in stripping buffer for 20-30 minutes at room temperature, followed by blocking them again in 5% milk in PBS-T and incubation with a new primary antibody.

Table 2.6: Antisera

Antibody	Company	Type	Dilution
Actin (AC-40)	Sigma	Mouse monoclonal	1:5000
Aldolase	Abcam	Mouse monoclonal	1:500
Aldolase	Abcam	Goat polyclonal	1:2000
HIF1 α	BD Bioscience	Mouse monoclonal	1:500
FLAG (M2)	Sigma	Mouse monoclonal	1:5000
GFP	Clontech	Mouse monoclonal	1:2000
LDH	Abcam	Mouse monoclonal	1:4000

LDH	Abcam	Goat polyclonal	1:2000
myc	Cell Signalling	Mouse monoclonal	1:1000
PHD1	Novus	Rabbit polyclonal	1:2000
PHD2	Kind gift by Kevin Gattner	Mouse monoclonal	1:200
PHD3	Kind gift by Kevin Gattner	Mouse monoclonal	1:50
Triosephosphate isomerase	Abcam	Mouse monoclonal	1:500
Triosephosphate isomerase	Abcam	Goat polyclonal	1:5000
Tubulin	Sigma	Mouse monoclonal	1:2000
Immunostaining			
FLAG-Cy3	Sigma	Mouse monoclonal	1:100
FLAG-FITC	Sigma	Mouse monoclonal	1:100
DNaseI-Alexa488	Invitrogen	100 µg/ml	1:50
Phalloidin-TRITC	Sigma	1 mg/ml	1:200

Table 2.7: Secondary antibodies

Secondary antibodies	Company	Dilution
Anti-mouse IgG, HRP-linked	Cell Signalling	1:5000
Anti-rabbit IgG, HRP-linked	Cell Signalling	1:5000
Anti-goat IgG, HRP-linked	Cell Signalling	1:5000

2.2.9 Immunoprecipitations

2.2.9.1 Dynabeads

24 hours before transfection cells were plated onto 10 cm tissue culture dishes. Cells were transfected with 4 µg DNA (FLAG-tagged PHD plasmids) using Lipofectamine 2000 transfection reagent. After 24 hours cells were treated appropriately (as described in section 2.2.5). After the treatment cells were washed twice in ice cold PBS and lysed in 1 ml cold TNN lysis buffer as described in section 2.2.6. 5% of the total lysate was kept for Western blot analysis.

1-2 mg of total protein was used for each immunoprecipitation. Immunoprecipitations were performed by adding 1 µg of the appropriate antibody (0.2 µl of FLAG-M2 antibody) to the lysate for 2-3 hours at 4°C. In the

meantime 20 μ l of Dynabeads- M280 sheep anti mouse IgG slurry (Invitrogen) was washed once with 1%BSA/PBS to block unspecific binding and once with TNN lysis buffer. The washed beads were then added to the lysate containing antibodies and the sample was incubated for 1 hour at 4°C. Afterwards the beads were washed twice in washing buffer. The dry beads were resuspended in 50 μ l 1x Laemmli sample buffer and boiled at 95°C for 5-10 minutes. Proteins were separated on a SDS-PAGE and analysed by Western blotting.

2.2.9.2 FLAG-sepharose

Immunoprecipitations were performed as described in section 2.2.9.1 with the following alterations: HCT116 cells were plated onto 15 cm plates 48 hours before transfection. Cells were transfected with 8 μ g DNA (FLAG-tagged PHD plasmids) using Lipofectamine 2000 transfection reagent. After transfection cells were incubated under normoxia or hypoxia for 24 hours before they were lysed in 1.5 ml TNN lysis buffer as described above. 100 μ l of FLAG-agarose slurry (Sigma) were washed three times with TNN lysis buffer, added to 25 mg of total protein and incubated for 2 hours at 4°C. The samples were centrifuged at 1000 x g for 5 minutes at 4°C and transferred into a spin column (Biorad, Catalogue number 732-6204). Samples were washed three times in washing buffer by sequential mixing of the beads with the buffer and removing the buffer by centrifuging the buffer into a microfuge tube. After the last wash the dry beads were incubated with 2-bed volumes of FLAG peptide (100 μ g/ ml, Sigma) in TBS for 5 minutes on ice with occasional vortexing. The eluate was removed by centrifuging it into a fresh microfuge tube. The elution step was repeated once more. Eluates that were previously labelled in heavy and light medium (SILAC) were mixed on a 1:1 ratio (volume to volume). The mixed samples were then concentrated by centrifugal filtration using a 3 kDa cut-off membrane (Microcon Ultracell YM-3, Millipore) at 14,000 x g, 15°C for 120 minutes. Concentrated samples were removed from the reservoir by placing the sample reservoir upside down in a clean tube and centrifuging it for 1 min at 1000xg. After determining the sample volume one quarter volume per volume of 4x NuPage sample buffer was added and the sample was denaturated at 57°C for 15 minutes. Samples were run on a 10% NuPage gel and further analysed by mass spectrometry (section 2.2.10).

2.2.9.3 GFP-agarose

Immunoprecipitations were performed as described in section 2.2.9.1 with a few alterations. HEK293 cells were plated onto 15 cm plates 24 hours before transfection. Cells were transfected with 4 µg DNA (GFP-actin) using Lipofectamine 2000 transfection reagent. The medium was changed to fresh medium 5 hours after transfection. Cells were lysed in 1.5 ml ice cold RIPA buffer as described above. Samples were immunoprecipitated using 40 µl of GFP-agarose slurry which was added to 30 mg total protein for 3 hours at 4°C. The beads were washed three times with RIPA buffer. The dry beads were resuspended in 40 µl 1x NuPage buffer and boiled for 10 minutes. One tenth of the sample was resolved on a 10% NuPage gel next to known amounts of BSA to estimate the amount of immunoprecipitated GFP-actin after staining with colloidal Coomassie. The rest of the sample was analysed by mass spectrometry which was performed by Richard Unwin at the University of Manchester (see section 2.2.11).

2.2.10 SILAC

Protein samples were separated on 10% Novex gel then stained with coomassie (SimplyBlue, Invitrogen). The gel lane was fractionated into 8-12 slices, which were each further reduced into 1x1 mm² fragments then, dehydrated with acetonitrile (MeCN). Proteins in each slice were reduced with 10 mM dithiothreitol in 50 mM ammonium bicarbonate (AmBic) for 20 min at 56°C then, alkylated with 55 mM iodoacetamide in 50 mM AmBic for 1 hr at room temperature. After this treatment, gel pieces were washed by sequential dehydration/hydration steps alternating between MeCN and 50 mM AmBic. Polypeptide material was subjected to endoproteolytic digestion with trypsin (modified porcine trypsin from Promega) for 90 minutes at 37°C. Digested material was extracted from gel pieces with 0.1% trifluoroacetic acid, 5% MeCN, and concentrated down to 20 µl volume. The digest was separated on an Ultimate 3000 nanoLC (Dionex, Sunnyvale, CA). Five µl of the sample were pre-concentrated using a PepMap100 trap column loaded at 20µl/min of A solvent (5% MeCN, 0.1% formic acid) and separated using a PepMap C₁₈ 75-µm i.d. x 15cm

analytical column over a 40 min gradient (8-25% B in 30 min then 25-50% B in 10 min) at a flow rate of 300nl/min (B: 80% MeCN, 0.1% formic acid).

The nano-LC was coupled to a Q-Star XL (Applied Biosystems, Concord, ON) and Analyst software was used for data dependant acquisition. Basic survey scan (1.5 s) from 400-1200 Da, was followed by data-dependent MS/MS, of the three most intense ions with charge state +2 to +4 for 1.5-2 s. These ions were then excluded from acquisition for 30 s. To improve the characterisation of low abundant peptide/protein, a gas phase fractionation strategy was applied sometimes in combination with an exclusion list generated from the previously acquired data. The acquisition was performed over 2 ranges: 400-680 (survey scan 2s and 3 EPI scan 4/5/5s) and 660-1500 Da (survey scan 4s and 3 EPI scan 4/7/10s).

Acquired tandem mass spectra were exported from Analyst using the script Mascot.dll 1.6b23 (matrix Science, London, UK). Mass spectra were recalibrated using an in-house script then, searched against UniprotKB-SwissProt database (UniProtKB Ver. 9.0-14; databases updated automatically every week) using Mascot 2.0 software (Matrix Science) for protein identification with a mass tolerance of 30 ppm for the parent and 0.12 Da for the fragments ions. The protein identification list was filtered using the non-MUDPit scoring with a threshold of 25 (this value was determined by searching the same dataset against a randomized database).

Peptides were quantified with MSQuant (<http://msquant.sourceforge.net/>) and subsequently normalized. Spectra were validated by visual inspection. Identified protein could be distributed in three subsets: A) non specific adsorption identified in the un-transfected control sample related to the interaction between beads and antibodies; B) Un-specific partners equally quantified in the un-transfected and EglN_X (with X = 1, 2, 3) immunoprecipitation; C) specific protein interactions with the EglN_X proteins. Protein subsets A and B were used to determine the threshold to consider a protein as specifically interacting with EglN_X. This value was defined as 1.3.

2.2.11 Hydroxylation of actin

Sites of proline hydroxylation were determined by mass spectrometry using the MIDAS (MRM-Initiated Detection and Sequencing) methodology on a 4000 Q-Trap hybrid triple quadrupole/ion trap mass spectrometer, as described by [122] with the following modifications. Gel bands were excised and destained using 100mM triethylammonium bicarbonate (TEAB; Sigma)/40% (v/v) acetonitrile. Gel pieces were then dehydrated in acetonitrile, and rehydrated in 20 μ L 50ng/mL modified trypsin (Promega) in 100mM TEAB, 5% (v/v) acetonitrile prior to overnight incubation at 37°C. Supernatant was removed, remaining peptides extracted with 50% (v/v) acetonitrile/0.1% formic acid (Sigma), pooled with the initial supernatant and dried in a speedvac. Samples were resuspended in 30 μ L 2% acetonitrile/0.1% formic acid and 2 μ L used to confirm protein identity by liquid chromatography-mass spectrometry [122]. For MIDAS analysis, a list of MRM transitions was generated which incorporated proline hydroxylation on all potential sites, with one modification and one missed tryptic cleavage allowed per peptide. Methionine oxidation was included for target peptide EITALAPSTMK, selected due to a potential hydroxylation consensus. Transitions with Q1 >390 were selected. Q3 mass was set at the predicted mass of a product ion, where possible generated by fragmentation at a proline. Collision energy was set at $(m/z*0.044)+3$ for 2+ precursors and $(m/z*0.04)+2$ for 3+ precursors, and dwell time was fixed at 60ms. Samples were analysed using this list if MRM transitions to trigger MS/MS fragmentation as previously described by Unwin [122]. Data was processed using MASCOT with proline hydroxylation as a variable modification, 1x missed cleavage. Putative sites of proline hydroxylation were confirmed by manual inspection.

2.2.12 Immunostaining

Cells were seeded on sterile cover slips in 6 well plates and transfected with GFP-actin as described in section 2.2.4 or treated as described in section 2.2.5. Cells were washed twice with PBS before they were fixed in 4% formalin for 10 minutes at room temperature. Cells were washed three times with PBS and then permeabilised in 1% triton X-100 for 10 minutes at 4°C. After another two washes with PBS unspecific binding was blocked with 10% BSA for 30 minutes at

room temperature. Samples were stained using Cy3- or FITC- linked anti FLAG antibody (Sigma), Phalloidin-TRITC (Sigma) or DNaseI-Alexa488 (Invitrogen) for 2 hours or overnight at room temperature in a humid environment. Phalloidin is a fungal toxin isolated from *Amanita phalloides*. Phalloidin binds to and stabilises actin filaments. It only binds actin oligomers and polymers but not actin monomers [123]. DNaseI however is used to visualise actin monomers. DNaseI binds actin monomers with high affinity and actin polymers with low affinity [124]. After staining samples were washed three times with PBS. Any excess liquid was drained from the cover slips before they were mounted onto microscopy slides using vectrashield mounting medium (Vector laboratories Inc.) and sealed with nail varnish. Samples were analysed using a Leica SP2 Confocal microscope with LCS software.

2.2.13 Quantification of filamentous actin

This assay was performed as described previously by Machesky and Hall [125]. Briefly, cells were seeded onto 6cm dishes, transfected as described in section 2.2.4 or treated as described in section 2.2.5 and then grown to confluency. Cells were washed twice in PBS, then lysed and fixed in 250 μ l lysis buffer containing a saturating amounts of Phalloidin (20 mM KPO₄ pH 8, 10 mM Pipes pH 8, 5 mM EGTA pH 8, 2 mM MgCl₂, 0.1% TritonX-100, 3.7% formalin, 2 μ M Phalloidin-TRITC) and incubated for 1 hour at room temperature whilst slowly rotating. Protein concentration was measured as described in section 2.2.6. The sample was centrifuged at 12,000 x g for 2 minutes in a table top centrifuge. The pellet was washed with washing buffer (0.1% Saponin, 20 mM KPO₄ pH 8, 10 mM Pipes pH 8, 5 mM EGTA pH 8, 2 mM MgCl₂) and centrifuged again at 12,000 x g for 2 minutes. The Phalloidin bound to the actin filaments was extracted with methanol. 200 μ l methanol were added to the pellet and incubated for 1 hour at room temperature whilst slowly rotating. Samples were centrifuged at 12,000 x g for 2 minutes in a table top centrifuge. The fluorescence emission of the supernatants was measured in a 96well plate at 570 nm and an excitation at 540 nm.

2.2.14 Wound healing scratch assay

Transfected or untransfected cells were grown to confluency and treated accordingly (as described in section 2.2.5). A p200 pipette tip was used to scratch a wound into the cell monolayer. Cells were washed once with sterile PBS to remove any debris before they were placed into a low serum medium (DMEM supplemented with 1% FBS and 2 mM L-glutamine). The closure of the wound was tracked using the Nikon TE 2000 timelapse microscope. Images were taken for three different fields of each condition every ten minutes for 290 minutes (U2OS cells) or 590 minutes (A375 cells). Analysis of wound closure was carried out using the single cell tracking device of ImageJ. This was done to account for differences in wound width and resulted in calculation of distances and cellular velocity.

2.2.15 Inverse invasion assay

This method is a modified version of the method described by Hennigan [126]. An aliquot of matrigel was thawed slowly on ice and then diluted 1:1 with ice cold PBS. 100 μ l of the matrigel/PBS solution was pipetted in each transwell chamber which was inserted into a well of a 24well plate (Fisher, catalogue number TKT-525-110X). The matrigel was left to settle for 1 hour at 37°C in a humidified incubator. In the meantime a cell suspension of 4×10^5 cells per ml was prepared in complete medium (DMEM containing 10% FBS). The transwells were inverted onto the lid of the 24well plate and 100 μ l of the cell suspension was pipetted onto the underside of each transwell filter (4×10^4 cells plated). The transwells were carefully covered with the base of the 24well plate so that the plate contacts the droplet of the cell suspension. The inverted plate was incubated at 37°C in a humidified incubator for 4 hours to allow the cells to attach. Each transwell was removed and sequentially dipped into 2x 1 ml of serum free medium to wash off the serum and then in placed the right way up in 1 ml of serum free medium in a fresh 24well plate. 100 μ l of complete medium (DMEM containing 10% FBS) were pipetted on top of the matrigel plug. The plate was incubated at 37°C for 3 days.

After that the transwells were transferred to a fresh 24well plate and overlaid with 1 ml of a 1 μ M Calcein-AM solution diluted in serum free medium (acetoxymethylester of calcein, Molecular Probes). Calcein stains the whole cell fluorescent green. After 1 hour incubation at 37°C the assay was analysed by confocal microscopy using a Leica SP2 microscope. Transwells were placed onto large coverslips on a 20x objective and analysed by optical sectioning (Z-sections). Optical sections were taken every 15 μ m starting from the bottom of the matrigel plug producing a series of images. Individual optical sections are placed alongside one another with increasing depth as indicated. Invasion assays were quantified by measuring the fluorescence intensity of cells penetrating the matrigel to a depth of 45 μ m and greater. This intensity was expressed as a percentage of the total fluorescence intensity of all cells within the plug. Data were normalized for each experiment such that invasion of cells transfected with scrambled control shRNA under normoxia =1. The fluorescence intensity of each image was quantified using ImageJ. Overall results were determined from at least three different experiments with duplicate samples.

2.2.16 ***Statistical analysis***

Experiments were repeated at least three times, images shown are representative results from one experiments. In graphs results are presented as mean \pm S.E.M. Statistical significance of differences between the means was determined by Mann-Whitney test analysis using GraphPad Prism 5. Values of $p < 0.05$ were selected to be statistically significant.

Chapter 3 – Quantitative proteomic screen

3 Quantitative proteomic screen to identify new targets of PHDs

3.1 Introduction

HIF prolyl hydroxylases (PHDs) have been implicated to function in different pathways, however their substrates are mostly unknown. In order to identify new potential substrates of PHDs, a quantitative proteomic approach (SILAC) was used. Co-immunoprecipitations using FLAG-tagged PHDs were performed under normoxia and hypoxia and binding of proteins was compared to each other or to a mock transfected sample. Cells were grown in two cultures, one in normal medium, the second one in medium containing ^{13}C -labelled arginine and lysine. Labelling of arginine and lysine leads to labelling of all peptides after tryptic digest but the carboxyterminal peptide of the protein due to the specificity of trypsin to cleave at these amino acids. Furthermore, cells are grown in dialysed serum so there are no other means of incorporating amino acids. Potential binding partners are identified by mass spectrometry after co-immunoprecipitations. Peptide pairs are separated by a distinct mass difference. Quantification of peptides is achieved by comparing peak ratios to each other whereby quantification is only limited by peptide signal and signal-to-noise ratio.

3.2 Results

3.2.1 PHD substrates can be trapped on the enzyme under hypoxia

Before identifying new potential substrates of prolyl hydroxylases in a quantitative proteomic approach, the best binding conditions between the enzyme and its substrate had to be identified. α -ketoglutarate-dependent oxygenases are thought to function by a common mechanism as was shown for the asparaginyl hydroxylase Factor Inhibiting HIF (FIH), which is involved in the regulation of HIF activity. First the enzyme binds the prime protein substrate and α -ketoglutarate before it binds molecular oxygen [30]. Under conditions

with sufficient concentrations of all co-substrates, the complex dissociates after hydroxylation of a specific prolyl residue. In order to identify new substrates of PHDs the enzyme-substrate complex had to be stabilised. According to the above model oxygen deprivation or blocking enzyme activity with α -ketoglutarate like inhibitors may prolong the interaction. Co-immunoprecipitations using FLAG-tagged PHD2 were performed under normoxic and hypoxic conditions as well as in the presence of hypoxia mimetic agents like DMOG, a non-cleavable α -ketoglutarate derivative that blocks PHD enzyme activity [18]. The enzyme-substrate interaction between PHD2 and HIF1 α was investigated under different conditions using a renal clear cell carcinoma cell line (RCC4), which lacks the von Hippel-Lindau protein (pVHL). As pVHL is the recognition component of the E3 ubiquitin ligase complex that targets the HIF α subunit for proteasomal degradation, HIF α cannot be degraded in these cells and is stable even under normoxia (Figure 3.1a, lane 1).

As shown in Figure 3.1a (lane 4) the enzyme and its substrate only showed a weak interaction under normoxic conditions even in the absence of pVHL. The PHD inhibitor DMOG (lane 5) had little effect on the binding. However, under hypoxic conditions the PHD-HIF interaction increased (lane 6). This indicates that the PHD2-HIF1 α complex is not a stable entity under normoxia, and is only slightly stabilised by DMOG. However, 1% oxygen significantly stabilises the enzyme-substrate complex. The α -ketoglutarate derivative DMOG might sterically hinder the binding of the substrate to the enzyme, which could account for the difference between hypoxia and pharmacological inhibition of the enzyme.

Similar results were obtained for the interaction of PHD3 and HIF1 α (Figure 3.1b). Although PHD3 is not thought to be the major hydroxylase of HIF1 α , it has been shown to be able to hydroxylate, and therefore must bind, HIF1 α *in vitro* [32]. In addition to the conditions described above, we also used a cell-permeable α -ketoglutarate derivative (T α KG) that increases intracellular α -ketoglutarate levels and reactivates PHDs under hypoxia [36]. It would not be expected to stabilise the enzyme-substrate complex. This is indeed the case in Figure 3.1b, lane 3.

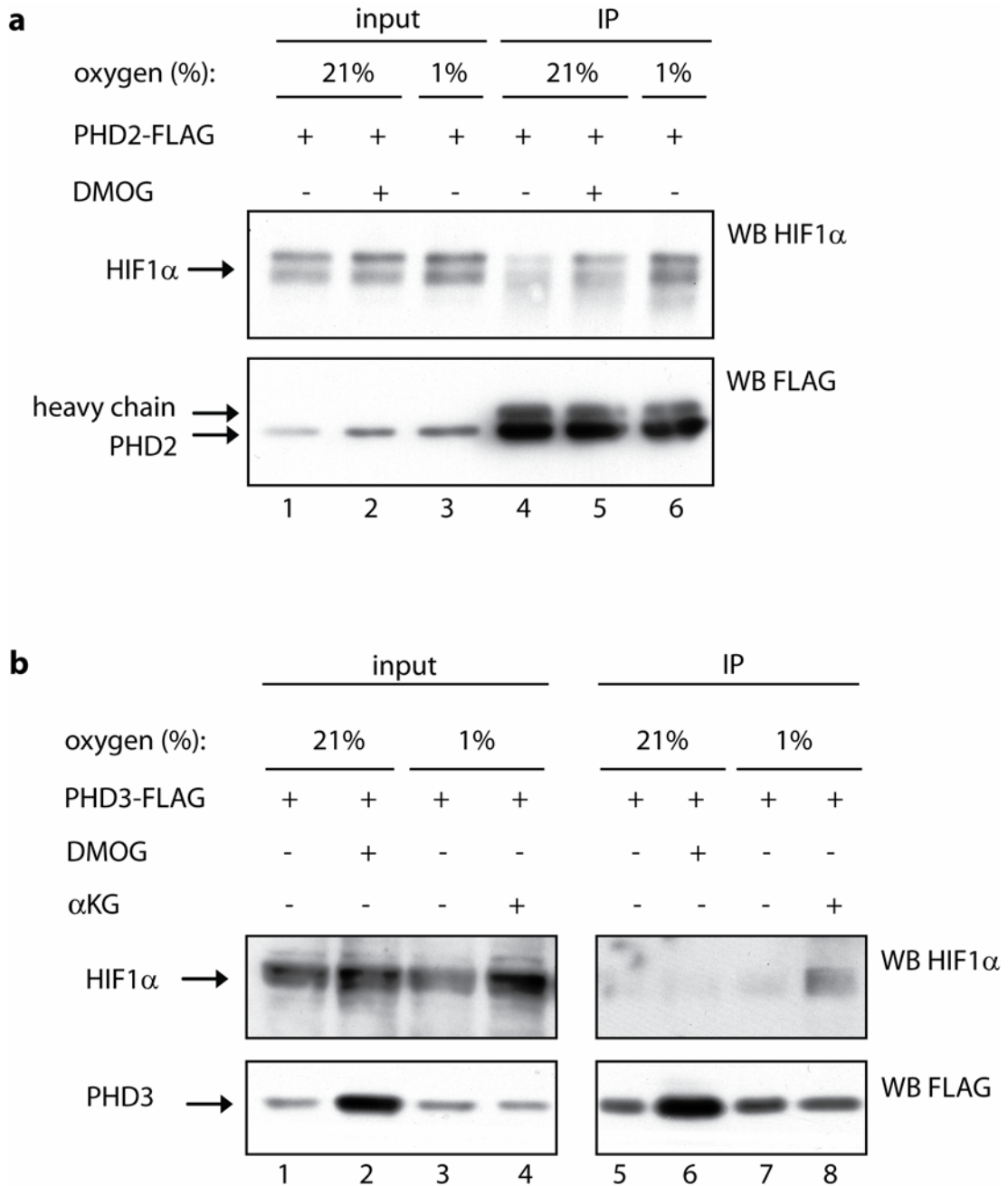


Figure 3.1: Binding conditions that stabilise the enzyme-substrate (PHD-HIF1 α) complex
 Binding conditions that stabilise the enzyme-substrate complex were tested in RCC4 cells. Co-immunoprecipitations of FLAG-tagged PHD2 (a) or PHD3 (b) with HIF1 α were performed under normoxia or hypoxia. Where indicated, cells were also treated with either a PHD inhibitor or an activator – DMOG or a cell-permeable α -ketoglutarate derivative (T α KG), respectively.

These results indicate that under normoxic conditions the enzyme and its substrates are only briefly in a complex. Under conditions where oxygen is limiting the prime protein substrate is trapped on the enzyme as oxygen is the last co-substrate to bind the enzyme. These results allowed us to define the optimal conditions under which to isolate PHD-binding proteins.

3.2.2 Incorporation of heavy amino acids in HCT116 cells

HCT116 cells were grown in heavy or light medium for two weeks, before incorporation of heavy amino acids was tested. HCT116 cells were used as they are routinely used in the lab and are well characterised regarding their hypoxic response. Total cell lysates were separated on a SDS-PAGE, bands were cut out as shown in Figure 3.2 and analysed by mass spectrometry.

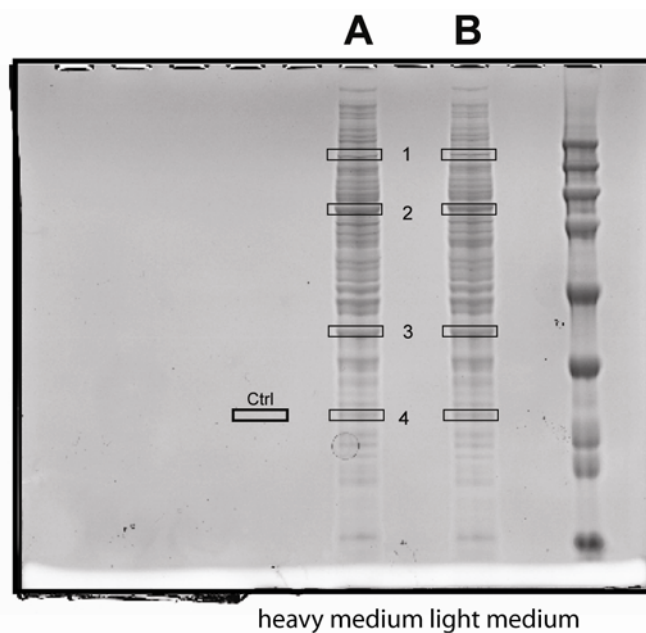


Figure 3.2: Check incorporation of amino acids
Total cell lysates of cells grown in heavy or light cultures were separated on SDS-PAGE, bands as indicated were cut out and analysed by mass spectrometry.

Incorporation time was tested previously in a time course experiments in which cells were lysed every day until incorporation reached 100%. For HCT116 cell

complete incorporation of labelled amino acids takes about two weeks. Complete incorporation was checked before each SILAC experiment.

3.2.3 SILAC screen

To be able to directly compare samples to each other, a quantitative proteomic approach was used [115]. FLAG-tagged PHDs were overexpressed in the human colon carcinoma cell line HCT116. Co-immunoprecipitations using anti-FLAG antibody were performed under normoxia and/or hypoxia. After eluting proteins from the column, equal amounts of eluates of labelled and unlabelled sample were mixed and concentrated using centricon tubes. These samples were resolved on SDS PAGE and after tryptic in-gel digest, peptides were identified by mass spectrometry. The tryptic peptides of each sample showed a specific mass difference, allowing samples to be directly compared to each other. The workflow is depicted in Figure 3.3. The mass spectrometric analyses of this quantitative screen were performed by Willy Bienvenut (Beatson Institute for Cancer Research).

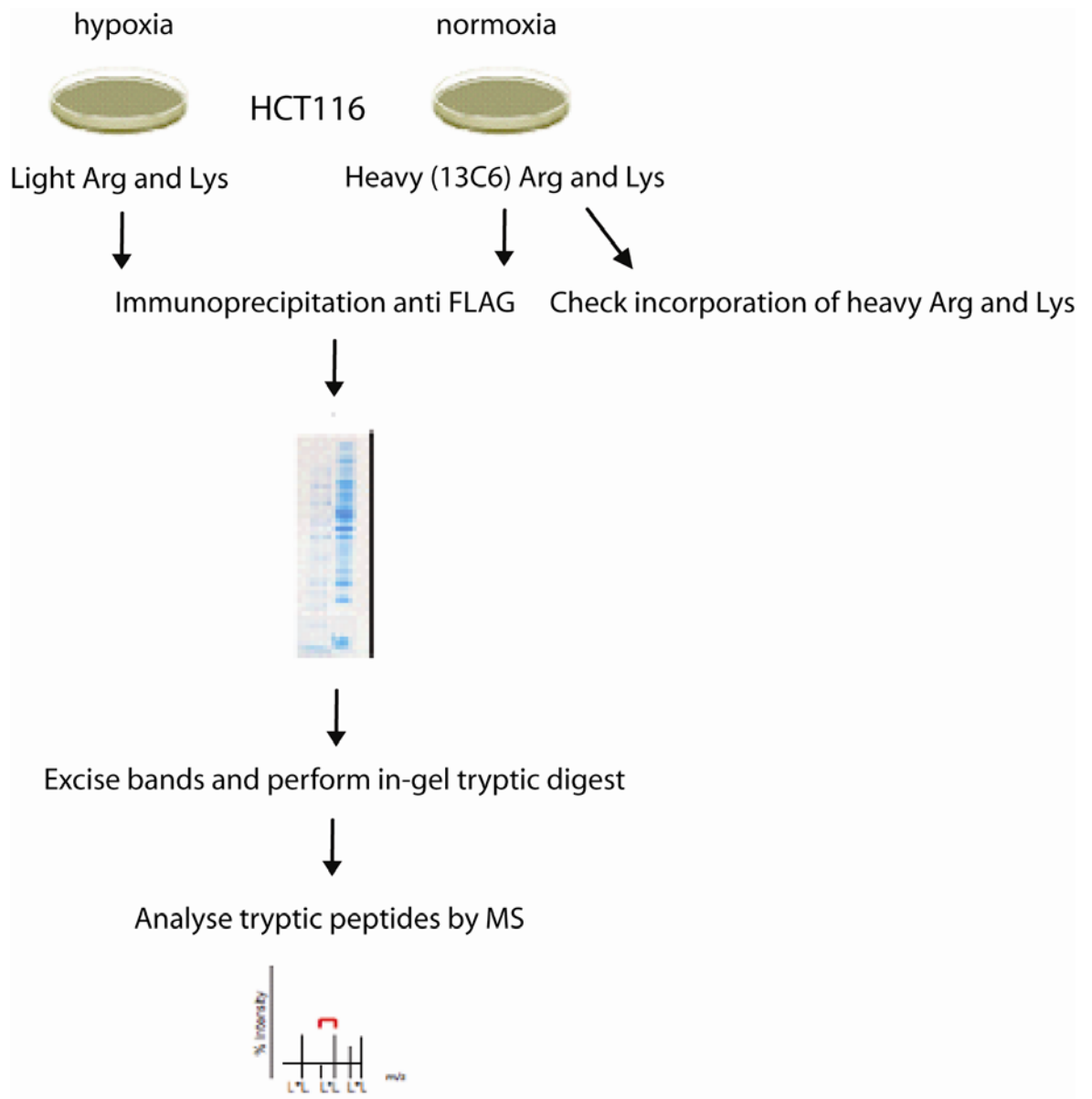


Figure 3.3: Scheme of the quantitative proteomic screen (SILAC).

HCT116 cells were grown in two different cultures (heavy and light amino acids containing medium). FLAG-tagged PHDs were overexpressed and co-immunoprecipitations using anti-FLAG antibody were performed under normoxia (heavy) or hypoxia (light) before samples were mixed in a 1:1 ratio and resolved on SDS PAGE. After tryptic in-gel digest, peptides were identified by mass spectrometry and quantified (the ratio between light and heavy of each identified peptide).

3.2.4 Assessment of the hypoxic response in HCT116 cells

HCT116 cells were incubated under normoxic or hypoxic conditions for either 6 or 18 hours. Hypoxic cells were either lysed under hypoxia or re-oxygenated for 10 minutes before lysis. The expression of each of the PHD isoforms as well as HIF1 α was analysed by immunoblot analysis (Figure 3.4).

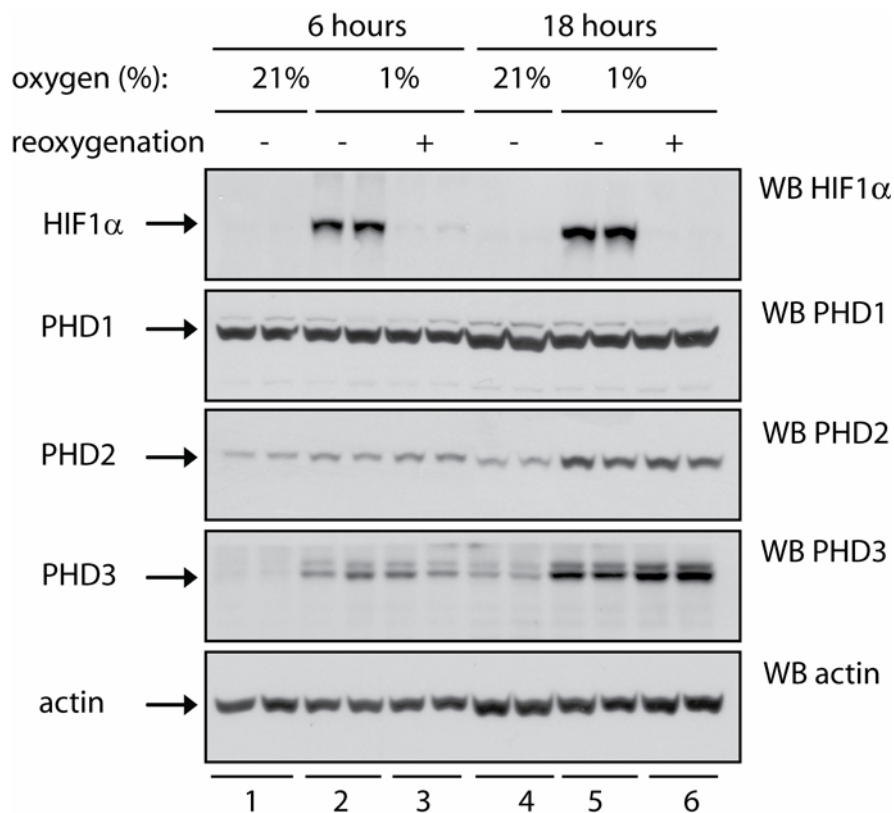


Figure 3.4: Assessment of the hypoxic response in HCT116 cells

Immunoblot analysis showing the expression of each of PHD isoforms and HIF1 α under normoxia, hypoxia and after 10 minutes of re-oxygenation at two different time points (6 hours or 18 hours).

As shown in Figure 3.4 expression of endogenous PHD1 was independent of ambient oxygen conditions whereas levels of endogenous PHD2 and PHD3 were upregulated under hypoxia. However, expression of PHD3 was upregulated at an earlier timepoint than expression of PHD2. HIF1 α was stabilised under hypoxia but degraded within 10 minutes of re-oxygenation.

3.2.4.1 Results for PHD3

Firstly, the conditions for the larger scale co-immunoprecipitation used for the SILAC screen were optimised. Co-immunoprecipitations were performed with overexpressed FLAG-tagged PHD3 using anti FLAG antibodies. Cultures overexpressing FLAG-tagged PHD3 were grown under normoxia or hypoxia. Experiments were controlled for by adding fresh media after transfection and using a constant protein amount for the immunoprecipitation.

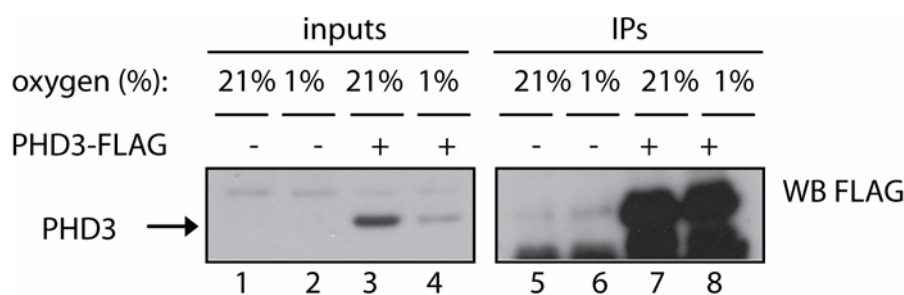


Figure 3.5: Testing the conditions for the large-scale co-immunoprecipitation using FLAG-tagged PHD3
 FLAG-tagged PHD3 was overexpressed in HCT116 cells in normoxic or hypoxic conditions and immunoprecipitated using anti FLAG antibodies covalently linked to sepharose beads.

FLAG-tagged PHD3 was immunoprecipitated efficiently using the conditions described in section 2.2.9.2 (Figure 3.5). However, it has to be kept in mind that overexpression of FLAG-tagged PHD3 was able to induce cell death as reported previously [71].

Next, cultures overexpressing FLAG-tagged PHD3 grown in normoxia as well as samples overexpressing an empty vector control grown in hypoxia were grown in heavy medium whereas samples overexpressing FLAG-tagged PHD3 grown in hypoxia and samples overexpressing an empty vector control grown in normoxia were grown in light (normal) medium. Different samples could then be compared to each other. The most important samples are the ones comparing PHD3-transfected samples under hypoxia and normoxia to each other using the substrate trap.

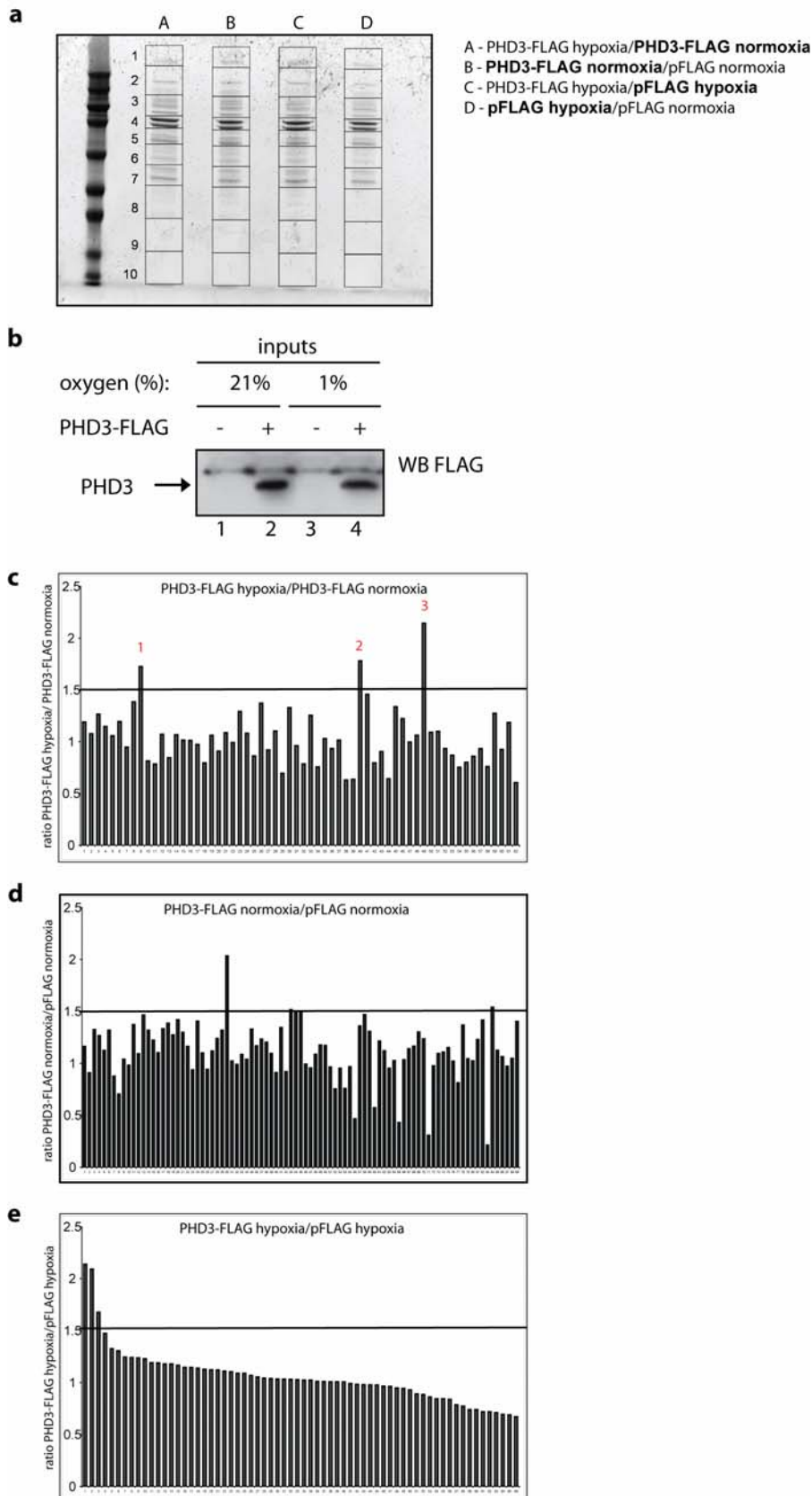


Figure 3.6: SILAC analysis of immunoprecipitations of PHD3-FLAG

(a) PHD3-FLAG or empty vector control (pFLAG) were overexpressed in HCT116 cells grown in heavy or light medium and immunoprecipitated using anti FLAG antibodies. Eluates after immunoprecipitation were mixed in a 1:1 ratio as indicated. Concentrated samples were resolved on SDS-PAGE, stained with coomassie, lanes were cut into strips as indicated and analysed by mass spectrometry. (b) Immunoblot analysis to confirm expression of PHD3-FLAG (c-e) ratios of mass spectrometric analysis of samples indicated. Ratios >1.5 were considered significant changes.

Table 3.1: SILAC analysis of samples overexpressing PHD3-FLAG

	Description	Accession number	number of peptides	ratio PHD3 hypoxia/ PHD3 normoxia >1.5
1	Methylosome subunit pICln	P54105	24	1.72
2	Actin, cytoplasmic 2	P63261	27	1.78
3	Creatine kinase B-type	P12277	3	2.14

	Description	Accession number	number of peptides	ratio PHD3 normoxia/ untransfected normoxia >1.5
1	Profilin-1	P07737	1	2.03
2	Actin, cytoplasmic 2	P63261	7	1.52
3	Mps one binder kinase activator-like 2	Q70IA6	1	1.54

	Description	Accession number	number of peptides	ratio PHD3 hypoxia/ untransfected hypoxia >1.5
1	Junction plakoglobin	P14923	7	2.14
2	Peroxiredoxin-1	Q06830	2	2.09
3	Filaggrin-2	Q5D862	2	1.68

While binding of most of the identified proteins did not change between normoxia and hypoxia, there were a few that showed a difference with increased binding under hypoxia (Figure 3.6b). The protein creatine kinase showed one of the highest ratios, but was only identified with 3 peptides in this screen. The second highest ratio was a 2-fold increase in binding under hypoxia for actin (identified with 27 peptides).

Furthermore samples transfected with PHD3-FLAG were compared to samples transfected with an empty vector control either under normoxia or under hypoxia. The proteins shown in Table 3.1 were identified to bind to PHD3 under these conditions, however these proteins were only identified with low peptide counts in one run of the experiment.

3.2.4.2 Results for PHD1

Subsequently, co-immunoprecipitations were performed overexpressing FLAG-tagged PHD1. Cultures were set up as described in section 3.2.4.1.

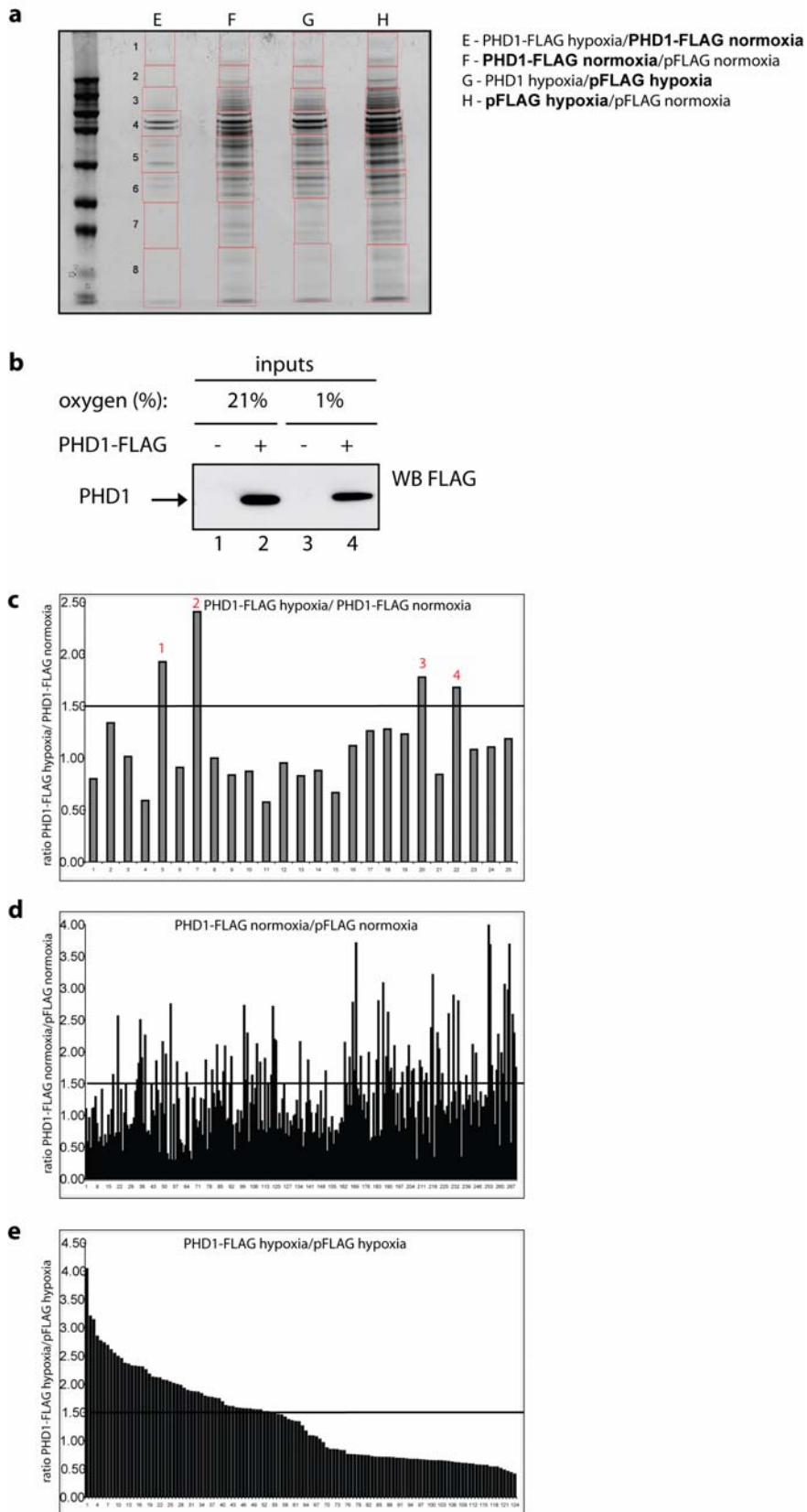


Figure 3.7: SILAC analysis of immunoprecipitations of PHD1-FLAG

(a) PHD1-FLAG or empty vector control (pFLAG) were overexpressed in HCT116 cells grown in heavy or light medium and immunoprecipitated using anti FLAG antibodies. Eluates after immunoprecipitation were mixed in a 1:1 ratio as indicated. Concentrated samples were resolved on SDS-PAGE, stained with coomassie, lanes were cut into strips as indicated and analysed by mass spectrometry. (b) Immunoblot analysis to confirm expression of PHD1-FLAG (c-e) ratios of mass spectrometric analysis of samples indicated. Ratios >1.5 were considered significant changes..

Table 3.2: SILAC analysis of samples overexpressing PHD1-FLAG

	Description	Accession number	number of peptides	ratio PHD1 hypoxia/ PHD1 normoxia >1.5
1	Actin, cytoplasmic 1	P60709	25	1.93
2	Glyceraldehyde-3-phosphate dehydrogenase	P04406	2	2.41
3	Heat shock protein HSP 90-alpha	P07900	19	1.78
4	Heat shock protein HSP 90-beta	P08238	23	1.68

	Description	Accession number	number of peptides	ratio PHD1 normoxia/ untransfected normoxia >1.5
1	Egl nine homolog 2	Q96KS0	14	33.83
2	LIM and SH3 domain protein 1	Q14847	1	2.56
3	Small nuclear ribonucleoprotein Sm D2	P62316	4	1.55
4	Methylosome protein 50	Q9BQA1	20	1.81
5	Methionine adenosyltransferase 2 subunit beta	Q9NZL9	2	2.50
6	60S ribosomal protein L7a	P62424	4	1.90
7	Mps one binder kinase activator-like 2	Q70IA6	1	2.26
8	Heterogeneous nuclear ribonucleoproteins A2/B1	P22626	4	1.50
9	Protein phosphatase 1A	P35813	24	1.85
10	Dolichyl-diphosphooligosaccharide--protein glycosyltransferase 48 kDa subunit	P39656	2	2.15
11	Serine/threonine-protein kinase 38	Q15208	9	1.96
12	Talin-1	Q9Y490	3	2.75
13	Protein arginine N-methyltransferase 5	O14744	55	1.84
14	Small nuclear ribonucleoprotein Sm D1	P62314	3	1.67
15	Spectrin beta chain, brain 1	Q01082	3	1.87
16	Protein phosphatase 1B	O75688	69	1.71
17	Eukaryotic translation initiation factor 3 subunit C	Q99613	4	2.11
18	Ubiquitin carboxyl-terminal hydrolase 15	Q9Y4E8	4	1.68
19	DNA replication licensing factor MCM2	P49736	1	2.09
20	Hypoxia up-regulated protein 1	Q9Y4L1	3	1.92
21	Serine hydroxymethyltransferase, mitochondrial	P34897	2	2.72
22	26S proteasome non-ATPase regulatory subunit 2	Q13200	4	1.55
23	Ras GTPase-activating-like protein IQGAP1	P46940	4	2.29
24	T-complex protein 1 subunit epsilon	P48643	7	1.63
25	T-complex protein 1 subunit alpha	P17987	7	2.12
26	C-1-tetrahydrofolate synthase, cytoplasmic	P11586	3	1.83
27	DNA replication licensing factor MCM3	P25205	3	1.89
28	Filamin-B	O75369	3	1.51
29	T-complex protein 1 subunit eta	Q99832	6	1.63
30	Importin subunit beta-1	Q14974	4	2.71
31	Heat shock protein 105 kDa	Q92598	4	2.19
32	Neutral alpha-glucosidase AB	Q14697	7	2.17
33	6-phosphogluconate dehydrogenase, decarboxylating	P52209	2	1.50
34	T-complex protein 1 subunit zeta	P40227	6	2.15
35	Vinculin	P18206	8	1.87
36	Glutathione reductase, mitochondrial	P00390	4	1.70

37	Ankyrin repeat and FYVE domain-containing protein 1	Q9P2R3	3	2.14
38	Lamin-A/C	P02545	3	1.50
39	Polypyrimidine tract-binding protein 1	P26599	3	1.91
40	60S ribosomal protein L22	P35268	2	2.77
41	Isocitrate dehydrogenase (NAD) subunit alpha, mitochondrial	P50213	1	1.70
42	Adenylate kinase isoenzyme 2, mitochondrial	P54819	2	3.71
43	DNA replication licensing factor MCM6	Q14566	1	1.92
44	Uncharacterized protein C11orf84	Q9BUA3	2	1.98
45	6-phosphofructo-2-kinase/fructose-2,6-biphosphatase 3	Q16875	4	1.87
46	Far upstream element-binding protein 2	Q92945	2	2.80
47	Serine/threonine-protein kinase RIO1	Q9BRS2	2	3.08
48	Poly (ADP-ribose) polymerase 1	P09874	4	1.92
49	Peroxiredoxin-5, mitochondrial	P30044	3	2.62
50	40S ribosomal protein S16	P62249	7	1.69
51	Nuclease-sensitive element-binding protein 1	P67809	2	1.73
52	Splicing factor, proline- and glutamine-rich	P23246	3	2.09
53	Polyadenylate-binding protein 1	P11940	8	1.67
54	Phosphatidylethanolamine-binding protein 1	P30086	1	1.76
55	BTB/POZ domain-containing protein KCTD5	Q9NXV2	4	2.10
56	Prohibitin	P35232	2	1.69
57	OTU domain-containing protein 4	Q01804	4	1.73
58	Splicing factor 3B subunit 1	O75533	1	1.86
59	ATP-dependent DNA helicase 2 subunit 1	P12956	2	1.75
60	Staphylococcal nuclease domain-containing protein 1	Q7KZF4	3	1.54
61	FACT complex subunit SPT16	Q9Y5B9	10	1.66
62	40S ribosomal protein S19	P39019	3	2.37
63	Spectrin alpha chain, brain	Q13813	2	3.21
64	Mitogen-activated protein kinase kinase kinase 7-interacting protein 1	Q15750	2	2.30
65	40S ribosomal protein S12	P25398	5	2.04
66	Heterogeneous nuclear ribonucleoprotein A1	P09651	2	1.65
67	Heterogeneous nuclear ribonucleoprotein A/B	Q99729	1	2.59
68	60S ribosomal protein L9	P32969	2	2.89
69	Tyrosine-protein kinase JAK1	P23458	3	2.80
70	40S ribosomal protein S11	P62280	2	1.53
71	Gelsolin	P06396	2	1.62
72	26S protease regulatory subunit 7	P35998	3	2.11
73	60S ribosomal protein L3	P39023	1	1.97
74	40S ribosomal protein S23	P62266	1	3.99
75	40S ribosomal protein S24	P62847	1	3.68
76	60S ribosomal protein L30	P62888	3	1.78
77	FACT complex subunit SSRP1	Q08945	2	1.71
78	Interleukin enhancer-binding factor 2	Q12905	2	2.27
79	Reticulocalbin-1	Q15293	2	1.98
80	Keratin, type II cytoskeletal 71	Q3SY84	2	1.65
81	Putative small nuclear ribonucleoprotein polypeptide E-like protein 1	Q5VYJ4	2	3.06
82	AN1-type zinc finger protein 1	Q8TCF1	2	2.97
83	U4/U6 small nuclear ribonucleoprotein Prp31	Q8WWY3	1	3.69
84	Synaptic vesicle membrane protein VAT-1 homolog	Q99536	1	2.58
85	UPF0160 protein MYG1	Q9HB07	1	2.29

86	RuvB-like 2	Q9Y230	2	1.75
----	-------------	--------	---	------

	Description	Accession number	number of peptides	ratio PHD1 hypoxia/ untransfected hypoxia >1.5
1	Egl nine homolog 2	Q96KS0	31	9.69
2	Histone H1.4	P10412	4	4.04
3	40S ribosomal protein S2	P15880	2	3.20
4	Tropomyosin alpha-4 chain	P67936	7	3.13
5	Phosphate carrier protein, mitochondrial	Q00325	1	2.84
6	Small nuclear ribonucleoprotein Sm D3	P62318	2	2.76
7	GTP-binding nuclear protein Ran	P62826	7	2.73
8	Nascent polypeptide-associated complex subunit alpha	Q13765	3	2.68
9	60S ribosomal protein L8	P62917	1	2.60
10	Rho GDP-dissociation inhibitor 1	P52565	2	2.54
11	40S ribosomal protein S3	P23396	11	2.49
12	Spindlin-1	Q9Y657	3	2.45
13	Glutathione transferase omega-1	P78417	2	2.36
14	40S ribosomal protein S4, X isoform	P62701	4	2.35
15	Chloride intracellular channel protein 1	O00299	6	2.32
16	Guanine nucleotide-binding protein subunit beta-2-like 1	P63244	3	2.31
17	Methylosome subunit pICln	P54105	21	2.30
18	Triosephosphate isomerase	P60174	12	2.30
19	Malate dehydrogenase, mitochondrial	P40926	11	2.25
20	Glutathione S-transferase P	P09211	4	2.17
21	Annexin A5	P08758	8	2.12
22	L-lactate dehydrogenase B chain	P07195	17	2.11
23	Elongation factor 1-delta	P29692	9	2.10
24	60S ribosomal protein L7	P18124	4	2.07
25	14-3-3 protein zeta/delta	P63104	19	2.06
26	14-3-3 protein theta	P27348	3	2.03
27	LIM and SH3 domain protein 1	Q14847	3	2.01
28	60S ribosomal protein L23a	P62750	1	1.99
29	40S ribosomal protein S18	P62269	7	1.97
30	Malate dehydrogenase, cytoplasmic	P40925	2	1.92
31	40S ribosomal protein S25	P62851	5	1.88
32	NAD(P)H dehydrogenase (quinone) 1	P15559	4	1.86
33	Heterogeneous nuclear ribonucleoprotein D0	Q14103	2	1.86
34	14-3-3 protein epsilon	P62258	13	1.85
35	60S ribosomal protein L27a	P46776	3	1.83
36	60S ribosomal protein L27	P61353	4	1.78
37	60S ribosomal protein L11	P62913	2	1.77
38	60S ribosomal protein L31	P62899	1	1.76
39	S-adenosylmethionine synthetase isoform type-2	P31153	1	1.75
40	Small nuclear ribonucleoprotein Sm D2	P62316	5	1.74
41	Methylosome protein 50	Q9BQA1	25	1.68
42	Methionine adenosyltransferase 2 subunit beta	Q9NZL9	1	1.62
43	60S ribosomal protein L7a	P62424	3	1.60
44	L-lactate dehydrogenase A chain	P00338	12	1.60
45	Mps one binder kinase activator-like 2	Q70IA6	5	1.57
46	Coproporphyrinogen III oxidase, mitochondrial	P36551	3	1.57

47	Peroxiredoxin-6	P30041	18	1.56
48	Heat shock protein beta-1	P04792	2	1.56
49	Annexin A3	P12429	7	1.56
50	Heterogeneous nuclear ribonucleoproteins A2/B1	P22626	4	1.54
51	60S acidic ribosomal protein P0	P05388	3	1.54
52	Nucleoside diphosphate kinase A	P15531	11	1.54
53	Creatine kinase B-type	P12277	3	1.51
54	Protein phosphatase 1A	P35813	29	1.51

In Figure 3.7 the results obtained for cells overexpressing PHD1-FLAG are shown. Only a few proteins were identified to show increased binding under hypoxia compared to normoxia (Table 3.2). Glyceraldehyde-3-phosphate dehydrogenase showed the highest ratio, but was only identified with two peptides in this screen. The second highest ratio was a 2-fold increase in binding under hypoxia for actin (identified with 25 peptides). Another protein identified to bind stronger under hypoxia was heat shock protein HSP-90.

Apart from this samples transfected with PHD1-FLAG were compared to samples transfected with an empty vector control either under normoxia or under hypoxia. Identified proteins are shown in Table 3.2. Most of these proteins were only identified with low peptide counts. Only a few proteins were identified with higher peptide counts and therefore higher confidence of a real interaction. Proteins binding stronger under normoxia compared to the control were protein phosphatase 1A/1B and protein arginine N-methyltransferase. The most prominent proteins binding stronger under hypoxia compared to the control were a few metabolic enzymes such as triosephosphate isomerase, malate dehydrogenase and lactate dehydrogenase among a other proteins such as peroxiredoxin, nucleoside diphosphate kinase and protein phosphatase 1A.

3.2.4.3 Results for PHD2

Lastly, co-immunoprecipitations were performed overexpressing FLAG-tagged PHD2. Cultures were set up as described in section 3.2.4.1.

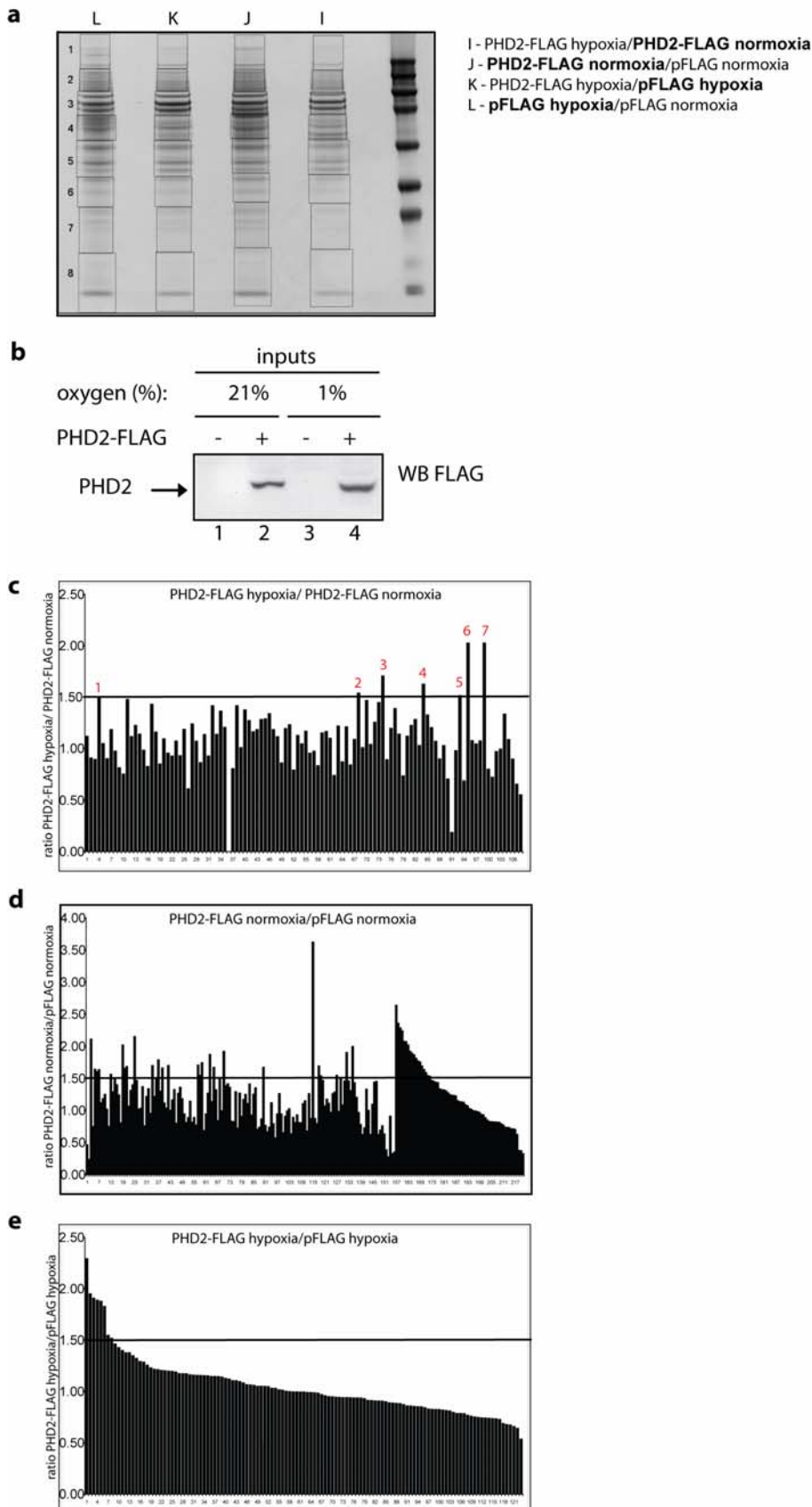


Figure 3.8: SILAC analysis of immunoprecipitations of PHD2-FLAG

(a) PHD2-FLAG or empty vector control (pFLAG) were overexpressed in HCT116 cells grown in heavy or light medium and immunoprecipitated using anti FLAG antibodies. Eluates after immunoprecipitation were mixed in a 1:1 ratio as indicated. Concentrated samples were resolved on SDS-PAGE, stained with coomassie, lanes were cut into strips as indicated and analysed by mass spectrometry. (b) Immunoblot analysis to confirm expression of PHD2-FLAG (c-e) ratios of mass spectrometric analysis of samples indicated. Ratios >1.5 were considered significant changes.

Table 3.3: SILAC analysis of samples overexpressing PHD2-FLAG

	Description	Accession number	number of peptides	ratio PHD2 hypoxia/ PHD2 normoxia >1.5
1	Small nuclear ribonucleoprotein Sm D3	P62318	3	1.50
2	Macrophage migration inhibitory factor	P14174	2	1.53
3	Fructose-bisphosphate aldolase A	P04075	4	1.25
4	Actin, cytoplasmic 2	P63261	38	1.70
5	L-lactate dehydrogenase B chain	P07195	6	1.38
6	Actin, cytoplasmic 1	P60709	1	1.62
7	L-lactate dehydrogenase A chain	P00338	6	1.32
8	Eukaryotic translation initiation factor 3 subunit F	O00303	2	1.51
9	Heat shock protein 75 kDa, mitochondrial	Q12931	2	2.02
10	Alpha-2-macroglobulin	P01023	2	2.02

	Description	Accession number	number of peptides	ratio PHD2 normoxia/ untransfected normoxia >1.5
1	Egl nine homolog 1	Q9GZT9	34	54.36
2	OTU domain-containing protein 4	Q01804	7	1.64
3	Splicing factor 3B subunit 3	Q15393	6	1.60
4	Mitogen-activated protein kinase kinase kinase 7-interacting protein 1	Q15750	4	1.63
5	60S ribosomal protein L24	P83731	5	1.56
6	Protein phosphatase 1A	P35813	4	1.50
7	Protein arginine N-methyltransferase 5	O14744	58	2.01
8	Ubiquitin carboxyl-terminal hydrolase 15	Q9Y4E8	5	1.65
9	Ankyrin repeat and FYVE domain-containing protein 1	Q9P2R3	3	1.68
10	Methylosome protein 50	Q9BQA1	28	2.15
11	Kinesin-like protein KIF11	P52732	2	1.69
12	Filamin-A	P21333	20	1.78
13	Protein phosphatase 1B	O75688	78	1.66
14	T-complex protein 1 subunit eta	Q99832	4	1.69
15	Polyadenylate-binding protein 1	P11940	3	1.70
16	T-complex protein 1 subunit alpha	P17987	8	1.54
17	Vinculin	P18206	7	1.74
18	RNA-binding protein 10	P98175	7	1.87
19	Methylosome subunit pICln	P54105	9	1.67
20	T-complex protein 1 subunit theta	P50990	15	1.51
21	Leucine-rich PPR motif-containing protein, mitochondrial	P42704	8	1.91
22	Stress-70 protein, mitochondrial	P38646	10	1.67
23	Non-POU domain-containing octamer-binding protein	Q15233	2	5.69
24	60S ribosomal protein L22	P35268	2	3.62
25	26S proteasome non-ATPase regulatory subunit 1	Q99460	3	1.69
26	14-3-3 protein zeta/delta	P63104	2	1.53
27	Adenosylhomocysteinase	P23526	9	1.46
28	Keratin, type I cytoskeletal 18	P05783	15	1.54

29	Tyrosine-protein kinase JAK1	P23458	10	1.90
30	DNA-dependent protein kinase catalytic subunit	P78527	5	1.99
31	Exportin-2	P55060	2	2.63
32	Kinesin-1 heavy chain	P33176	2	2.35
33	Lamin-A/C	P02545	2	2.28
34	Coatomer subunit beta'	P35606	2	2.24
35	60S ribosomal protein L18	Q07020	2	2.07
36	Ribose-phosphate pyrophosphokinase 2	P11908	2	2.07
37	Vigilin	Q00341	2	2.01
38	Integrin beta-1	P05556	3	1.92
39	3-hydroxyacyl-CoA dehydrogenase type-2	Q99714	2	1.89
40	40S ribosomal protein S3a	P61247	3	1.86
41	FACT complex subunit SPT16	Q9Y5B9	4	1.81
42	6-phosphofructokinase type C	Q01813	1	1.77
43	Splicing factor 3B subunit 1	O75533	1	1.75
44	ATP-dependent RNA helicase A	Q08211	4	1.69
45	Eukaryotic translation initiation factor 2 subunit 1	P05198	4	1.63
46	Eukaryotic translation initiation factor 3 subunit I	Q13347	4	1.58
47	Methionine adenosyltransferase 2 subunit beta	Q9NZL9	2	1.54
48	Coatomer subunit alpha	P53621	5	1.53

	Description	Accession number	number of peptides	ratio PHD2 hypoxia/ untransfected hypoxia >1.5
1	Egl nine homolog 1	Q9GZT9	33	7.42
2	Ig kappa chain V-II region Cum	P01614	1	5.22
3	Keratin, type I cytoskeletal 10	P13645	4	4.42
4	Creatine kinase B-type	P12277	3	2.29
5	S-adenosylmethionine synthetase isoform type-2	P31153	2	1.95
6	Fascin	Q16658	3	1.90
7	OTU domain-containing protein 4	Q01804	2	1.88
8	Splicing factor 3B subunit 3	Q15393	3	1.87
9	Mitogen-activated protein kinase kinase kinase 7-interacting protein 1	Q15750	3	1.82
10	Small nuclear ribonucleoprotein Sm D3	P62318	2	1.54
11	Keratin, type I cytoskeletal 9	P35527	3	1.51

In Figure 3.8 the results obtained for cells overexpressing PHD2-FLAG are shown. As seen before some proteins were identified to show increased binding under hypoxia compared to normoxia (Table 3.3), however most of them were only identified with low peptide counts. Actin was found to have the highest ratio as well as the highest peptide count under these conditions.

When samples transfected with PHD2-FLAG were compared to samples transfected with an empty vector control either under normoxia or under hypoxia, most identified proteins were only identified with low peptide counts, especially under hypoxic conditions. The most prominent proteins binding stronger under normoxia compared to the control were tyrosine-protein kinase JAK1, protein phosphatase 1B, filamin-A and protein arginine N-methyltransferase.

Overall, using the substrate trap actin appears to be the most promising candidate as it was identified to bind stronger under hypoxia than under normoxia in two experimental runs for PHD3 as well for PHD1 and PHD2 with high ratios and high peptide counts. Therefore, it was validated further as a potential substrate.

3.3 Conclusions

In initial binding experiments, we found that the substrate can be trapped on the enzyme under hypoxia. This suggests that PHDs function by a similar binding mechanism to the one described for other α -ketoglutarate-dependent oxygenases such as FIH [30]. Molecular oxygen is the last substrate to bind the enzyme-substrate complex after the protein substrate and the co-substrate α -ketoglutarate bind.

In order to get reliable results from a proteomic screen, it is important to find the right set up for the experiment. The idea that substrates can be trapped on the enzyme appeared to be the best option. Comparing binding to PHDs between hypoxic and normoxic conditions gave us a reasonable number of potential substrates to work with for each of the PHDs. Furthermore, samples overexpressing PHDs were compared to control transfected samples. In general more proteins were identified with these samples. However these proteins might not be substrates but rather proteins that show no differences in binding between normoxia and hypoxia such as regulators, inhibitors or scaffold proteins. All identified proteins should be validated as true interaction partners

of PHDs either by a second SILAC screen or by other assays (see following chapter). Even though SILAC is more specific than other non-quantitative proteomic approaches false positives still have to be ruled out. As with all proteomic approaches it should be kept in mind that identification of low abundant proteins in the presence of high abundant proteins is difficult as the signal of these low abundant proteins can be masked. This can lead to failure to identify some proteins as they are only identified above a certain threshold. Previously cut-offs to distinguish between background proteins and specific interactions have been chosen to be between 1.3-2fold difference in binding [116]. Here we chose a cut-off at 1.5.

Overall, PHD3 seemed to be less expressed than other PHDs, which might account for the fact that there are less proteins identified to bind to PHD3 than to the other PHDs. β -actin (or in some cases γ -actin) showed about a 2fold increase in binding to all three PHDs under hypoxia. It is one of the most consistent interactions using the substrate trap, but no interaction was found in any of the other conditions tested. It is difficult to distinguish between β - and γ -actin in this screen as these proteins are 98% identical. Other potential substrates we are particularly interested in are triosephosphate isomerase, malate dehydrogenase and lactate dehydrogenase, that were found to bind to PHD2 using the substrate trap and to PHD1 under hypoxia compared to the mock transfected control. As PHD1 was reported to be involved in metabolic signalling identifying PHD substrates involved in metabolism could shed some light on the underlying mechanism [79, 80].

Overall, potential new binding partners of PHDs were identified in this chapter using a quantitative proteomic approach. In the next chapter some of these potential interactions are validated.

Chapter 4 – Validation of potential substrates

4 Validation of potential PHD substrates

4.1 Introduction

In the previous chapter potential new PHD targets were identified in a proteomic screen however, these interactions have to be validated to rule out false positives. The most likely candidates as PHD substrates were identified as L-lactate dehydrogenase, triosephosphate isomerase, fructose-bisphosphate aldolase and actin. The latter one had one of the highest scores in the SILAC screen whereas the first three were also identified in a second screen performed by Hendrik Daub. L-lactate dehydrogenase, triosephosphate isomerase and fructose-bisphosphate aldolase are metabolic enzymes involved in the molecular breakdown of glucose. PHD1 has been linked to be involved in metabolic regulation in skeletal muscles and hepatocytes, however substrates of PHD1 and pathways inducing these changes are unclear [79, 80]. Actin is part of the cytoskeleton that regulates processes such as locomotion, adhesion and cell shape. Polymerisation of monomeric (G-) actin into filaments (F-actin), turnover of these filaments as well as size of the intracellular G-actin pool is tightly regulated by different classes of actin-binding proteins [127]. Several lines of evidence link hypoxia to increased migration and tumour invasion [88, 91]. However not much is known about the influence of hypoxia on the actin cytoskeleton. In this chapter the interaction of PHDs and the above named proteins is tested. Furthermore the hydroxylation status of validated substrates and their intracellular localisation are investigated.

4.2 Results

4.2.1 Validation of potential PHD targets

4.2.1.1 Interaction of PHDs and specific metabolic enzymes

Specific binding of potential PHD substrates was validated. Potential targets that were identified in the SILAC screen include the following metabolic enzymes: L-lactate dehydrogenase, triosephosphate isomerase and fructose-bisphosphate aldolase. To validate binding between PHD1 and the above named metabolic enzymes, FLAG-tagged PHD1 was expressed in the melanoma cell line A375 or in the colon carcinoma cell line HCT116 followed by immunoprecipitation using anti FLAG antibodies. These experiments were performed with A375 cells as A375 cells stably knocked-down for individual PHD isoforms were established in the lab, which can be used for functional studies [128]. Co-immunoprecipitations were performed under normoxia and under hypoxia followed by immunoblot analysis. Even though only L-lactate dehydrogenase and triosephosphate isomerase were identified as potential binding partners of PHD1, all three enzymes were tested for their ability to bind PHD1.

As shown in Figure 4.1 L-lactate dehydrogenase, triosephosphate isomerase and fructose-bisphosphate aldolase are expressed under normoxia and hypoxia. L-lactate dehydrogenase and fructose-bisphosphate aldolase are slightly upregulated under hypoxia as they are HIF target genes. However, no interaction was detected between PHD1 and these enzymes under the tested conditions.

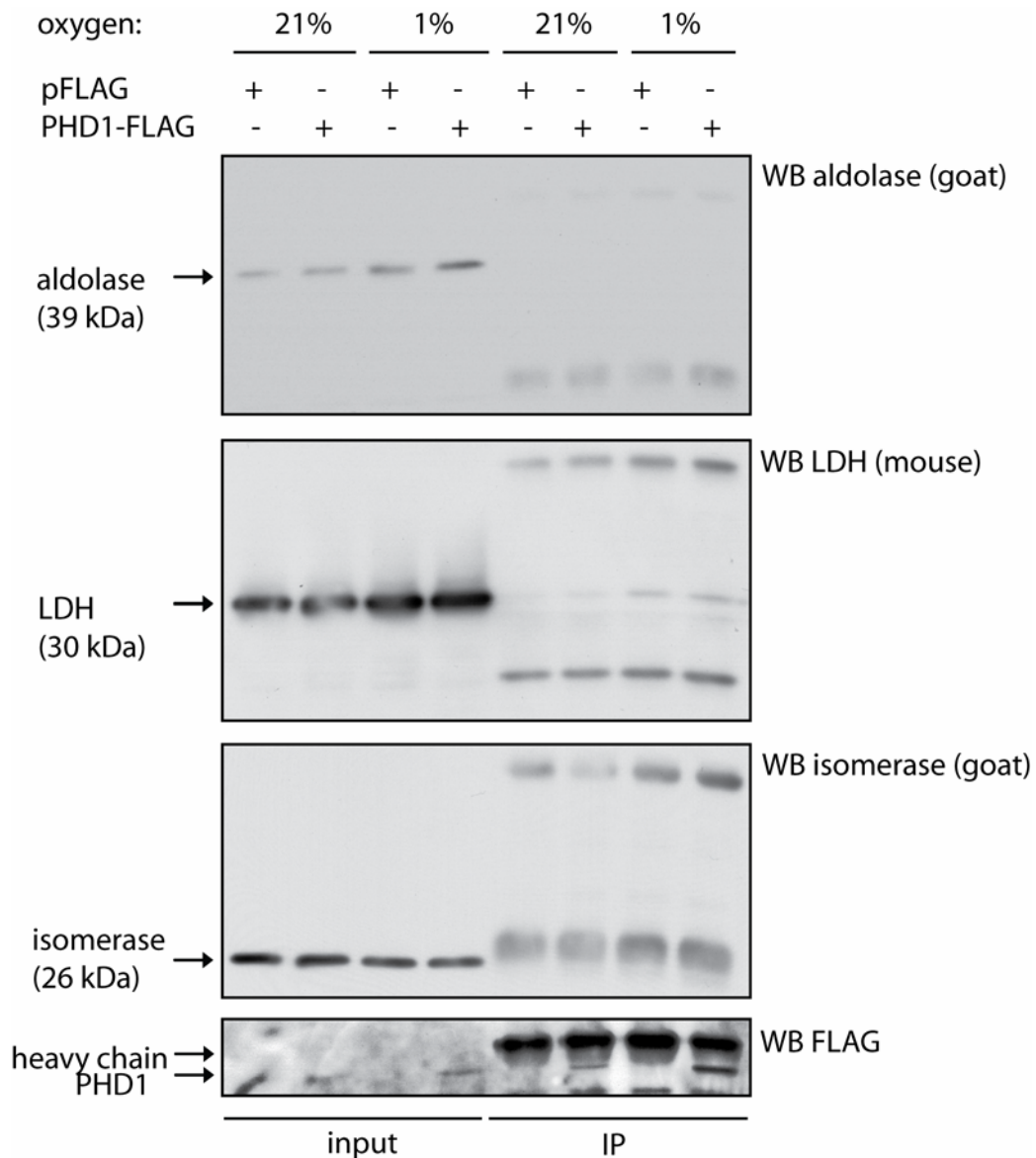


Figure 4.1: Validation of binding between PHD1 and lactate dehydrogenase, triosephosphate isomerase and fructose-bisphosphate aldolase
Co-immunoprecipitations were performed using FLAG-tagged PHD1 in A375 cells under normoxic or hypoxic conditions as indicated.

To validate if either of the other PHDs interact with L-lactate dehydrogenase, triosephosphate isomerase and fructose-bisphosphate aldolase, co-immunoprecipitations were performed under normoxia or hypoxia. FLAG-tagged PHD2 or PHD3 were overexpressed and immunoprecipitated using anti FLAG antibodies. L-lactate dehydrogenase and fructose-bisphosphate aldolase were identified as potential binding partners of PHD2 in the SILAC screen, but all three enzymes were tested for their ability to bind either PHD2 or PHD3. As

mentioned previously, overexpression of PHD3 can induce cell death [71], leading to less overexpression of PHD3 compared to other PHD isoforms.

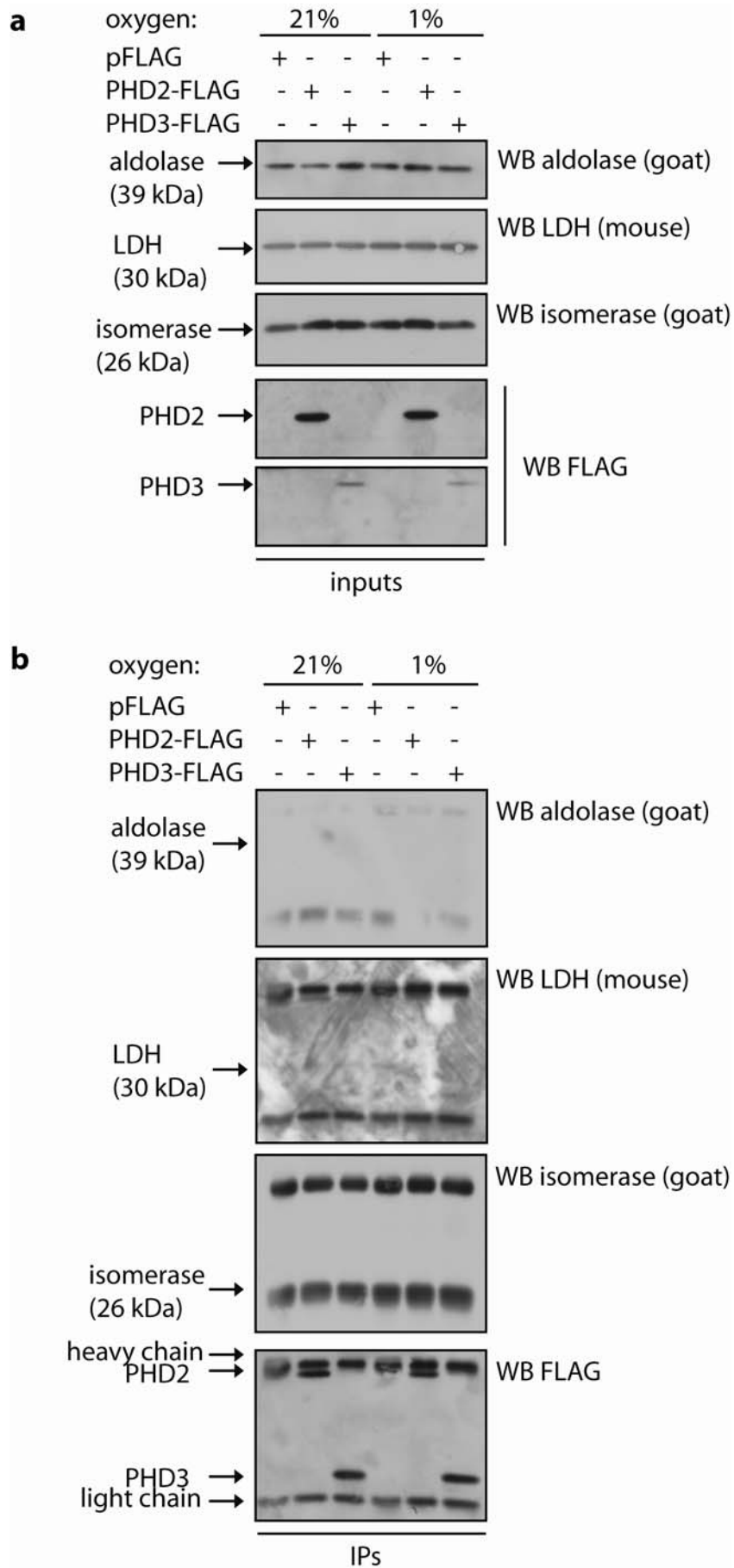


Figure 4.2: Validation of binding between PHD2 or PHD3 and lactate dehydrogenase, triosephosphate isomerase and fructose-bisphosphate aldolase (a) protein expression in total protein lysates of A375 cells (b) Co-immunoprecipitations were performed using FLAG-tagged PHD2 or PHD3 under normoxia or hypoxia.

Figure 4.2a shows the expression of these proteins in total cell lysates. PHD3 is slightly less expressed than PHD2 as was seen in previous experiments. As shown in Figure 4.2 none of these metabolic enzymes (L-lactate dehydrogenase, triosephosphate isomerase and fructose-bisphosphate aldolase) seem to interact with either PHD2 or PHD3. In conclusion, none of these potential substrates could be validated as targets of PHDs.

4.2.1.2 Binding of actin and PHDs

To validate the specific binding of actin to PHDs, co-immunoprecipitations followed by immunoblot analysis were performed in HCT116. In order to validate the interaction, FLAG-tagged PHDs were overexpressed in HCT116 cells and immunoprecipitated using anti FLAG antibodies. Firstly, all three PHDs (PHD1-3) were tested for their ability to bind actin under normoxic and hypoxic conditions.

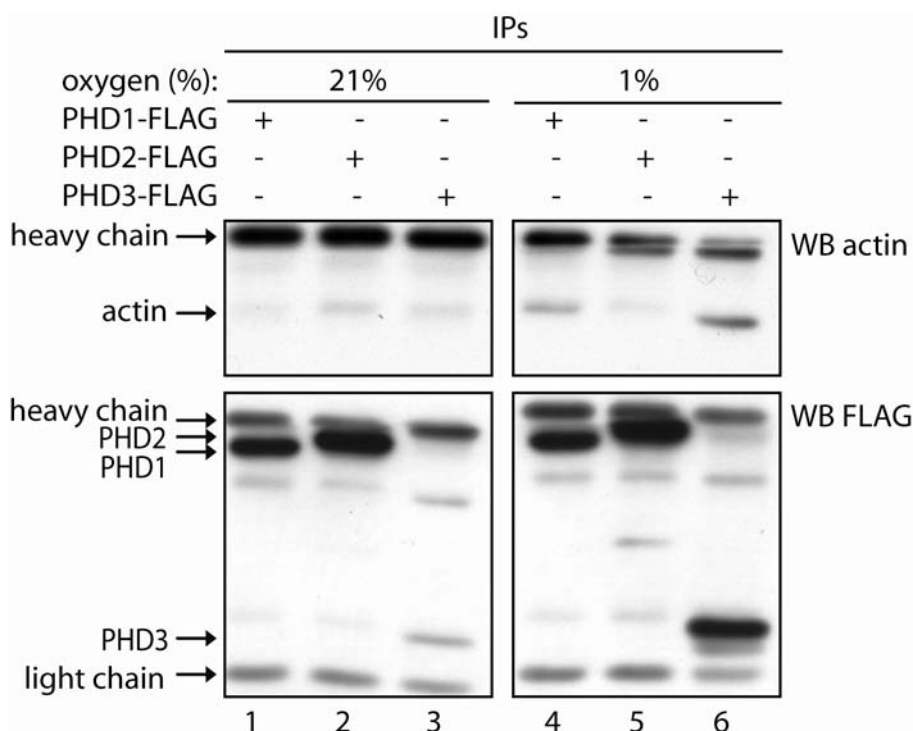


Figure 4.3: Validation of interaction between PHDs and actin in HCT116 cells
Co-immunoprecipitations were performed using FLAG-tagged PHDs in HCT116 cells under normoxic or hypoxic conditions as indicated.

Little binding was detected under normoxia for all PHDs (lanes 1-3). Under hypoxia no binding was detected between PHD2 and actin (lane 5), PHD1 was found to bind only weakly (lane 4). However, PHD3 strongly bound actin in a hypoxia specific manner (lane 6). PHD3 appeared to be less expressed under hypoxia and therefore less immunoprecipitated, however actin still strongly binds to PHD3 under hypoxia whereas PHD1 and PHD2 are higher expressed under hypoxia than PHD3 and still show less binding.

For further validation and to confirm specific interaction, co-immunoprecipitations of overexpressed PHDs were also performed using the osteosarcoma cell line U2OS. U2OS cells were also used later on in this study when investigating the actin cytoskeleton as HCT116 cells do not have a distinctive actin cytoskeleton.

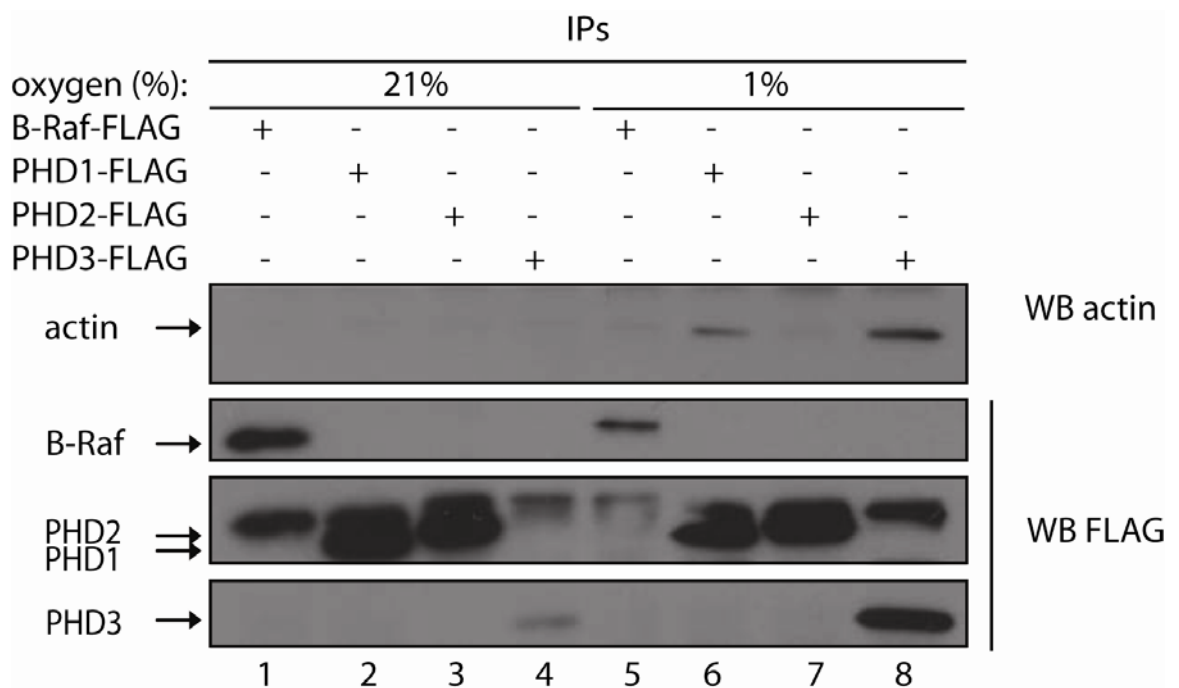


Figure 4.4: Validation of interaction between PHDs and actin in U2OS cells
Co-immunoprecipitations were performed using FLAG-tagged PHDs and FLAG-tagged B-Raf in U2OS cells under normoxic or hypoxic conditions as indicated.

The results shown in Figure 4.4 confirmed the previous results obtained HCT116 cells. PHD3 is slightly less precipitated under normoxia than under hypoxia. Under normoxia all of the PHDs showed little to no binding to actin. Under hypoxia only PHD3 showed a strong interaction, PHD1 weakly interacted whereas

PHD2 did not bind to actin. FLAG-tagged B-Raf was used as a non-specific control and it did not interact with actin under any of the tested conditions. The interaction between actin and PHD3 shows the same pattern of substrate trap as found for the interaction of PHDs and HIF1 α .

4.2.1.3 Binding to PHD3 under different oxygen conditions

To validate the interaction of PHD3 and actin further and to make sure that the interaction is restricted to hypoxia, U2OS cells were incubated under normoxia or hypoxia or in the presence or absence of the PHD inhibitor DMOG, a non-metabolisable α -ketoglutarate derivative.

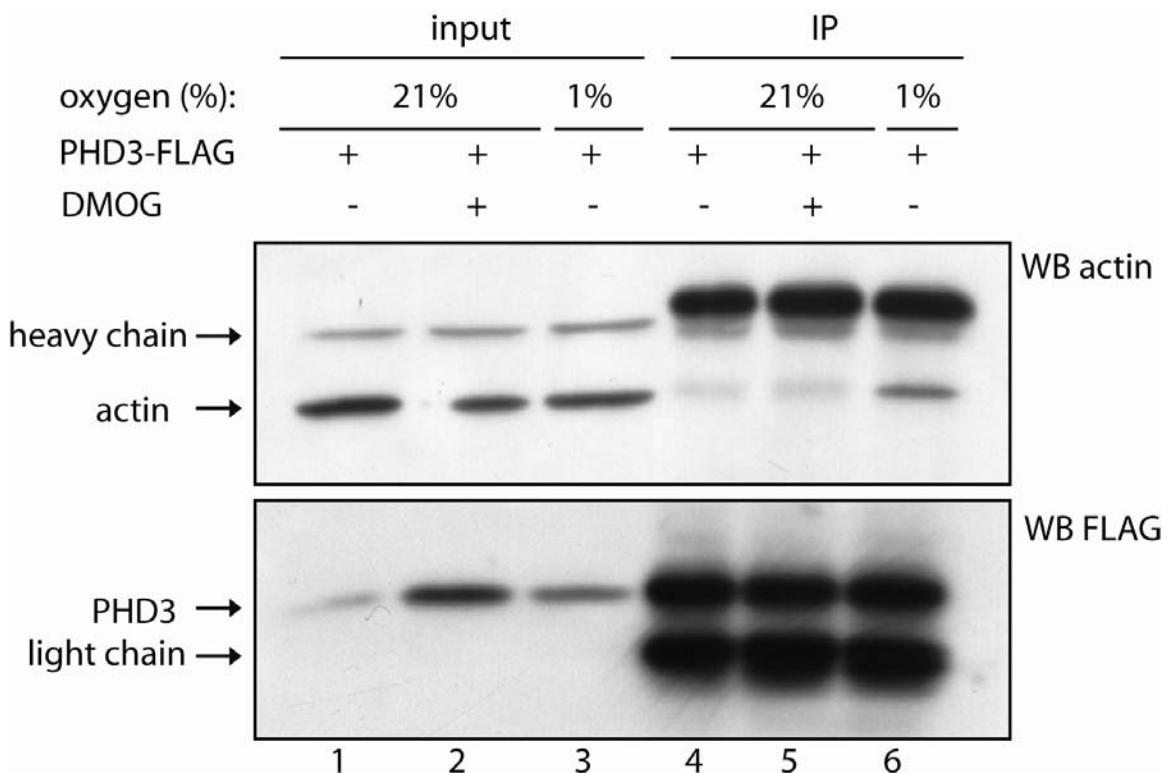


Figure 4.5: Validation of specific binding of PHD3 and actin under hypoxia
Co-immunoprecipitations were performed using FLAG-tagged PHD3 in U2OS cells under normoxia or hypoxia or in the presence of the PHD inhibitor DMOG

As shown in section 4.2.1.2 the interaction between actin and PHD3 was specific for hypoxia, and only weak binding was detected under normoxia or using the

PHD inhibitor (Figure 4.5). Equal amounts of PHD3 precipitated. Similar results were obtained in the renal clear cell carcinoma cell line RCC4 (Figure 4.6). An additional treatment of T α KG was added, a cell-permeable α -ketoglutarate derivative which induces intracellular α -ketoglutarate levels and reactivates PHDs even under hypoxia.

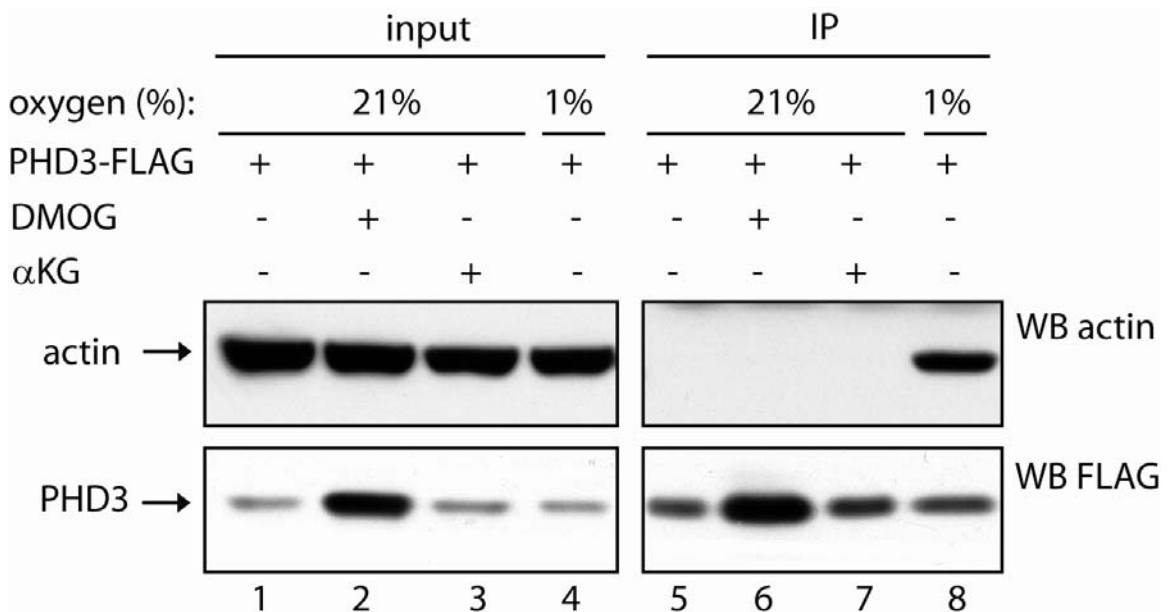


Figure 4.6: Validation of specific binding of PHD3 and actin under hypoxia

Co-immunoprecipitations were performed using FLAG-tagged PHD3 in RCC4 cells under normoxia or hypoxia, in the presence or absence of the PHD inhibitor DMOG or the PHD activator T α KG

As shown with the other cell lines PHD3 binds to actin specifically under hypoxia, but not under other conditions. The reasons for the changes of PHD3 expression under different conditions are unclear but could be due to PHD3 inducing cell death.

Taken together these results showed specific binding between PHD3 and actin, which is stabilised under hypoxia. Therefore β -actin was a good candidate for a PHD3 substrate.

4.2.2 Actin as PHD3 substrate

Detection of hydroxy-proline is quite difficult. The preferred method these days, especially for lower abundant proteins is analysis by of a 16 Da mass shift of hydroxylated peptides by mass spectrometry. However one has to be careful to rule out an isobaric mass shift of oxidised methionine or other amino acids in these peptides.

Based on studies of PHD-binding to HIF1 α , a conserved LXXLAP motif is thought to be the substrate-binding motif for prolyl hydroxylases [53]. However, this represents only a loose consensus, as mutations in all residues apart from the hydroxyl acceptor have been shown to be tolerated [54, 57]. We identified two putative binding motifs similar to the described LXXLAP motif in β -actin around the prolyl residues at position 322 and 332. To investigate if either of these or any other prolyl residues in β -actin were hydroxylated: actin fused to the Green Fluorescent Protein (GFP-actin) was overexpressed in human embryonic kidney HEK293 cells and then immunoprecipitated using anti GFP antibodies. HEK293 cells were used to express large amounts of GFP-actin in order to be able to identify possible hydroxylation sites. The samples were separated on SDS-PAGE and stained with coomassie. The appropriate band was cut out and analysed by mass spectrometry (Figure 4.7). Mass spectrometric analyses were carried out by Richard Unwin (University of Manchester).

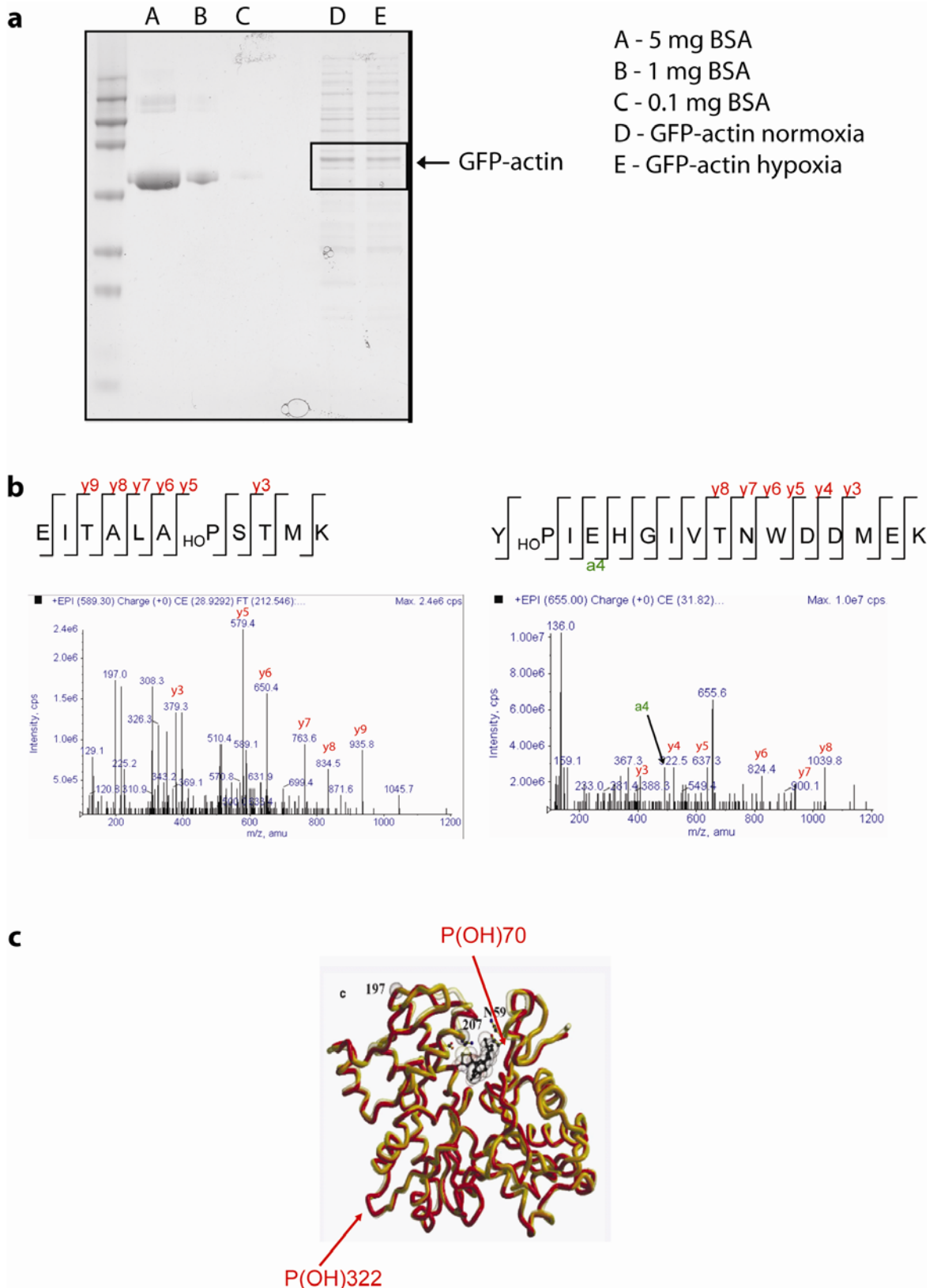


Figure 4.7: β -actin is hydroxylated at two specific proline residues (Pro70 and Pro322)
GFP-actin was overexpressed in HEK293 cells and immunoprecipitated using anti GFP antibodies. (a) Samples were resolved on SDS-PAGE, stained with coomassie and the appropriate band was cut out and analysed by mass spectrometry. (b) Shown are the spectra of the two peptides that are hydroxylated at specific proline residues. (c) Structure of an actin monomer showing the positions of the hydroxylated residues.

Figure 4.7a shows the gel and the bands that were cut out from it to analyse hydroxylation sites. In lanes A-C different amounts of BSA were run on the gel to be able to compare how much GFP-actin was precipitated. 10% of the samples were run in lanes D and E. Two hydroxylation sites were identified in the following peptides which showed a 16 Da mass shift: YP(OH)IEHGIVTNWDDMEK (Pro70) and EITALAP(OH)STMK (Pro322) with P being the hydroxyl acceptor. The spectra are shown in Figure 4.7b. Pro322 lies within an IXXLAP sequence which resembles the LXXLAP binding motif described in the literature, although one of the leucines is replaced by the structurally very similar isoleucine. The second site of proline hydroxylation (Pro70) lies in a slightly less conserved IXXLXXP sequence. Figure 4.7c shows the crystal structure of an actin monomer and the position of the hydroxylated prolyl residues.

4.2.3 Co-localisation of actin and PHD3

To confirm the interaction of PHD3 and actin in cells, the intracellular localisation of all PHDs and their co-localisation with actin was investigated using immunofluorescence in U2OS cells as HCT116 cells were not suitable for analysis of the actin cytoskeleton. Firstly, overexpressed FLAG-tagged PHDs were detected with fluorescently labelled FLAG antibody and actin filaments with fluorescently labelled phalloidin, a toxin that specifically binds to and stabilises filamentous actin [123]. Co-staining was investigated under normoxia and hypoxia.

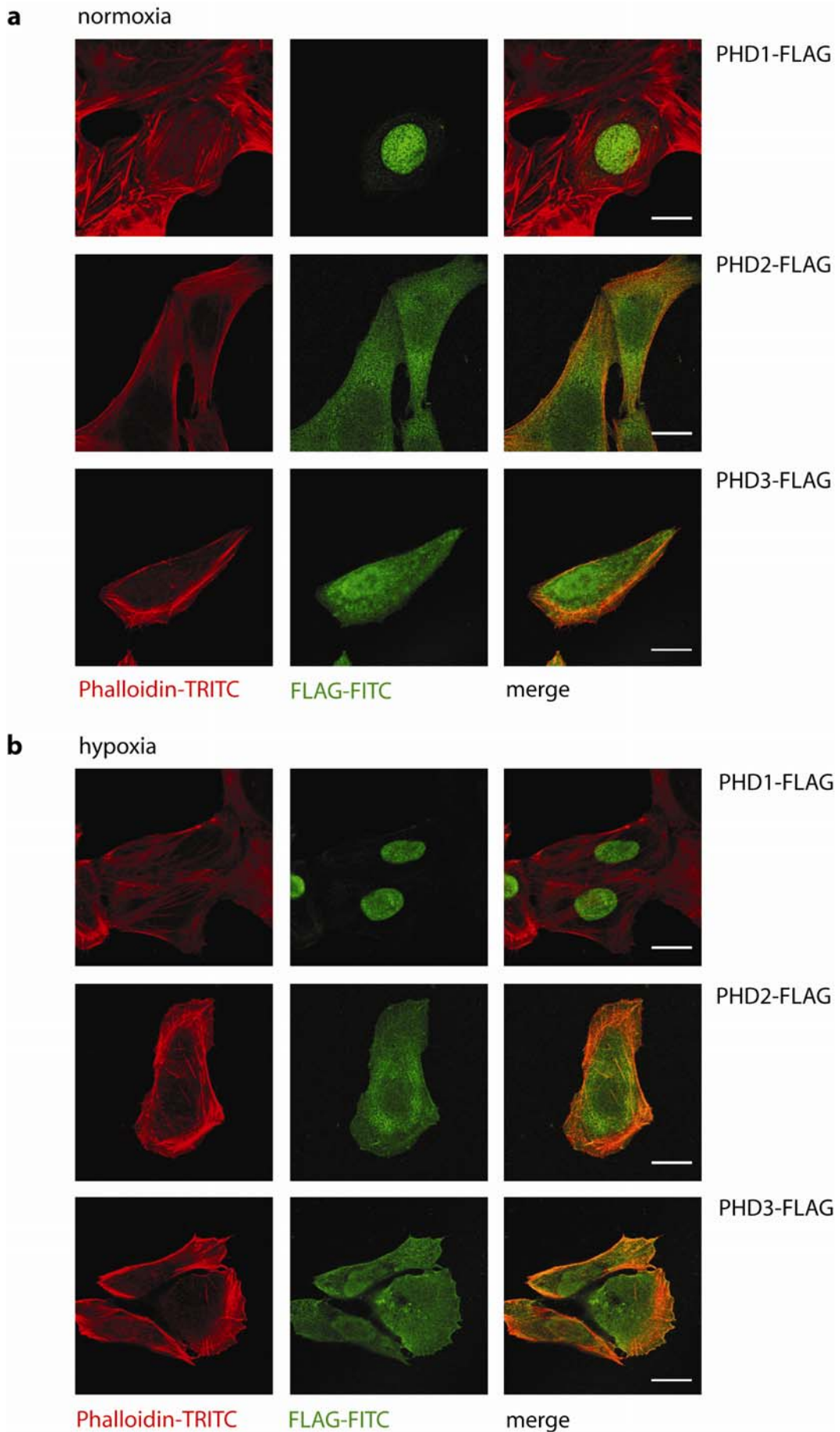


Figure 4.8: Colocalisation of PHDs and phalloidin-stained actin cytoskeleton
 FLAG-tagged PHDs were expressed in U2OS cells. After incubation in normoxia (a) or hypoxia (b) cells were stained with anti FLAG-FITC conjugated antibodies (green) and phalloidin-TRITC (red). Scale bars 20 μ m.

As described previously, we confirmed that PHD1 is localised to the nucleus, PHD2 to the cytoplasm whereas PHD3 was found in both compartments (Figure 4.8). The localisation of PHDs did not change under different oxygen conditions. None of the PHDs appeared to co-localise with the phalloidin-stained stress fibres either under normoxic or under hypoxic conditions.

To address the question of whether PHDs co-localised with other forms of actin rather than larger actin patterns such as stress fibres, GFP-actin was used to visualise different actin population (Figure 4.9). FLAG-tagged PHDs and GFP-actin were overexpressed, and the cells stained with fluorescent FLAG antibodies.

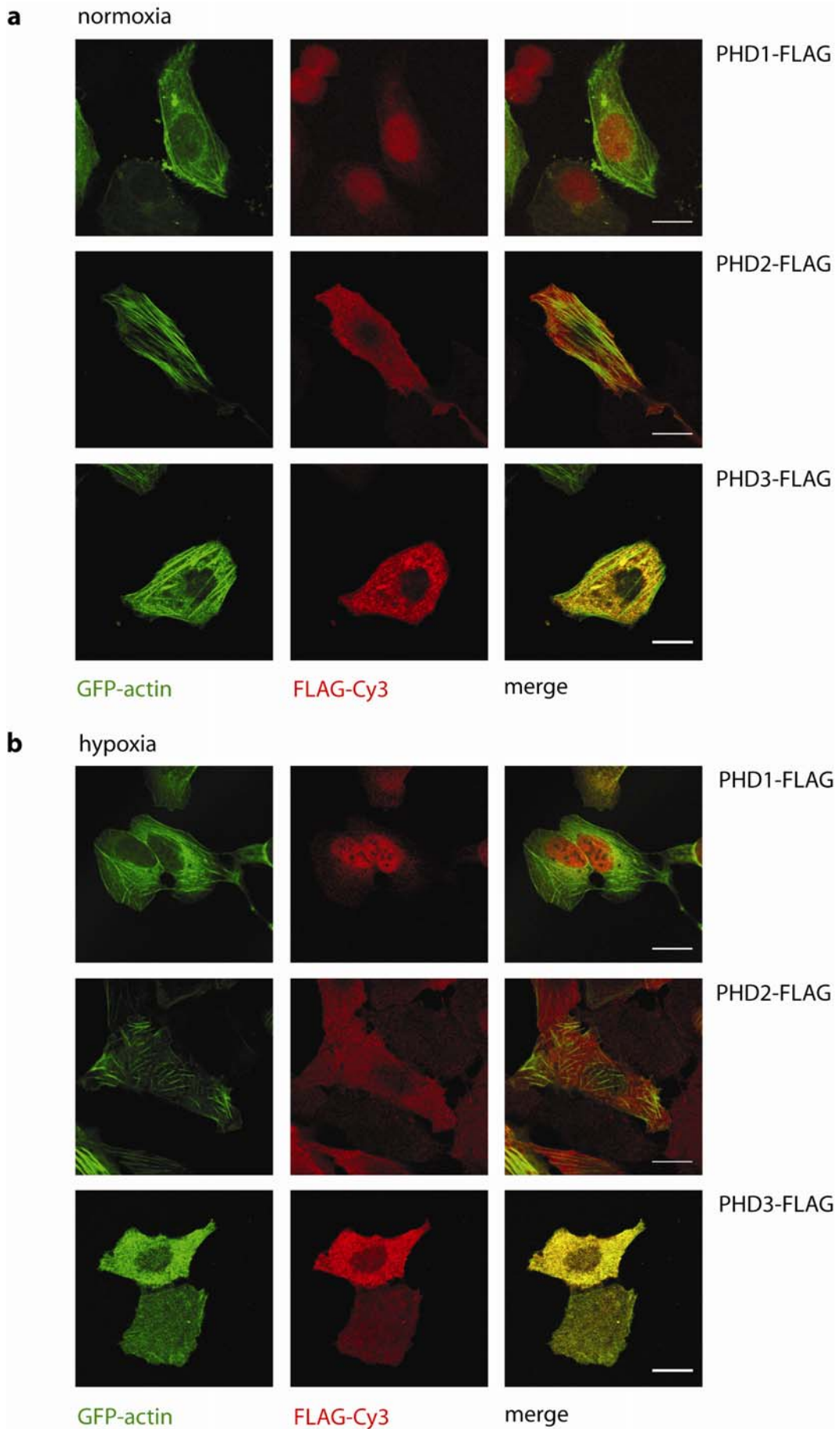


Figure 4.9: Colocalisation of PHDs and GFP-actin
 GFP-actin (green) as well as FLAG-tagged PHDs were overexpressed in U2OS cells grown in normoxia (a) or hypoxia (b). FLAG-tagged PHDs were stained with anti FLAG-Cy3 antibodies (red). Scale bars 20 μ m.

PHD1 did not co-localise with GFP-actin. PHD2 and PHD3 are both cytoplasmic proteins, but only PHD3 appeared to show some co-localisation with GFP-actin whereas PHD2 did not show any co-localisation (Figure 4.9). Under conditions of low oxygen a rearrangement of the actin cytoskeleton was found.

To investigate if this actin rearrangement is dependent on oxygen levels, cells were grown under the following oxygen conditions: normoxia, hypoxia or re-oxygenation after incubation under hypoxia.

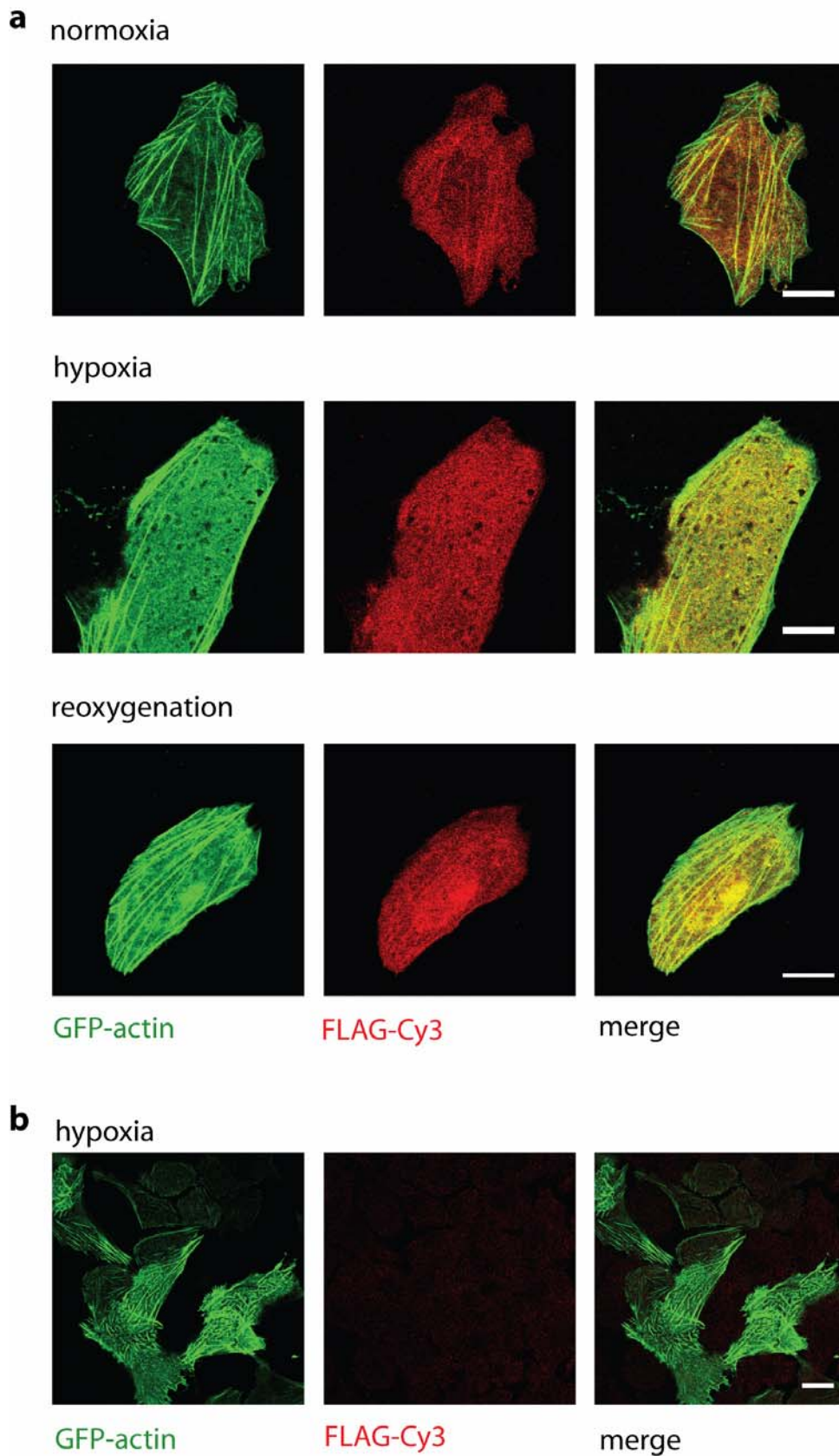


Figure 4.10: Actin rearrangement under different oxygen conditions when PHD3 is overexpressed

GFP-actin (green) as well as FLAG-tagged PHD3 were overexpressed in U2OS cells. FLAG-tagged PHD3 was stained with anti FLAG-Cy3 antibodies (red). Cells were incubated under normoxia, hypoxia or reoxygenated for 30 minutes after incubation under hypoxia. Scale bars 20 μ m. (b) Antibody control for FLAG-Cy3 in mock transfected cells.

Figure 4.10 shows that actin stress fibres disappear under hypoxia, but at least partially reappear after reoxygenation. Our results might suggest that PHD3 binds to smaller actin formations, visualised as diffuse staining, rather than larger actin patterns such as stress fibres. However it is not entirely clear from these experiments which states of actin might colocalise with PHD3.

Investigating this further, co-immunoprecipitations followed by immunoblot analysis were performed in HCT116 and U2OS cells. FLAG-tagged PHD3 was overexpressed in HCT116 or U2OS cells, which were treated with either latrunculin A or cytochalasin D, two different drugs that disrupt the actin cytoskeleton, and immunoprecipitated using anti FLAG antibodies.

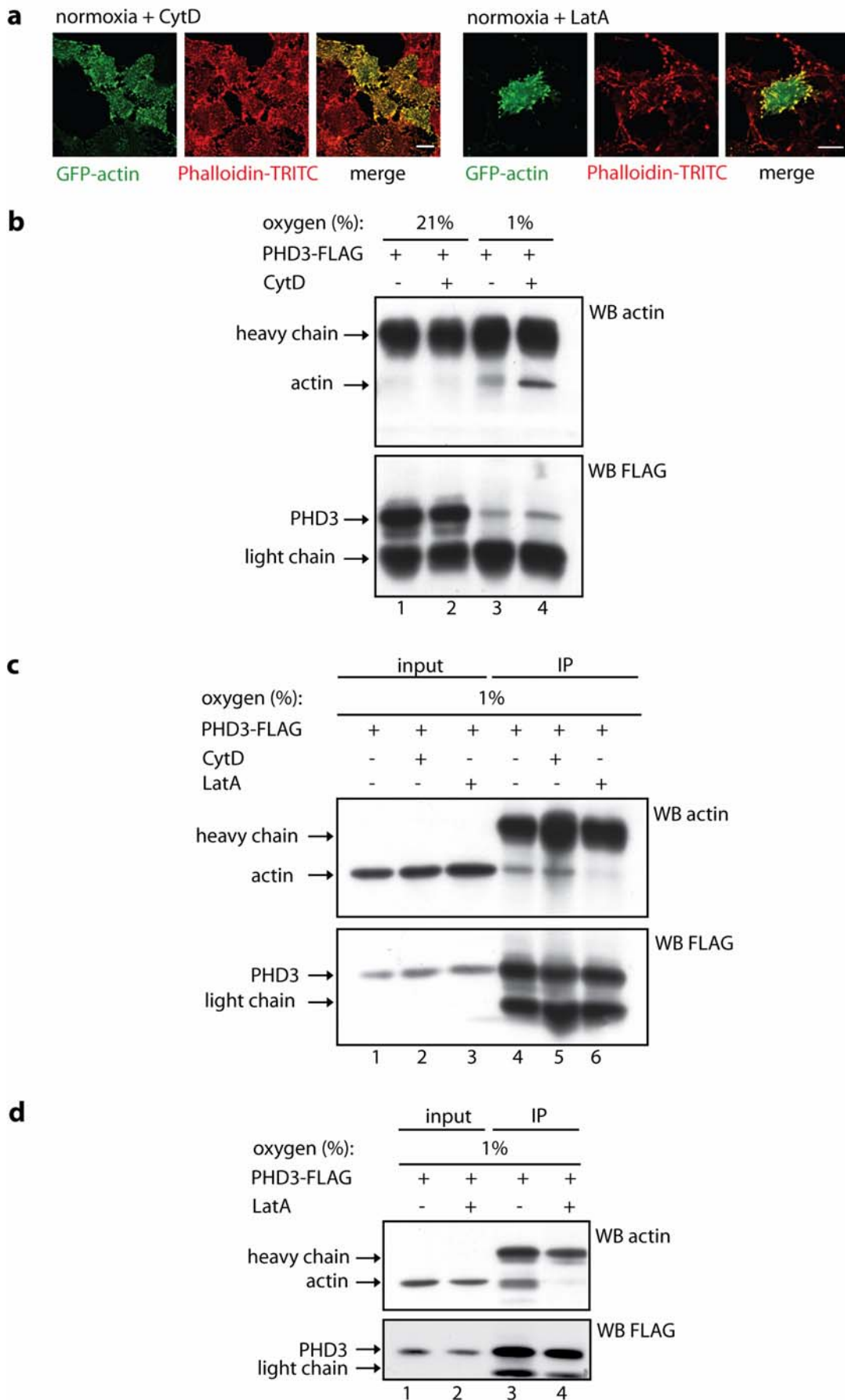


Figure 4.11: Binding of actin and PHD3 after treatment with actin drugs
(a) Immunostaining of the actin cytoskeleton after treatment with cytochalasin D or latrunculin A. **(b-d)** Co-immunoprecipitations were performed using FLAG-tagged PHD3 in HCT116 cells **(b)** or U2OS cells **(c-d)** under hypoxia. Cells were treated with cytochalasin D or latrunculin A as indicated.

In Figure 4.11b co-immunoprecipitations were performed under normoxia and hypoxia using HCT116 cells that were treated with cytochalasin D, a drug that disrupts the actin cytoskeleton by binding to the (+) end of the filaments and therefore inhibiting binding of further actin monomers [121]. No binding was detected under normoxia. Under hypoxia binding between PHD3 and actin was increased when cells were treated with cytochalasin D.

In Figure 4.11c-d co-immunoprecipitations were performed under hypoxic conditions using U2OS cells that were treated with cytochalasin D or latrunculin A. Latrunculin A disrupts the actin cytoskeleton by binding to actin monomers inhibiting the growth of the filaments [120]. In Figure 4.11c an increase in binding between actin and PHD3 is observed when cells are treated with cytochalasin D. However a decrease in binding is found when cells are treated with latrunculin A which was also confirmed in Figure 4.11d. Figure 4.11a shows the actin cytoskeleton after treatment with cytochalasin D and latrunculin A.

4.3 Conclusions

In the previous chapter potential substrates of PHDs were identified in a quantitative proteomic screen. The interaction between PHDs and some of these potential targets were further validated. First, the binding of metabolic enzymes such as L-lactate dehydrogenase, triosephosphate isomerase and fructose-bisphosphate aldolase to PHDs was analysed as these proteins were also identified to have potential hydroxylation sites. None of these metabolic enzymes could be confirmed as substrates of PHDs under the conditions tested. The ratios for binding between L-lactate dehydrogenase or fructose-bisphosphate aldolase to PHD2 probably did not show enough difference to be genuine substrates. These low ratios coincided with low peptide counts. Binding between L-lactate dehydrogenase or triosephosphate isomerase and PHD1 was identified in the SILAC screen when comparing PHD1 transfected samples with control transfected samples under hypoxia and not with the substrate trap. This could confirm that the substrate trap is the best indication for binding between PHDs and their substrates.

Subsequently the interaction between actin and PHDs was validated. Using the substrate trap actin was identified to potentially bind to all PHDs. In all cases actin was identified with ratios >1.5 and with high peptide counts. Validating the interaction we showed that PHD3 was the only PHD isoform that strongly binds actin specifically under hypoxic conditions in co-immunoprecipitation experiments. Weak binding to PHD1 was found in immunoprecipitations, but could not be confirmed in immunofluorescence experiments. Therefore it is likely that the weak interaction found in immunoprecipitations is due to the loss of intracellular compartments during the experiment rather than the interaction of PHD1 with nuclear actin. Subsequently β -actin was found to be hydroxylated at Pro70 and Pro322, suggesting that it is indeed a substrate of prolyl hydroxylases. These prolyl residues lie within sequences resembling the LXXLAP binding motif described in the literature for HIF1 α [53], even though one or both leucine residues are replaced by the structurally similar isoleucine. However so far it could not be proven that this hydroxylation is dependent on PHD3. As hydroxylated and non-hydroxylated peptides have the same retention time in the mass spectrometer, it can be estimated that about 10% of actin is hydroxylated. In immunofluorescence experiments, co-localisation of PHD3 and actin was observed confirming the specific interaction of PHD3 and actin. However, PHD3 did not co-localise with larger actin patterns such as stress fibres but rather with smaller, more diffuse states of actin. None of the other PHDs co-localises with phalloidin-stained stress fibres or with GFP-actin. Furthermore, the actin cytoskeleton appeared to change under hypoxia, especially when PHD3 was overexpressed. A normoxic phenotype could be recovered after reoxygenation. To investigate the possibility that PHD3 rather binds to monomeric actin than actin filaments, immunoprecipitations were performed in the presence of actin drugs that disrupt the actin cytoskeleton and therefore increasing the intracellular G-actin concentration. Cytochalasin D binds to the (+) end of filaments inhibiting further addition of monomers, therefore increasing the concentration of free monomers. Treatment with cytochalasin D was shown to increase binding between actin and PHD3 in hypoxic conditions as would be expected if PHD3 binds to monomeric forms of actin. Latrunculin A binds to the actin monomers inhibiting their binding to actin filaments. Treatment of cells with latrunculin A decreased binding between actin and PHD3 in hypoxic conditions compared to untreated samples. Both drugs induce the

intracellular concentration of actin monomer, but as described above they work by different mechanisms. Given the differences how these two drugs were shown to bind to actin it could give an insight to where PHD3 binds to actin. Increasing actin monomers in the cells increased interaction, however binding seems to be inhibited by latrunculin A, possibly by competing with PHD3 for binding to the monomers. Latrunculin A binds to a region near the ATP binding pocket of actin and could therefore compete the binding of PHD3 hydroxylating Pro70 which is also near the ATP binding pocket.

In this chapter one of the potential substrates identified in a quantitative proteomic approach could be confirmed to interact with PHD3 whereas others could not be validated. This proves the importance of validating the results from a proteomic screen to rule out false positives. We showed the specific interaction between PHD3 and actin and identified a new post-translational modification of actin, the hydroxylation of two specific prolyl residues. However it is still unclear if this hydroxylation is due to the function of PHD3 and changes under conditions in which PHD3 is inhibited. In the next chapter the biological function of the interaction between β -actin and PHD3 was analysed.

Chapter 5 – Biological role of actin hydroxylation

5 The biological role of actin hydroxylation

5.1 Introduction

In the previous chapter β -actin was found to specifically interact with PHD3 and to be hydroxylated at two specific proline residues. However the biological function of this interaction remains unclear. Hypoxia was linked to an increase in cell migration and tumour invasion however signalling pathways involved as well as the impact on the actin cytoskeleton under these conditions are mostly unknown [88, 91]. In this chapter the effects of PHD3 activity on the actin cytoskeleton, cell migration and invasion are investigated.

5.2 Results

5.2.1 Loss of PHD3 activity leads to rearrangement of the actin cytoskeleton

Possible changes in the actin cytoskeleton under low oxygen conditions that were found when validating the binding between PHD3 and actin (chapter 4) were further investigated. To visualise different actin populations the following tools were used: either GFP-actin was overexpressed in cells to show G- as well as F-actin, or cells were stained with fluorescently labelled phalloidin to show F-actin within stress fibres or with fluorescently labelled DNase1 to look at G-actin [124]. The actin cytoskeleton was investigated under normoxic conditions, using pharmacological PHD inhibitors (DMOG), under hypoxia and adding a cell-permeable α -ketoglutarate derivative to reactivate PHDs under hypoxia (T α KG) [36].

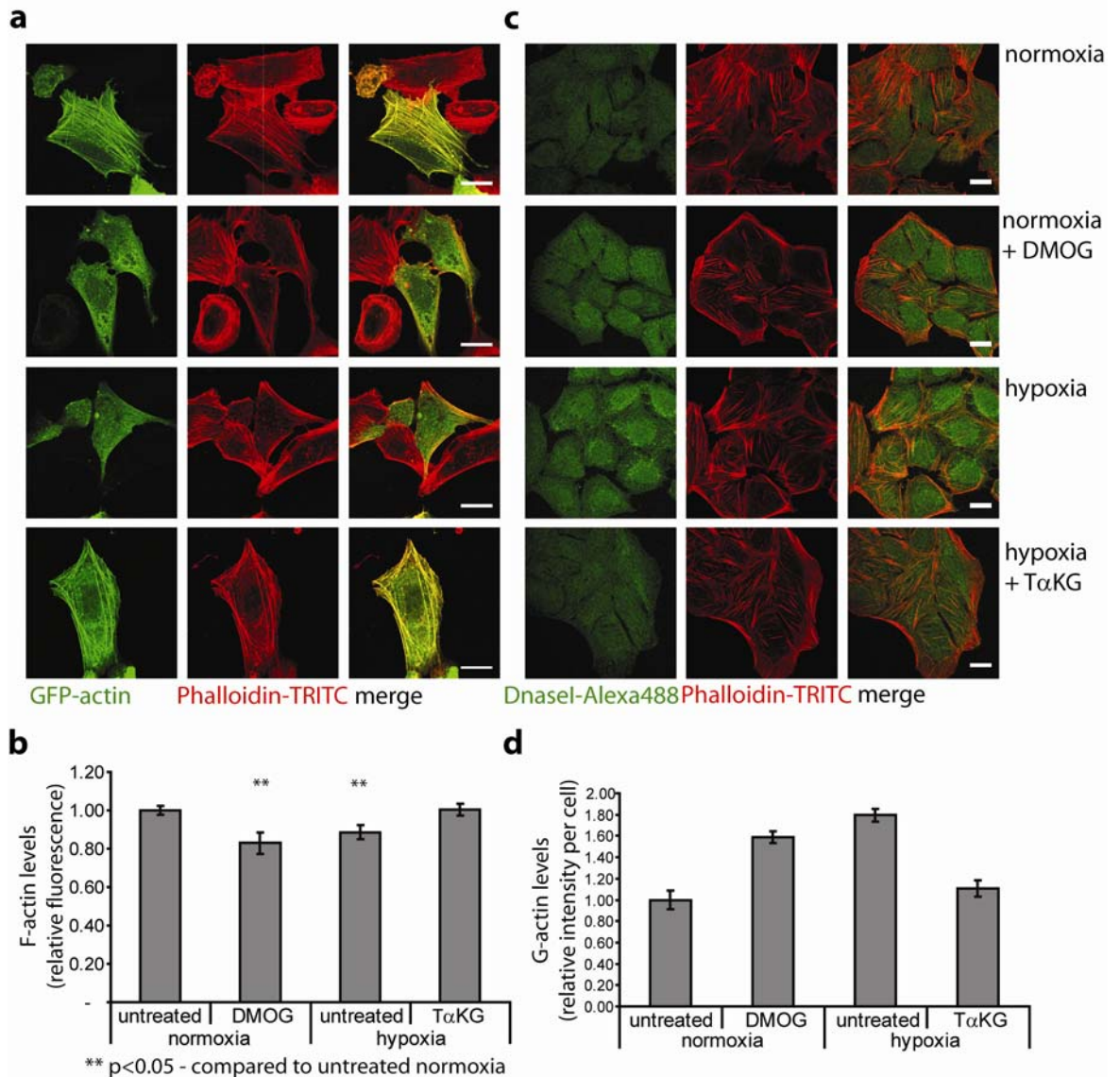


Figure 5.1: Rearrangement of the actin cytoskeleton following inhibition of PHDs

(a) GFP-actin (green) was overexpressed in U2OS cells, which were co-stained with fluorescent phalloidin (red). Cells were grown under normoxic and hypoxic conditions and treated with either DMOG or TαKG as indicated. (b) Intracellular F-actin levels were quantified by labelling actin filaments with saturating amounts of phalloidin-TRITC. Cells were treated as in panel a. F-actin content is shown as comparison to untreated samples measured on the same day (means \pm SEM). Each condition is a representation of 9 individual samples. P-values as compared to untreated normoxia: normoxia + DMOG 0.0379, hypoxia 0.0340, hypoxia + TαKG 0.9156. (c) Cells were treated as indicated and actin filaments were stained with phalloidin-TRITC (red) and actin monomers with DNase1-Alexa488 (green). Scale bars 20 μ m. (d) Quantification of G-actin levels. Images in panel c were used to quantify intracellular G-actin levels. The intensity of DNase1-staining per cell was analysed using ImageJ. Intensities per cell are shown as comparison to untreated normoxic samples.

Firstly, GFP-actin was overexpressed in U2OS cells and stained with fluorescent phalloidin (Figure 5.1a). Under conditions, where PHDs are inhibited, namely the addition of DMOG and hypoxia, fewer stress fibres and a more diffuse cytosolic actin staining was visible. A normoxic phenotype can be restored when PHDs are reactivated using the cell-permeable α -ketoglutarate derivative under hypoxia (T α KG). In a second approach and to confirm these results in an endogenous system, U2OS cells were stained with phalloidin and DNaseI (Figure 5.1c). DNaseI staining increased in conditions where PHDs were inactive confirming the data using GFP-actin. Reactivation of PHDs led to a similar DNaseI staining level as seen under normoxia. Images like those shown in Figure 5.1c were used to quantify intensities per cell of DNaseI-staining using ImageJ (Figure 5.1d). In Figure 5.1a differences in larger actin patterns such as stress fibres are visible. Linked to this observation, possible changes in intracellular F-actin levels were quantified using an assay described by Machesky and Hall [125]. Briefly, cell extract was labelled with a saturating amount of phalloidin-TRITC. The amount of bound phalloidin was quantified after its extraction by fluorescence emission and normalised for its protein content. The data are shown as a percentage compared to untreated cells processed on the same day. Inhibition of PHDs led to a decrease in intracellular F-actin content. Reactivation of PHDs under hypoxia with T α KG brought the F-actin content back to normoxic levels (Figure 5.1b).

To investigate which of the PHDs was important for this actin cytoskeleton rearrangement, PHDs were inhibited by knocking them down individually.

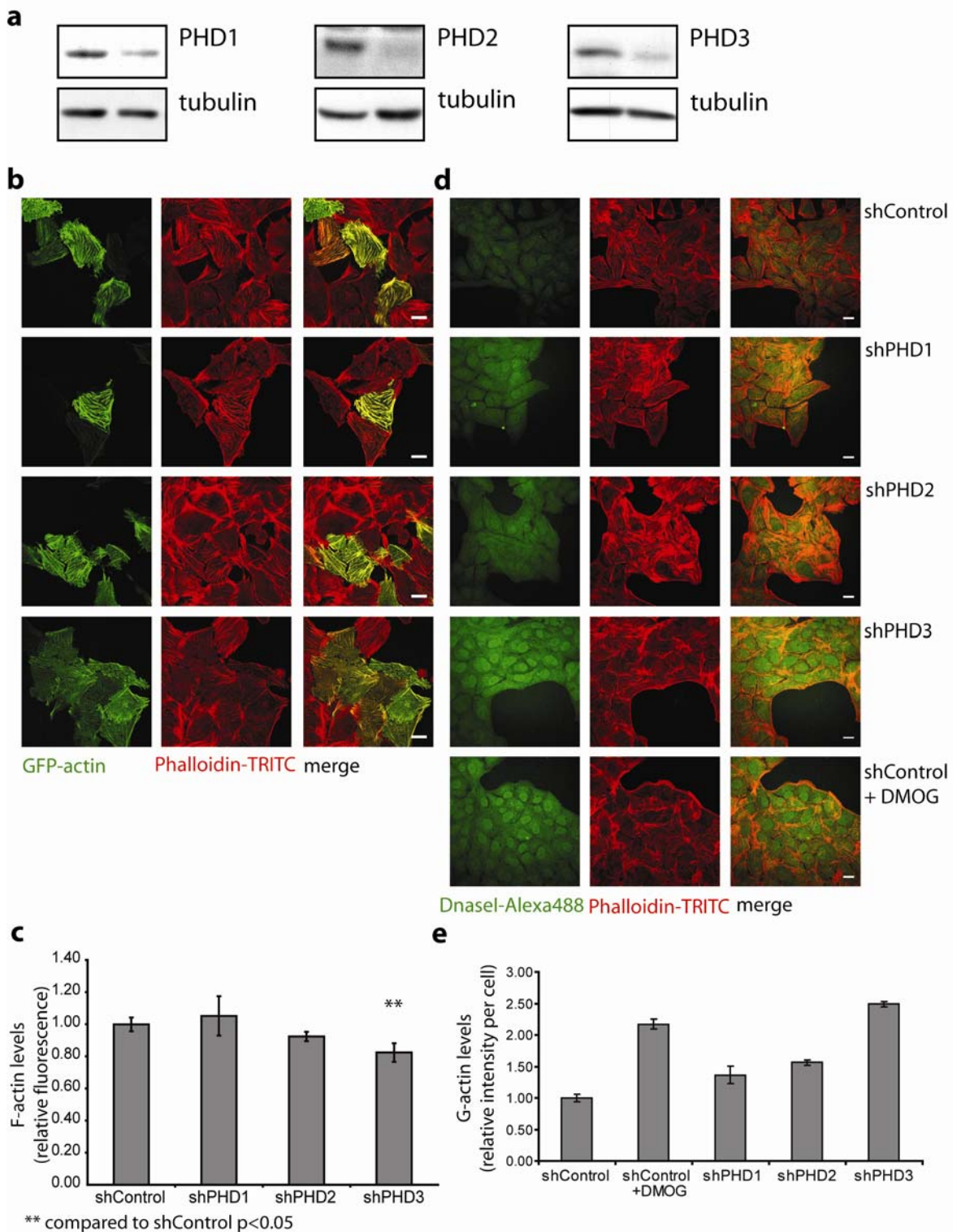


Figure 5.2: Rearrangement of the actin cytoskeleton is dependent on PHD3 activity.

(a) Immunoblot analysis to confirm efficient knockdown of each of the PHDs after transient transfection of short hairpin RNA plasmids into U2OS cells. Knockdown was confirmed on FLAG-tagged PHDs and on endogenous proteins. (b) Normoxic U2OS cells, in which each of the PHDs was knocked-down individually, were stained with GFP-actin (green) and phalloidin-TRITC (red). (c) Quantification of F-actin levels by measuring fluorescent emission after labelling actin filaments with phalloidin-TRITC. F-actin content is shown as comparison to samples transfected with shControl measured on the same day (means \pm SEM). Each condition is a representation of 9 individual samples. P-values as compared to shControl: shPHD1 0.6585, shPHD2 0.9296, shPHD3 0.0304. (d) Endogenous actin was stained with phalloidin-TRITC (red) and DNaseI-Alexa488 (green). Scale bars 20 μ m. (e) Images in panel d were used to quantify intracellular G-actin levels. The intensity of DNaseI-staining per cell was analysed using ImageJ. Intensities per cell are shown as comparison to untreated shControl cells.

The knockdown of each PHD was confirmed by immunoblot analysis (Figure 5.2a). Using GFP-actin and phalloidin staining in immunofluorescence experiments we found that the reduction of PHD1 or PHD2 under normoxia did not have an effect on the actin cytoskeleton, only the reduction of PHD3 led to loss of stress fibres similar to hypoxia or pharmacological inhibition of PHDs (Figure 5.2b). These results were confirmed by DNaseI and phalloidin staining (Figure 5.2d). The knockdown of PHD1 or PHD2 only had minor effects on the actin cytoskeleton. However, the G-actin staining increased to a similar extent as pharmacological inhibition of PHDs when PHD3 was knocked down. Quantification of the F-actin content showed a decrease in F-actin when PHD3 was lost, whereas loss of PHD1 or PHD2 did not have an effect on the F-actin levels (Figure 5.2c). Images in Figure 5.2c were used to quantify intensities per cell of DNaseI-staining using ImageJ (Figure 5.2d).

Similar results were obtained with A375 cells. Under conditions in which the PHDs were inhibited the intracellular F-actin content was decreased, whereas the G-actin content increased. This was shown by both immunofluorescence as well as quantitation of the F-actin level using phalloidin (Figure 5.3). GFP-actin was overexpressed in A375 cells and cells were stained with phalloidin (Figure 5.3a). Fewer stress fibres were visible when PHDs are inhibited as seen in U2OS cells. Using T α KG to reactivate PHDs under hypoxia a normoxic phenotype can be restored. These results were confirmed in an endogenous system staining A375 cells with phalloidin and DNaseI (Figure 5.3c). DNaseI staining increased when PHDs were inactive. Reactivation of PHDs with T α KG decreased DNaseI levels to normoxic levels. Samples stained with DNaseI were used to quantify intensities per cell using ImageJ (Figure 5.3d). Changes in intracellular F-actin levels were also quantified as described above. A decrease in F-actin content was detected when PHDs were inhibited. A normoxic phenotype was restored when PHDs were reactivated by T α KG under hypoxia (Figure 5.3b).

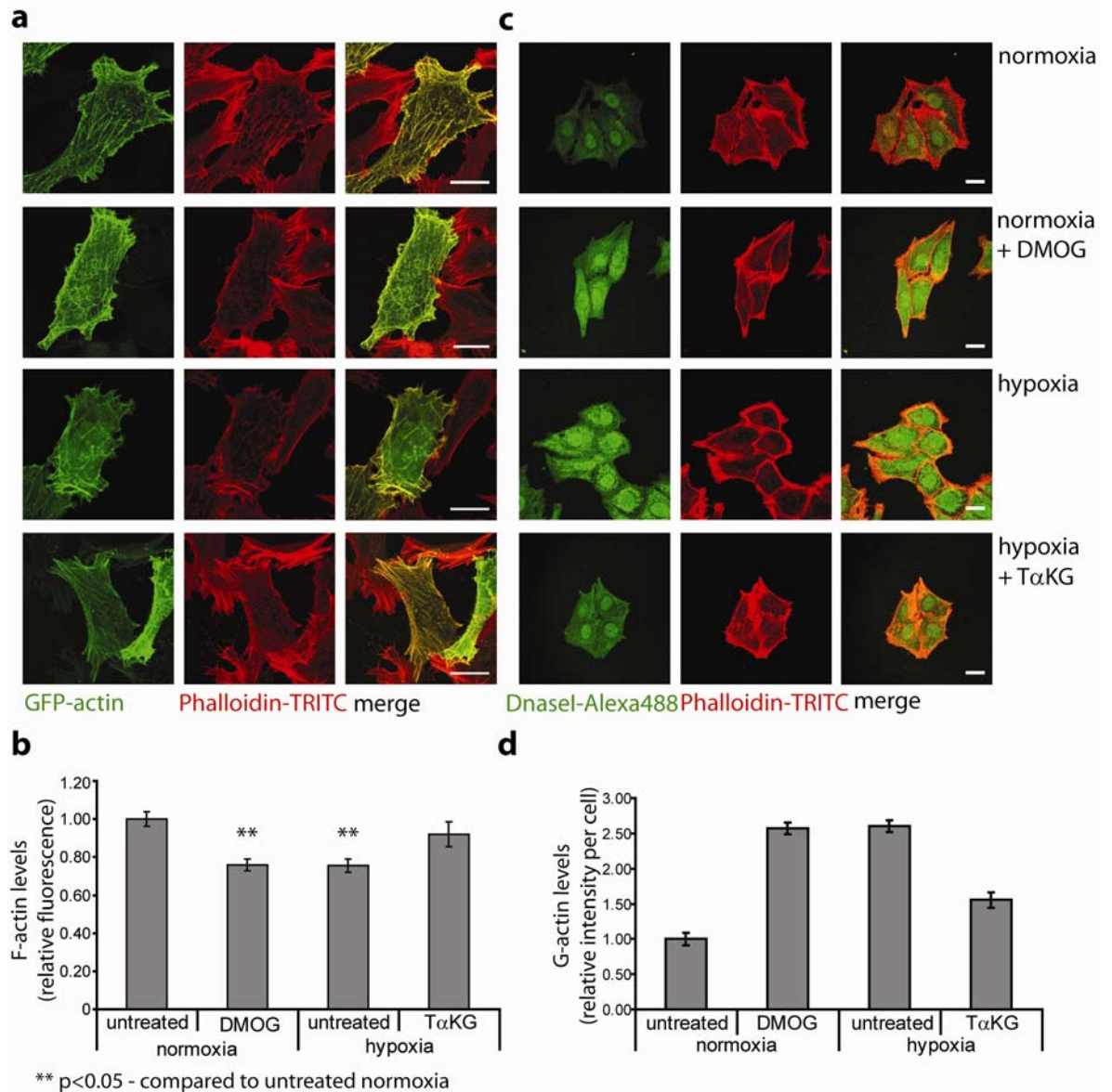


Figure 5.3: Actin rearrangement in A375 cells is dependent on PHD activity. A375 cells were incubated under normoxic or hypoxic conditions for 24 hours and treated as indicated. (a) Cells overexpressing GFP-actin (green) were co-stained with phalloidin-TRITC (red). (b) Quantification of endogenous F-actin levels. F-actin content is shown as comparison to normoxic untreated samples measured on the same day (means \pm SEM). Each condition is a representation of 9 individual samples. P-values as compared to untreated normoxia: normoxia + DMOG 0.0032, hypoxia 0.0013, hypoxia + T α KG 0.2856. (c) Actin filaments were stained with phalloidin-TRITC (red) and actin monomers with DNaseI-Alexa488 (green). Scale bars 20 μ m. (d) Quantification of G-actin levels. Images like in panel c were used to quantify intracellular G-actin levels. The intensity of DNaseI-staining per cell was analysed using ImageJ. Intensities per cell are shown as comparison to untreated normoxic samples.

These experiments were repeated in A375 cells stably knocked-down for individual PHD isoforms. For each of the PHD isoforms two stable clones were used. The stable cell lines were established by Dan Tennant [128]. Levels of achieved knockdown were identified by quantification of mRNA levels as described by Dan Tennant [128] (Figure 5.5).

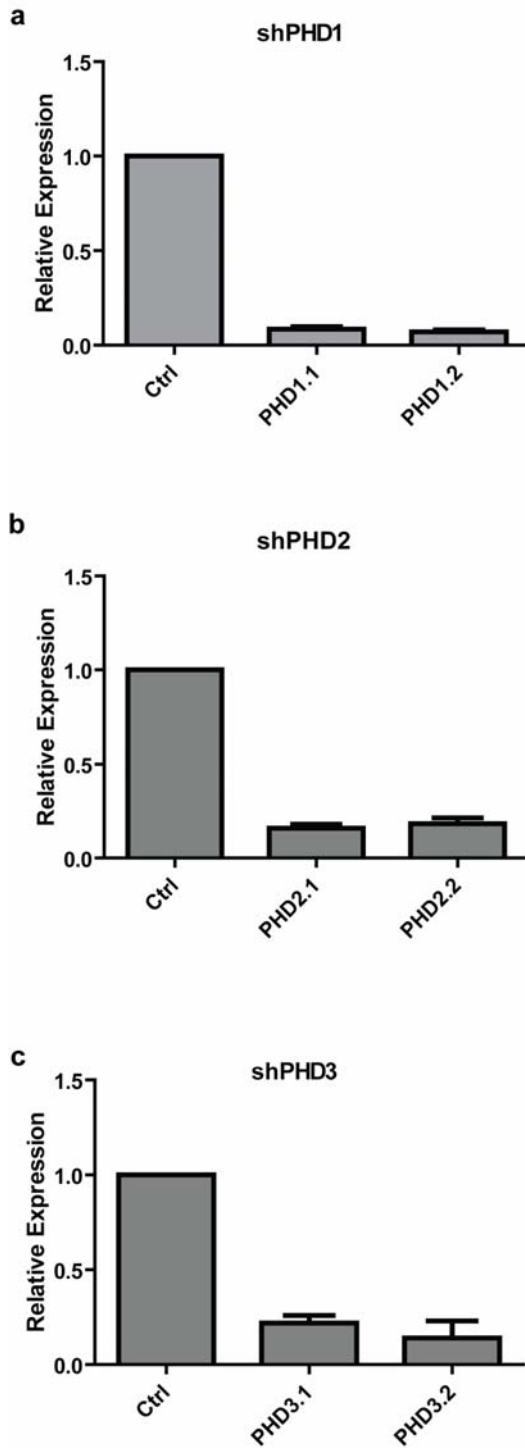


Abbildung 5.4: Assessment of stable PHD knockdown clones as shown by Dan Tennant [128]
mRNA expression levels for two independent clones relative to β -actin and control (shControl) clone for (a) PHD1, (b) PHD2 and (c) PHD3.

Then, the actin cytoskeleton of A375 cells stably knocked-down for PHD3 was investigated.

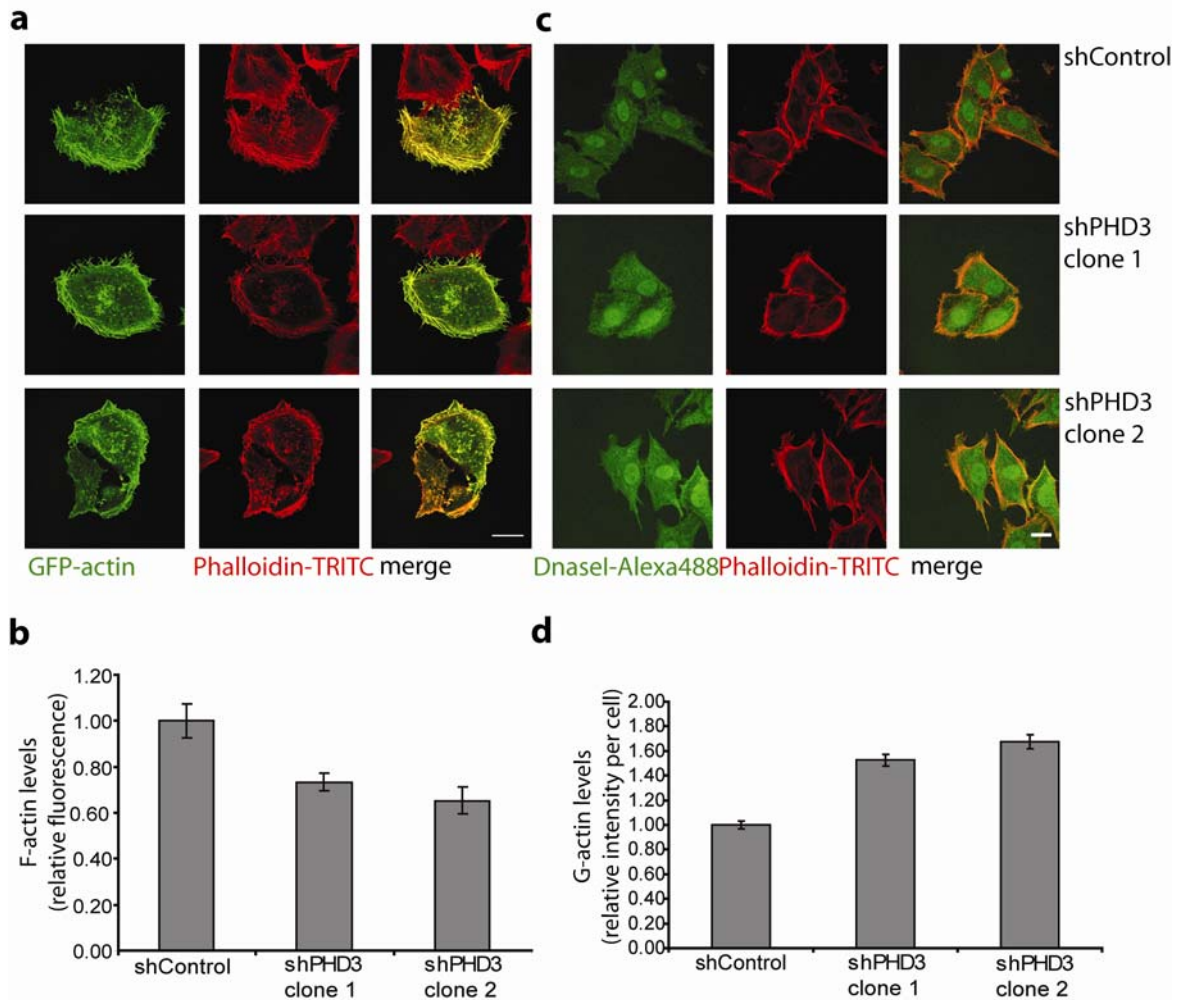


Figure 5.5: Actin rearrangement in A375 cells is dependent on PHD3 activity.

(a) A375-derived stable PHD3 knockdown clones overexpressing GFP-actin (green) were co-stained with phalloidin-TRITC (red). (b) Quantification of endogenous F-actin levels. F-actin content is shown as comparison to a shControl cell line measured on the same day (means \pm SEM). Each condition is a representation of 6 individual samples. P-values as compared to shControl cell line: shPHD3 clone 1 0.0247, shPHD3 clone 2 0.0161. (c) Actin filaments were stained with phalloidin-TRITC (red) and actin monomers with DNaseI-Alexa488 (green). Scale bars 20 μ m. (d) Quantification of G-actin levels. Images like in panel c were used to quantify intracellular G-actin levels. The intensity of DNaseI-staining per cell was analysed using ImageJ. Intensities per cell are shown as comparison to untreated normoxic samples.

Two stable PHD3 knockdown clones of A375 cells showed an increase in G-actin using GFP-actin or DNaseI and phalloidin staining compared to a control cell line (Figure 5.5a+c). A decrease in F-actin content was found in these cells as shown

in a quantitative approach (Figure 5.5b). The actin cytoskeleton in these cells was less prominent than in U2OS or A375 cells shown before. Other cell lines derived from A375 cells with stable knockdowns of either PHD1 or PHD2 were also analysed for their actin organisation in immunofluorescence experiments (Figure 5.6).

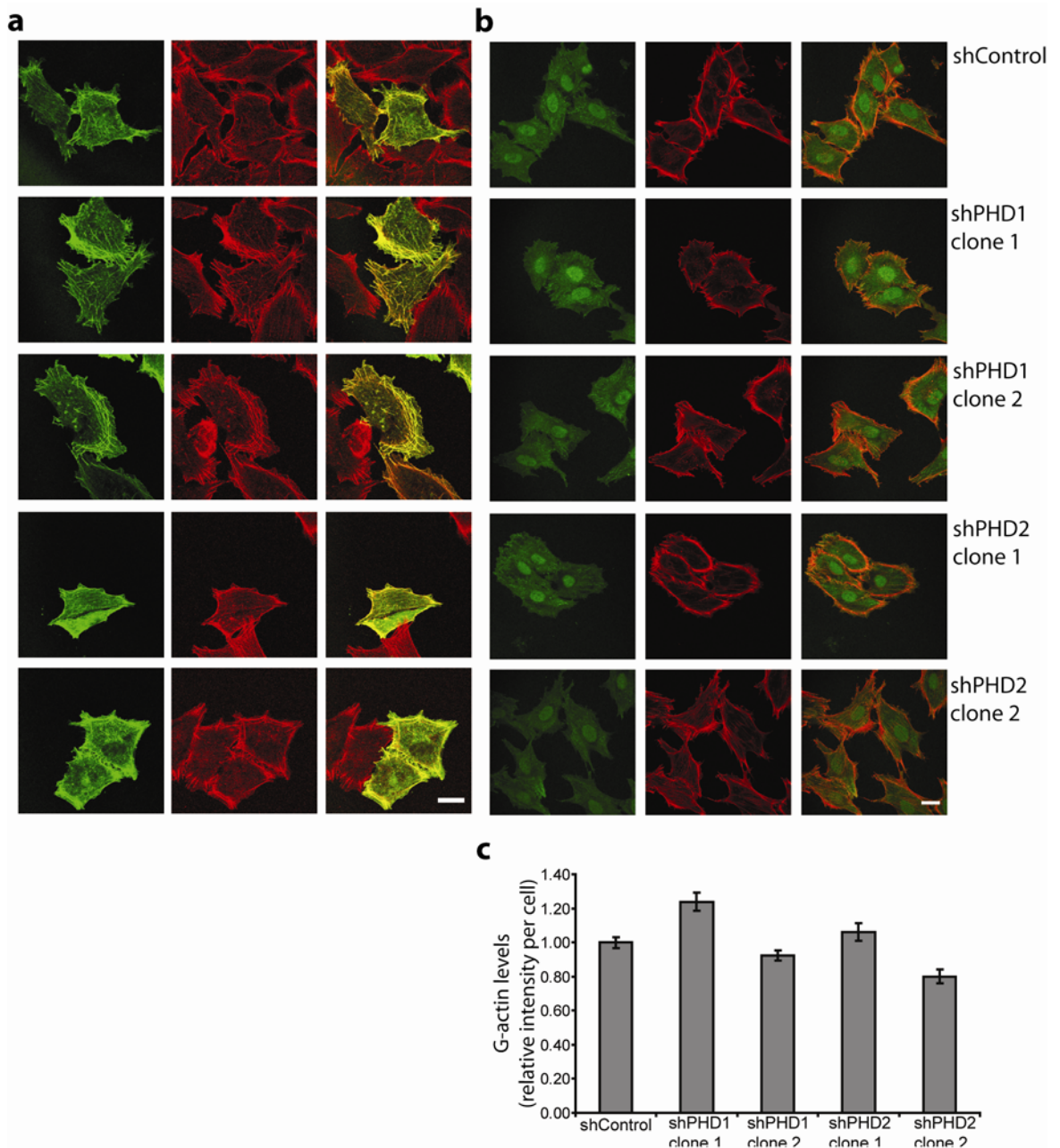


Figure 5.6: Actin organisation in A375-derived knock down cells

A375-derived stable PHD1 or PHD2 knockdown clones overexpressing GFP-actin (green) were co-stained with phalloidin-TRITC (red). (c) Actin filaments were stained with phalloidin-TRITC (red) and actin monomers with DNaseI-Alexa488 (green). Scale bars 20 μ m. (c) Quantification of G-actin levels. Images like in panel c were used to quantify intracellular G-actin levels. The intensity of DNaseI-staining per cell was analysed using ImageJ. Intensities per cell are shown as comparison to untreated normoxic samples.

Two stable clones of each PHD1 or PHD2 knockdown cell lines were analysed in immunofluorescence experiments. No changes in the actin cytoskeleton were found compared to a control cell line using GFP-actin and phalloidin staining or when using DNaseI and phalloidin staining (Figure 5.6a+b). Intensities in DNaseI staining were quantified but no significant differences could be found (Figure 5.6c). Results for the quantification of intracellular F-actin levels were inconclusive. Different levels were observed when compared to different control cells. The actin cytoskeleton in these cells is less pronounced than in U2OS or parental A375 cells and DNaseI staining stained the nucleus more than in above experiments.

Taken together, the results of U2OS and A375 cells showed a rearrangement of the actin cytoskeleton when PHDs are inhibited either by hypoxia or by pharmacological inhibitors such as DMOG. Intracellular F-actin decreased under these conditions to levels similar to those observed when using drugs that disrupt actin filaments. At the same time intracellular G-actin levels were increased under the same conditions. This phenotype was reversed when PHDs were reactivated under hypoxia. The hypoxia-induced actin reorganisation is mediated by the decrease of PHD3 as only the reduction of PHD3 levels but not the reduction of other PHDs led to the same phenotype.

5.2.2 Loss of PHD3 activity leads to increased migration and invasion

It has been shown that some pathways involved in migration and invasion can be regulated by hypoxia [91]. To study whether actin rearrangement under hypoxia resulted in different behaviour in cell migration, wound healing scratch assays were performed. U2OS cells were grown until they formed a confluent monolayer before a wound was scratched into this monolayer using a pipette tip and cell movement into the wound was monitored.

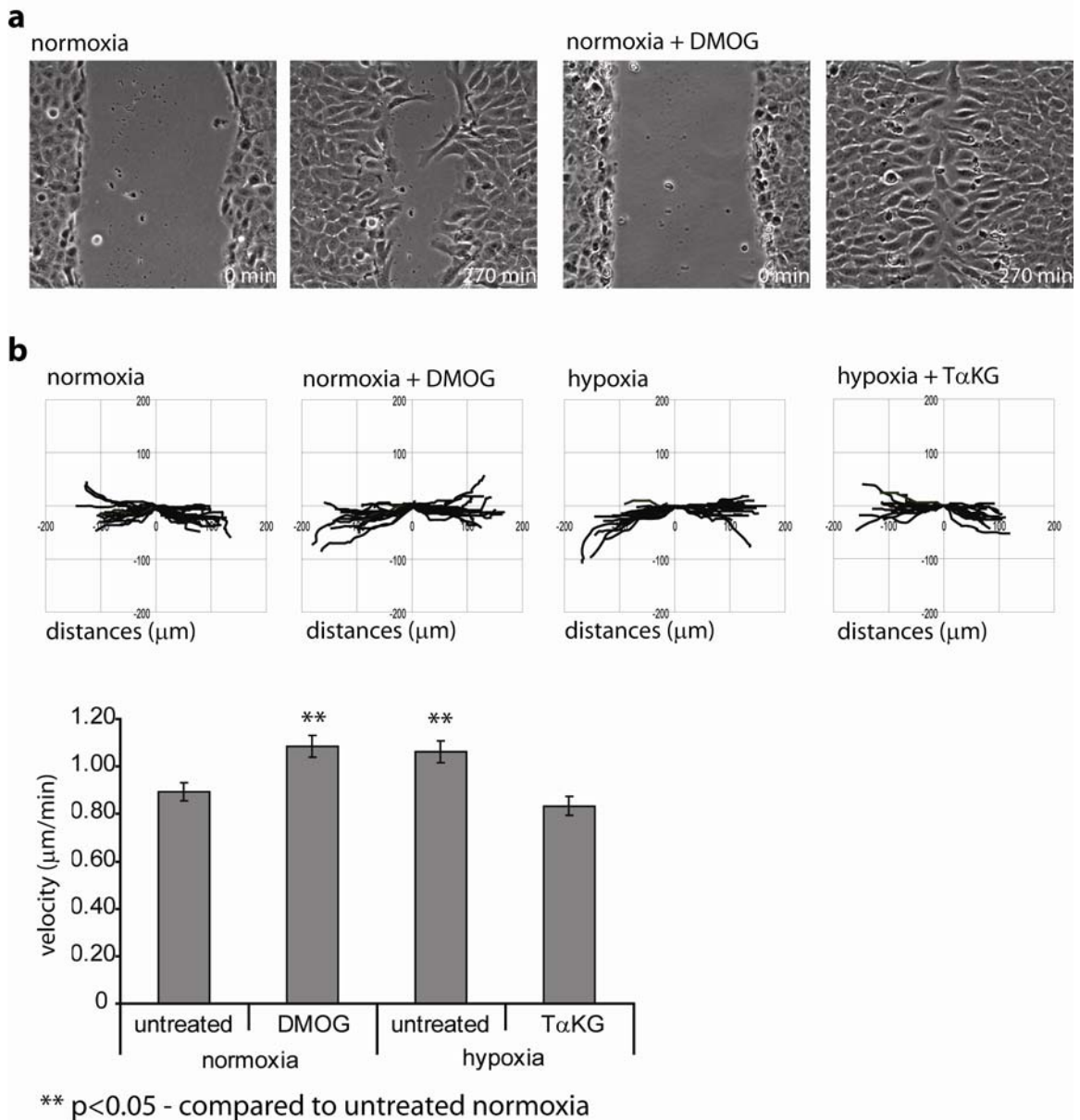


Figure 5.7: Cell migration is dependent on PHD activity

(a) monolayers of U2OS cells were scratched by a pipette and left to migrate into the gap in the presence or absence of DMOG. Bright field images were taken at time points indicated. (b) Wound closure was performed as in panel a at the indicated conditions and cells were tracked by time-lapse microscopy. The single cell tracking device of ImageJ was used to analyse distance and velocity of cell migration. Data shown is the analysis of representative experiment (a least 30 cells per condition; means \pm SEM). P-values as compared t untreated normoxia: normoxia + DMOG 0.0025, hypoxia 0.0112, hypoxia + T α KG 0.2114.

Cells migrated faster in this 2D migration assay when PHDs were inhibited either by hypoxia or DMOG (Figure 5.7) as was shown in bright field images taken at different time points as well as by quantification using the single cell tracking device of ImageJ. Shown are distance plots as well as velocities of cells. Reactivating PHDs under hypoxia using cell permeable T α KG derivative resulted in a decreased velocity of cells to levels similar to normoxia.

These migration assays were repeated under normoxia after having knocked down each PHD individually (Figure 5.8).

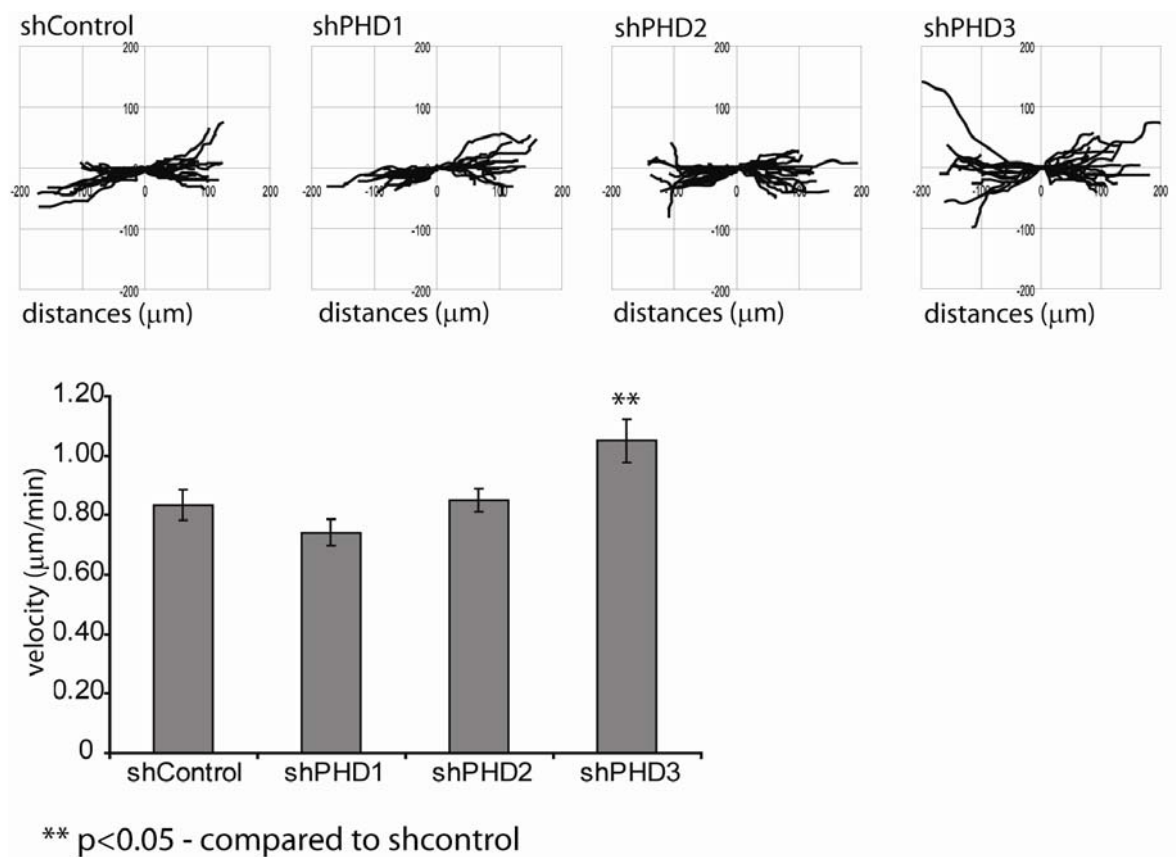


Figure 5.8: Cell migration is dependent on PHD3 activity
PHDs were knocked down individually in U2OS cells and cell migration assays were performed under normoxic conditions. P-values as compared to shControl: shPHD1 0.1957, shPHD2 0.5791, shPHD3 0.0261.

Decrease of PHD1 or PHD2 did not change the velocity of cells. However, the decrease of PHD3 resulted in an increase in velocity similar to that observed under hypoxia. It is currently accepted that an optimal G- to F-actin ratio is

required for maximal cell motility and invasiveness. Indeed, efficient cell movement requires actin polymerization, but high levels of F-actin and stress fibres can oppose cell migration by increasing cell adhesion. As cell migration is dependent on a fine balance of the intracellular G- to F-actin levels, it is hard to predict how changes in the actin cytoskeleton influence cell migration, wound healing scratch assay were performed using different concentrations of latrunculin A, a drug that disrupts the actin cytoskeleton (Figure 5.9).

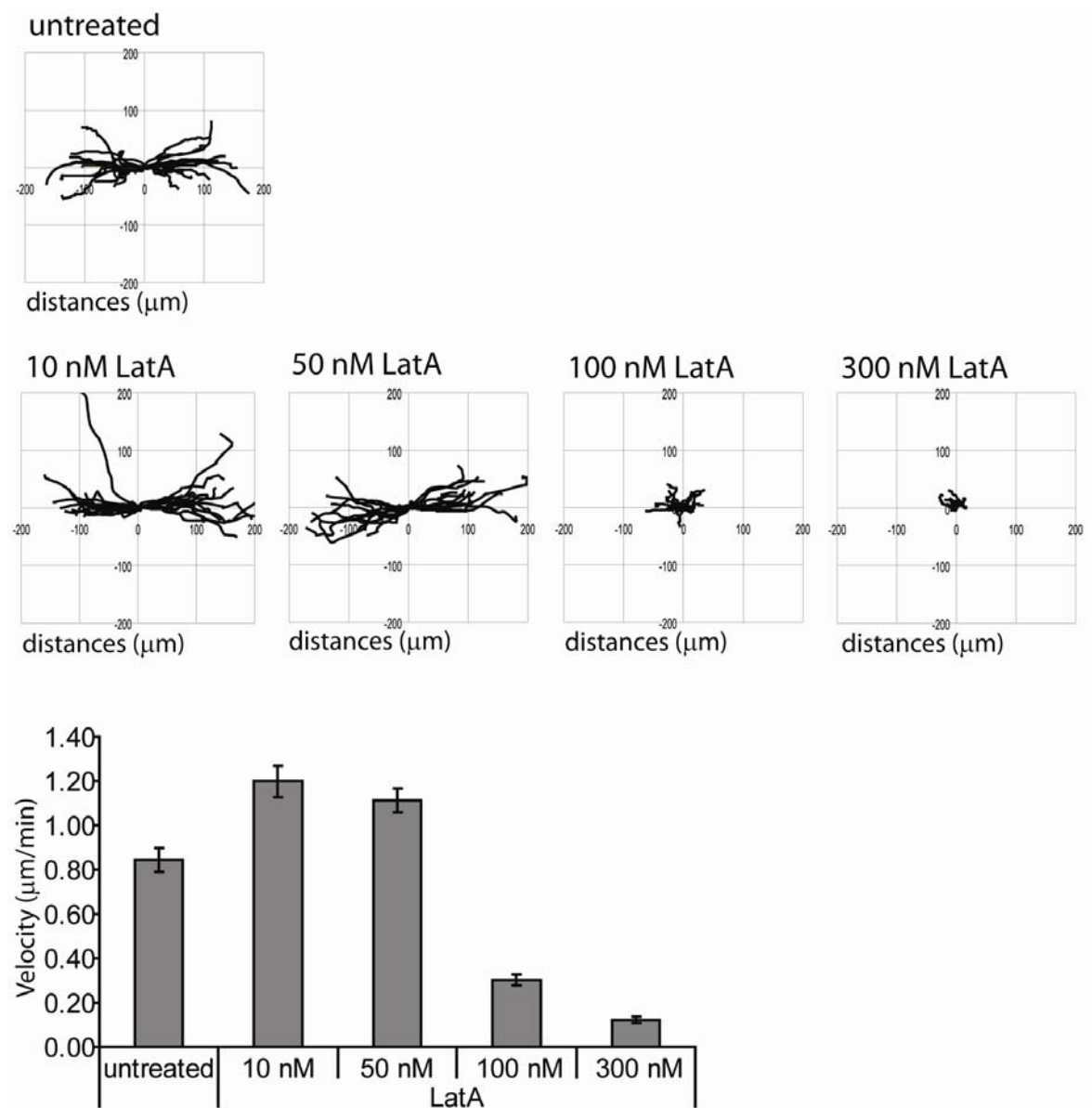
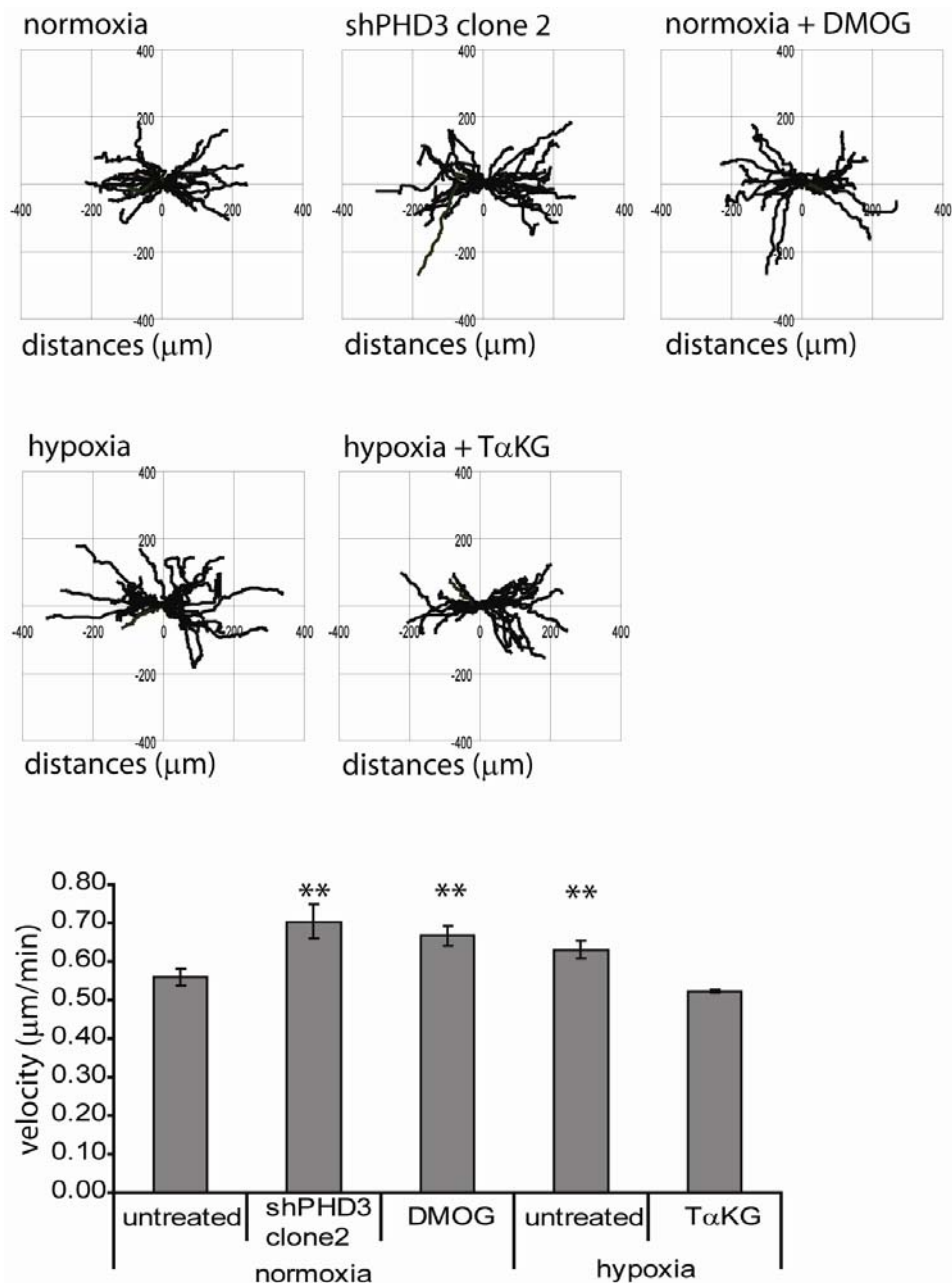


Figure 5.9: Dependency of cell migration on ability of actin to polymerise
Wound closure was performed under normoxia and U2OS cells were treated with different concentrations of latrunculin A. Cells were tracked by time-lapse microscopy. The single cell tracking device of ImageJ was used to analyse distance and velocity of cell migration. Data shown is the analysis of a representative experiment (at least 20 cells per condition; means \pm SEM). P-values compared to untreated samples: 10 nM latA 0.0004, 50 nM latA 0.0018, 100 nM latA <0.0001, 300 nM latA <0.0001.

Low doses of latrunculin A enhanced cell motility, whereas higher concentration of latrunculin A led to a decrease in migration until cell migration was halted. This shows that a fine balance of G- to F-actin and the amount of polymerisable actin in the cells are important for cell migration. This indicates that fine changes in the G- to F-actin ratio regulate cell motility. As a proof of principle this titration was only performed with latrunculin A, however similar results would be expected for a titration using cytochalasin D.

These wound healing scratch assays were also performed with A375 cells (Figure 5.10). Although A375 cells migrated slower than U2OS cells in this 2D assay, they showed similar results to those using U2OS.



** $p < 0.05$ - compared to untreated normoxia

Figure 5.10: Distance and velocity analysis of A375 cells in wound healing scratch assays
Wound closure was tracked by time-lapse microscopy. The single cell tracking device of ImageJ was used to carry out analyses. Data shown is the analysis of a representative experiment (at least 30 cells per condition; mean \pm SEM). A375 and stable clones of PHD3 knockdown cells were treated as indicated. P-values as compared to untreated normoxia: normoxia + DMOG 0.0089, normoxia shPHD3 0.0011, hypoxia 0.0015, hypoxia + TαKG 0.5679.

When incubated under hypoxia or with DMOG, A375 cells migrated faster. This was also observed in cells with stable PHD3 knock down. A normoxic phenotype was restored in hypoxic cells when PHDs were reactivated. The migration of stable PHD1-2 knockdown A375-derived cells was analysed as well (Figure 5.11).

Two clones of each knockdown were used. A375-derived PHD1 or PHD2 stable knockdown cells did not show any significant differences in migration compared to a control cell line. Cells in this experiment appeared to migrate a little slower than A375 cells in previous experiments.

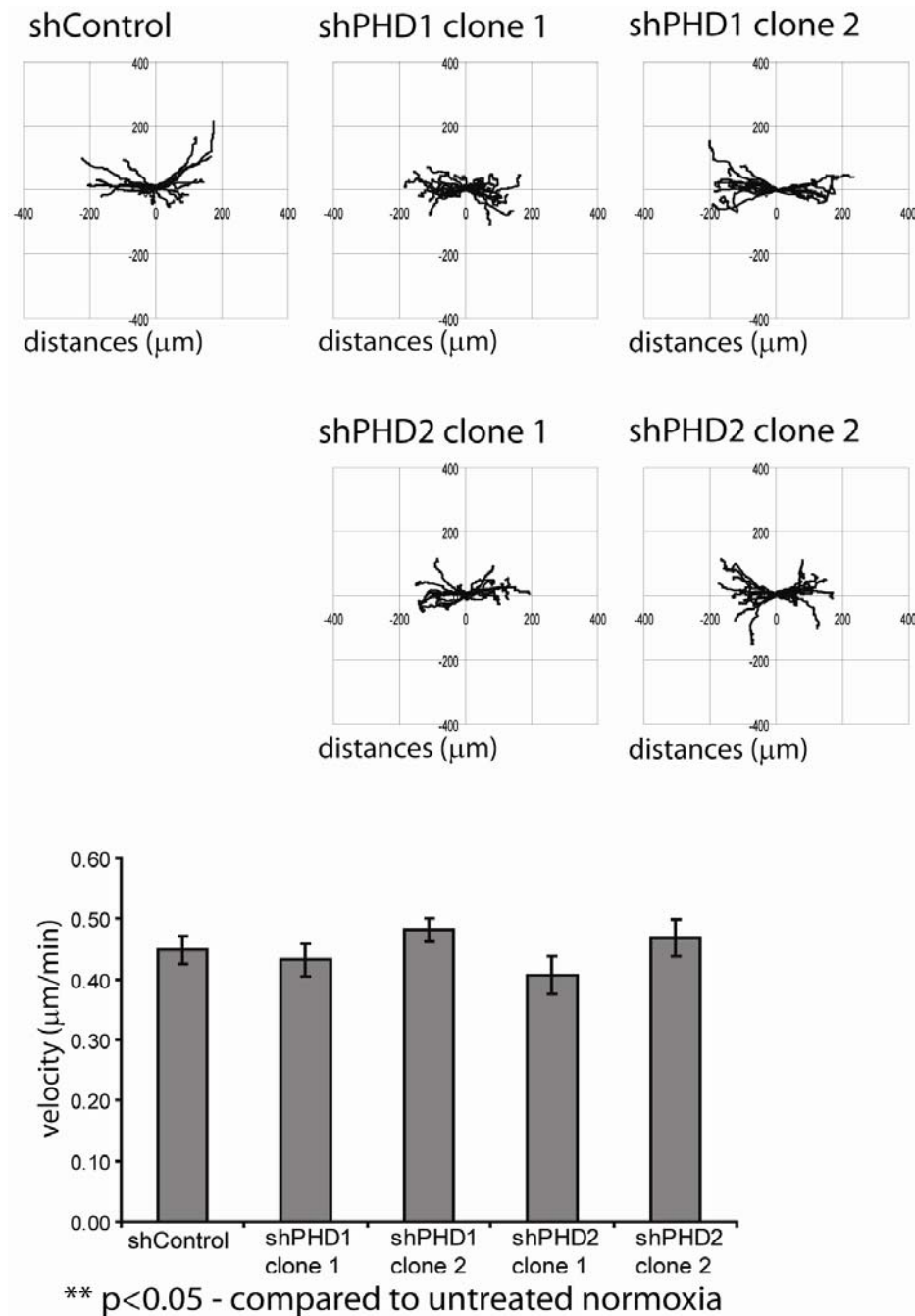


Figure 5.11: Distance and velocity analysis of A375-derived PHD1-2 knockdown cells in wound healing scratch assays

Wound closure was tracked by time-lapse microscopy. The single cell tracking device of ImageJ was used to carry out analyses. Data shown is the analysis of a representative experiment (at least 30 cells per condition; mean \pm SEM).

The next question was whether this increased migration in a 2D environment would also lead to an increase in invasion in a 3D model. The ability of cells to invade into a matrigel plug towards a chemotactic gradient was assessed under either normoxic or hypoxic conditions. U2OS cells were found to invade poorly into the matrigel plug, so A375 cells were used for this assay. Invasion assay were performed by Patrick Caswell (Beatson Institute for Cancer Research).

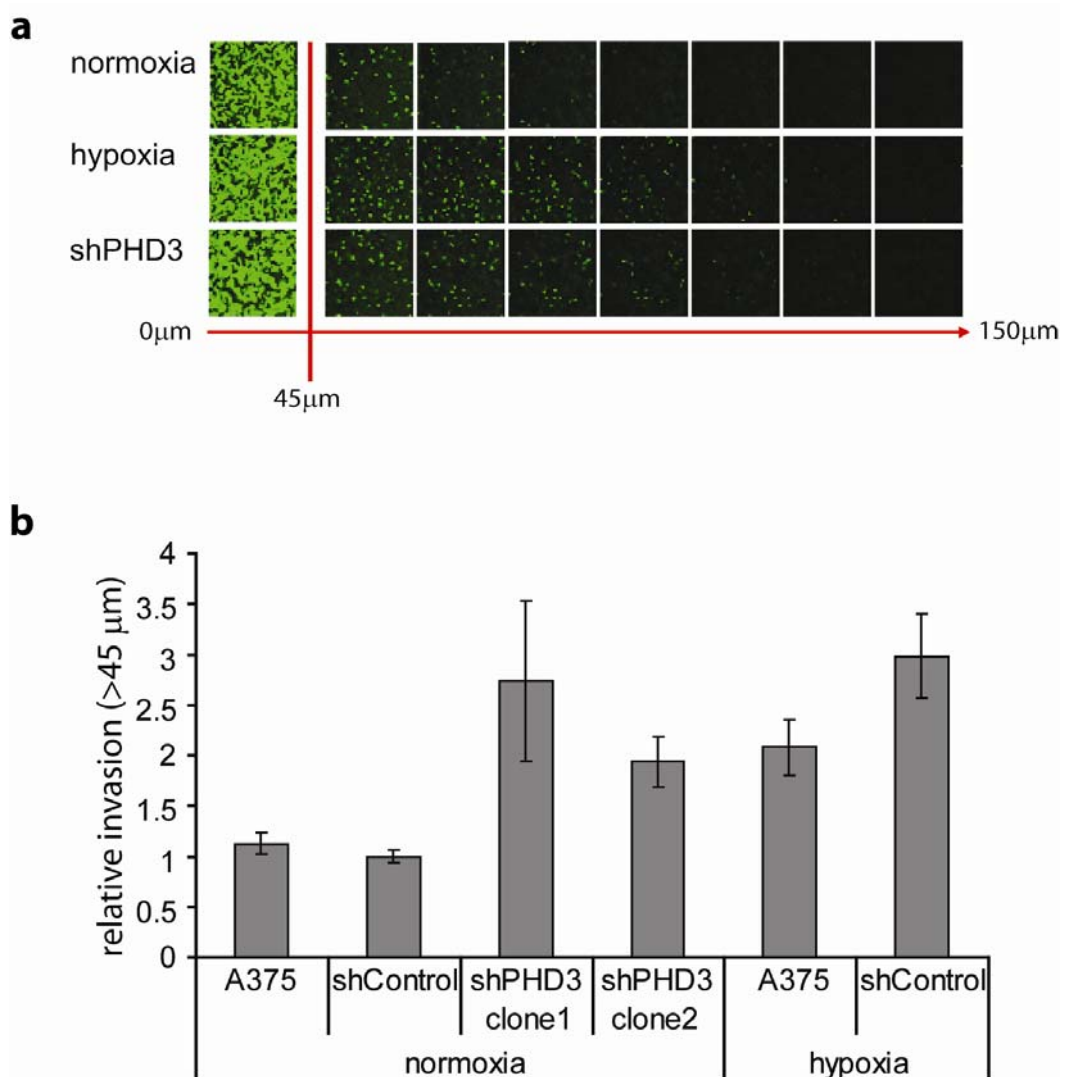


Figure 5.12: Invasion of A375 cells and derived shPHD3 stable clones into matrigel
Invasion of A375 cells and derived shPHD3 stable clones into matrigel was analysed microscopically under normoxic and hypoxic conditions. (a) Shown are microscopic focal planes at defined distances into the matrigel. Cells invading further than 45 μm were considered invasive. Data shown are representative results of confocal sections (every 15 μm) throughout the matrigel plug as well as (b) the quantitative analysis of 6 individual samples (means \pm SEM).

Compared to invasion under normoxia, A375 cells invaded further under hypoxia (Figure 5.12). The reduction of PHD3 increased invasion under normoxia compared to a control cell line as well. Taken together, these results showed that hypoxia-induced cell migration and invasion can be mimicked by decreasing PHD3 expression levels.

It would have been interesting to repeat these invasion assays in the presence of drugs influencing PHD activity such as DMOG or T α KG or influencing the actin cytoskeleton such as latrunculin A or cytochalasin D however, it was difficult to find the right conditions for treatment of the cells with these drugs over the period of time the assay was running.

5.2.3 Mutation of Pro70 and Pro322 effects the actin cytoskeleton and cell migration

To investigate the importance of residues Pro70 and Pro322 of β -actin in cytoskeleton rearrangement induced by PHD3 reduction or hypoxia one or both of these residues were mutated to alanine in a GFP-actin expression vector. These GFP-tagged wildtype and mutant constructs were overexpressed in U2OS cells, while concomitantly knocking down endogenous actin using different siRNA sequences, which targeted the 3'UTR sequence of actin.

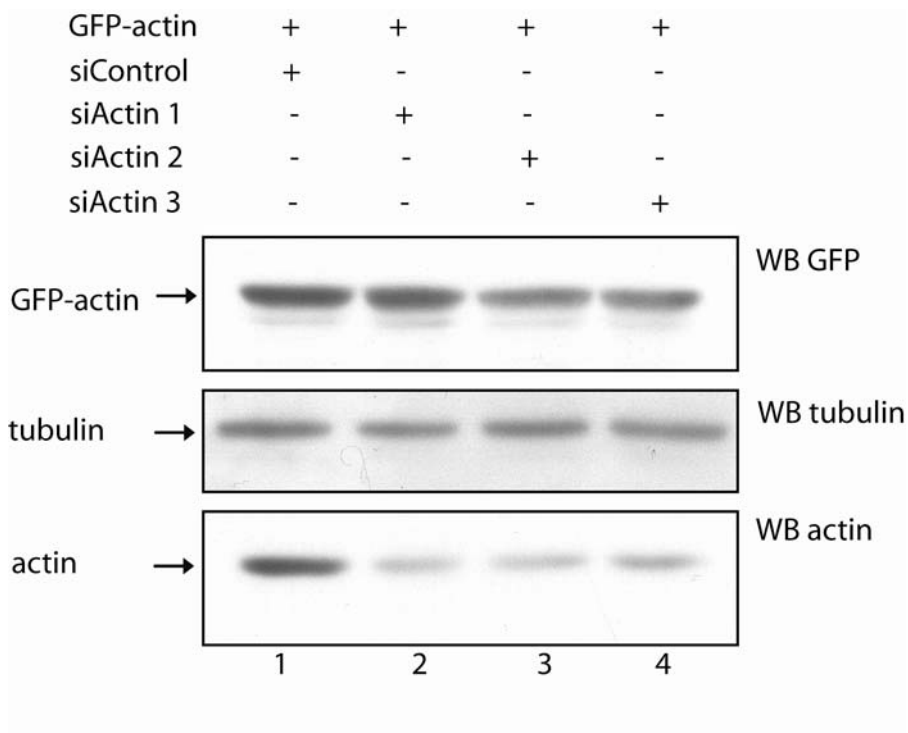


Figure 5.13: Immunoblot analysis confirming the knockdown of endogenous actin and expression of wildtype GFP-actin and its mutants
 Immunoblot analysis was used to confirm the knockdown of endogenous actin as well as the rescue of cells with the exogenously expressed GFP-actin.

The knock down of endogenous actin was confirmed by immunoblot analysis (Figure 5.13). The actin cytoskeleton was investigated by overexpressing these GFP-tagged plasmids and staining the actin filaments with phalloidin.

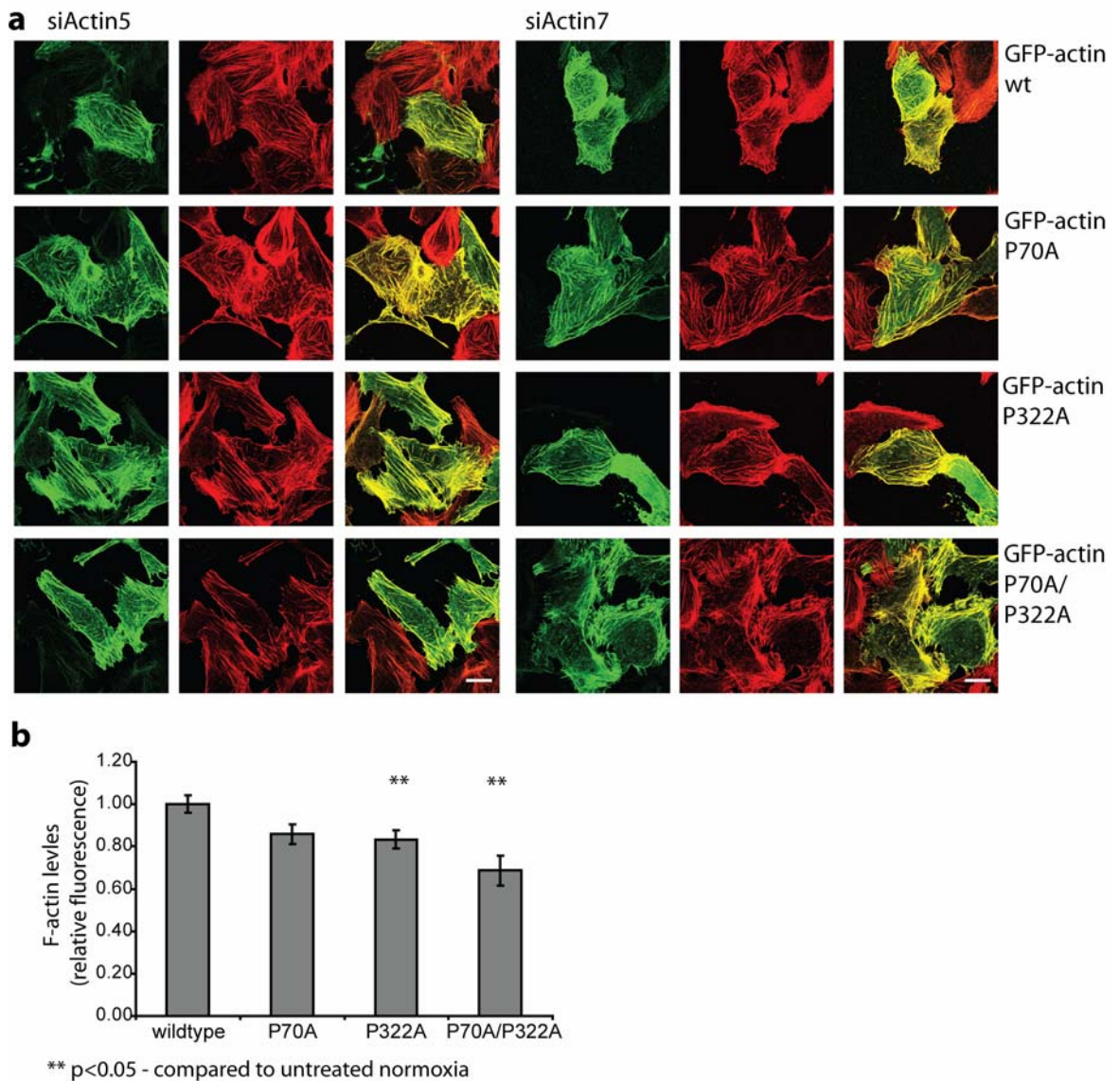


Figure 5.14: Pro70 and Pro322 of β -actin regulate the state of actin

(a) Wildtype (wt) GFP-actin or the indicated proline mutations on GFP-actin fusion proteins were expressed in U2OS cells while endogenous actin was knocked down by two different siRNA. Cells were co-stained with phalloidin-TRITC (red). Scale bar 20 μ m. **(b)** Quantification of endogenous F-actin levels. F-actin content is shown as comparison to cells overexpressing wildtype GFP-actin measured on the same day (means \pm SEM). Each condition is a representation of 10 individual samples. P-values as compared to wildtype GFP-actin: P70A 0.0536, P322A 0.0178, P70A/P322A 0.0004

Mutation of either Pro70 or Pro322 only had a minor effect on the organisation of filamentous actin compared to GFP-actin whereas mutation of both of these residues resulted in a significant decrease of actin filaments (Figure 5.14). The results were similar with both siRNAs for endogenous actin tested. This could also be quantified using the phalloidin-binding assay (Figure 5.14b). The influence of these actin mutants on cell migration was investigated in wound healing scratch assays.

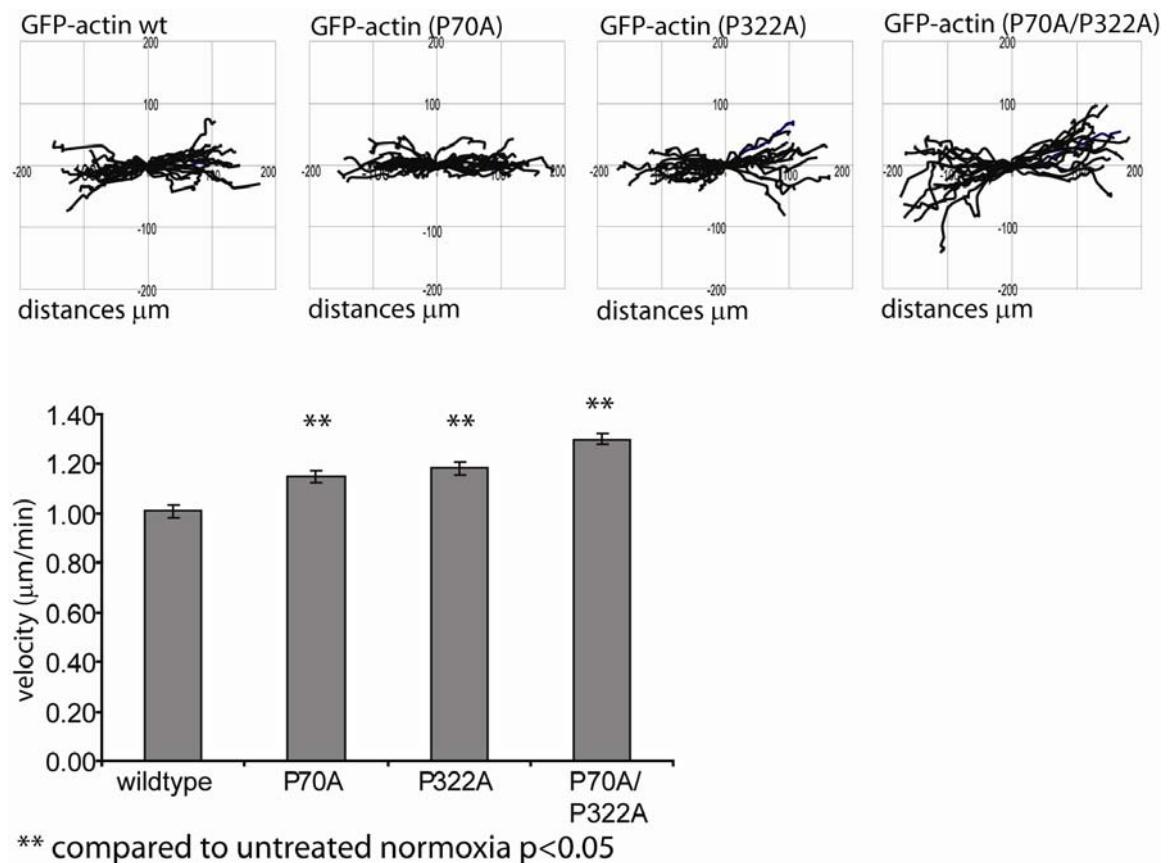


Figure 5.15: Pro70 and Pro322 of β -actin regulate cell migration

The effect of actin mutants on cell migration was analysed by time-lapse microscopy under normoxic conditions using U2OS cells. Distance plots and velocity of cells are shown. Data shown is the analysis of a representative experiment (at least 30 cells per conditions; means \pm SEM). P-values as compared to wildtype GFP-actin: P70A < 0.001 , P322A < 0.0001 , P70A/P322A < 0.0001 .

A significant increase in migration was found when overexpressing either of the single mutants compared to the wildtype GFP-actin whereas the double mutant showed a greater, additive effect, which correlates with a further increase in velocity (Figure 5.15). Taken together these results suggest that both of these prolyl residues are important for actin cytoskeleton rearrangement and cell migration. It would be interesting to follow up these results with matrigel invasion assays however these assays have not been done yet.

5.2.4 Effect of HIF1 α and HIF2 α on the actin cytoskeleton and cell migration

To investigate if these changes in organisation of actin are dependent on HIF activity HIF mutants were overexpressed in U2OS cells. The two proline residues (Pro402 and Pro564 in HIF1 α /Pro405 and Pro531 in HIF2 α) as well as the asparagine residue (Asp803 in HIF1 α) were mutated to alanine, preventing these HIF proteins from hydroxylation and subsequent degradation therefore these mutants are constantly active.

The overexpression of HIF mutants was confirmed by immunoblot analysis (Figure 5.16a). Using GFP-actin and phalloidin staining in immunofluorescence experiments overexpression of HIF mutants only had minor effects on the actin cytoskeleton under normoxia (Figure 5.16b). Similar results were obtained with DNaseI and phalloidin staining (Figure 5.16d+e). These results were also quantified using the images from Figure 5.16d. The results obtained using immunofluorescence were confirmed when intracellular F-actin levels were quantified (Figure 5.16c). These results indicate that changes in the actin cytoskeleton are independent on HIF levels and activity.

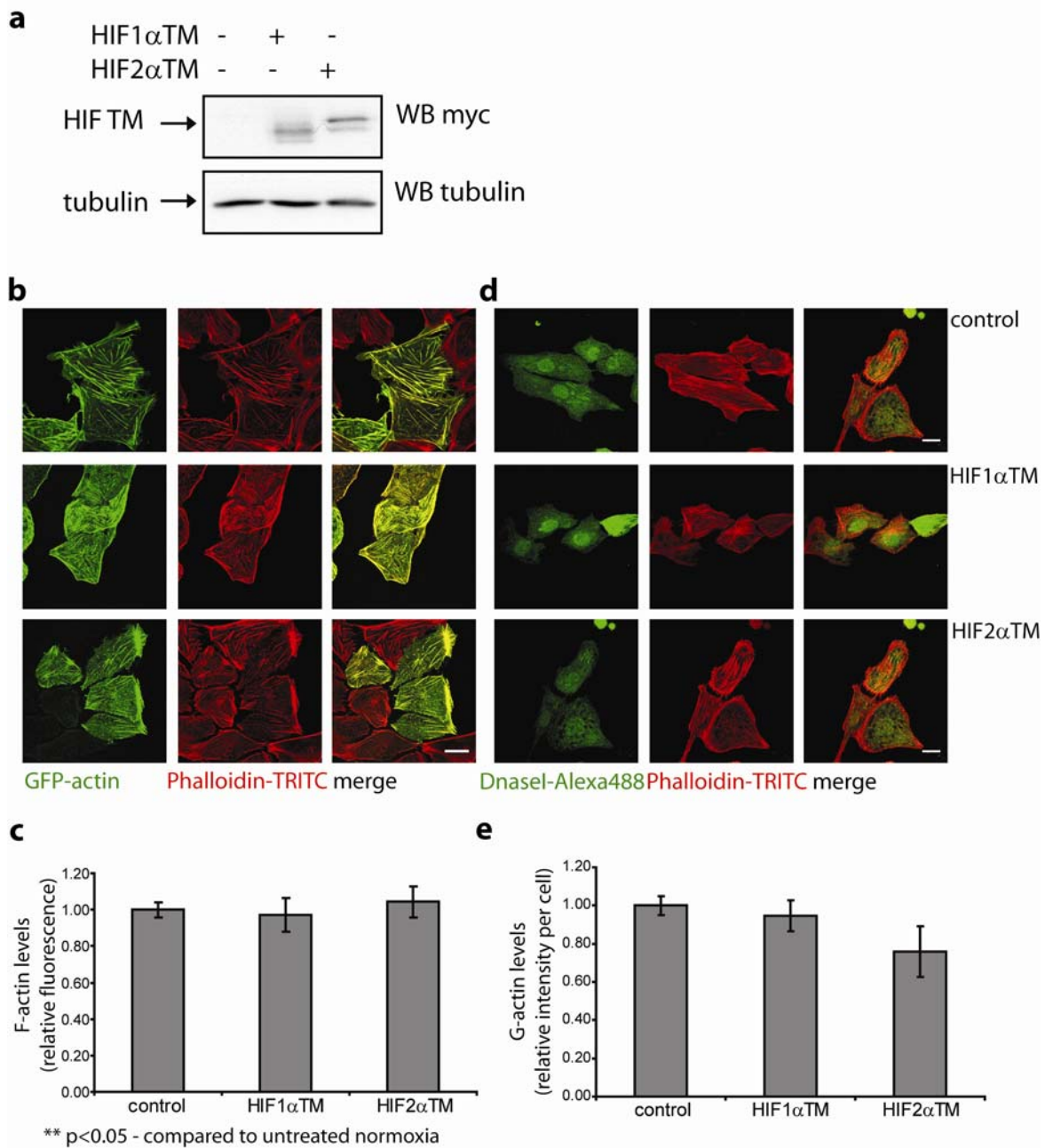


Figure 5.16: Effect of HIF1 α and HIF2 α on actin cytoskeleton

(a) Immunoblot analysis to confirm expression of HIF1 α and HIF2 α triple mutants (HIF1 α TM or HIF2 α TM) after transient transfection into U2OS cells. (b) Normoxic U2OS cells overexpressing HIF mutants, were stained with GFP-actin (green) and phalloidin-TRITC (red). (c) Quantification of F-actin levels by measuring fluorescent emission after labelling actin filaments with phalloidin-TRITC. F-actin content is shown as comparison to samples transfected with shControl measured on the same day (means \pm SEM). Each condition is a representation of 6 individual samples. P-values as compared to a control sample: HIF1 α TM 0.8324, HIF2 α TM 0.2229. (d) Endogenous actin was stained with phalloidin-TRITC (red) and DNaseI-Alexa488 (green). Scale bars 20 μ m. (e) Images in panel d were used to quantify intracellular G-actin levels. The intensity of DNaseI-staining per cell was analysed using ImageJ. Intensities per cell are shown as comparison to untreated control cells.

The next question was whether cell migration is increased in a HIF dependent mechanism. HIF mutants were overexpressed in U2OS cells and wound closure was monitored by time-lapse microscopy.

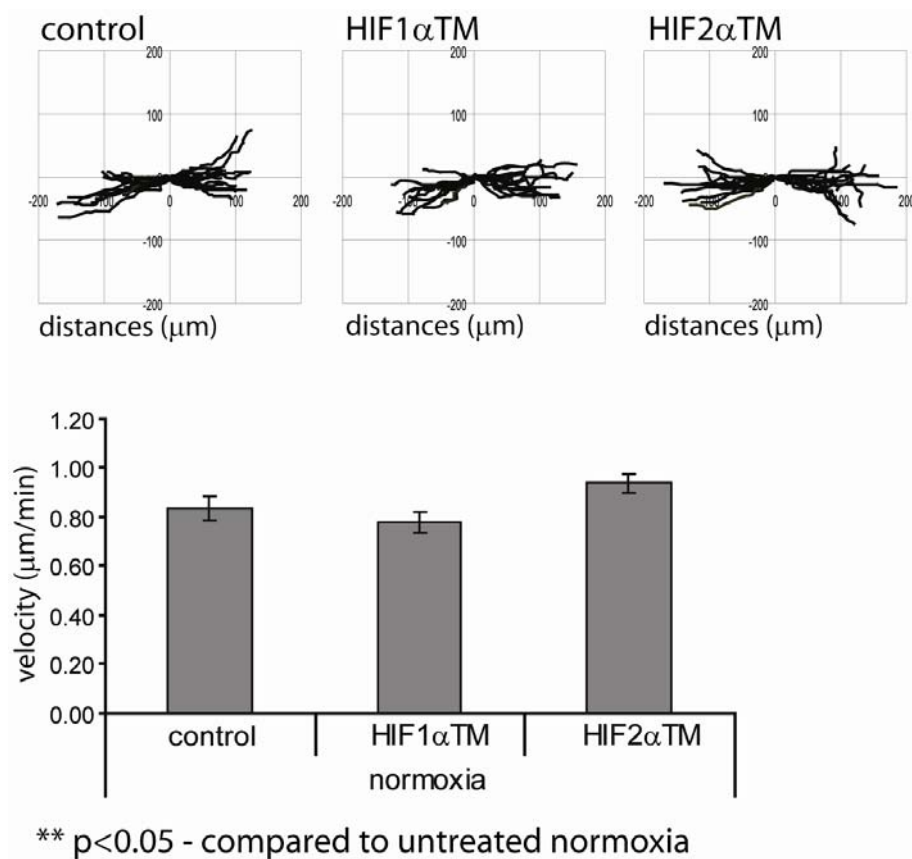


Figure 5.17: Effect of HIF triple mutants on cell migration

Monolayers of U2OS cells were scratched by pipettes and left to migrate into the gap. Cells were tracked by time-lapse microscopy. The single cell tracking device of ImageJ was used to analyse distance and velocity of cell migration. Data shown is the analysis of representative experiment (a least 30 cells per condition; means \pm SEM). P-values as compared to control cells: HIF1 α TM 0.5249, HIF2 α TM 0.0624.

Overexpression of HIF mutants did not lead to significant changes in cell migration compared to control cells. Even though overexpression of HIF2 α TM led to an increase in migration, the changes were not statistically significant. Overall, changes in the actin cytoskeleton as well as cell migration appear to be induced by a HIF-independent mechanism.

5.3 Conclusions

Hypoxia-induced changes in the actin cytoskeleton were found to be dependent on PHD3 expression levels as knock down of PHD3 was sufficient to increase the intracellular G- to F-actin ratio as was shown by immunofluorescence as well as in a quantitative approach. Using immunofluorescence, loss of stress fibres as well as an increase in G-actin was shown, whereas the quantitative approach showed loss of phalloidin-stained actin filaments. Subsequently, hypoxia-induced cell migration and invasion were shown to be dependent on PHD3 levels as well. All these experiments were performed using U2OS cells, A375 cells and A375-derived stable PHD knock down cells. Although A375 cells, especially the stable knock down cells, show a less distinct actin cytoskeleton and migrate slower in wound healing scratch assays similar results were obtained in all cell lines. As the width of the wound varied the single cell tracking device of ImageJ was used to analyse these assays. Changes in the distance plots are less obvious than changes in graphs for velocity where a 20-30% change is found. Using U2OS cells it could be shown that the rate of cell migration is dependent on the intracellular G- to F-actin ratio. Increasing amounts of the actin disrupting drug latrunculin A led to an increase in cell migration until migration stops at higher concentration of the drug. Both hydroxylated prolyl residues in actin (Pro70 and Pro322) appear to be important for the function described as mutation of these residues to alanine led to rearrangement of the actin cytoskeleton and increased cell migration. Single mutations appeared to have some effect, but the mutation of both prolyl residues had a greater, additive effect on the actin cytoskeleton and cell migration.

To reveal if PHD3-dependent actin cytoskeleton rearrangement and migration is dependent on HIF activity, non-degradable and therefore constantly active HIF1 α and HIF2 α mutants used to investigate their effect on the actin cytoskeleton and cell migration. PHD3-dependent changes in the actin cytoskeleton and migration were found to be independent on HIF1 α and HIF2 α as overexpression of HIF mutants did not change the actin cytoskeleton as was shown by immunofluorescence and in a quantitative approach and did not increase cell migration.

In this chapter a new link between oxygen-sensing pathways and hypoxia-induced cell migration was found, in which PHD3 appears to signal directly to components of the cytoskeleton. However the underlying mechanisms how hydroxylation of actin leads to rearrangement of the actin cytoskeleton and increased cell migration and invasion still remain to be elucidated.

Chapter 6 – General summary and outlook

6 General summary and outlook

Here we show a new link between oxygen-sensing pathways and hypoxia-induced cell migration. We describe a HIF-independent pro-invasive pathway, in which PHD3 activity affects the actin cytoskeleton. We identified the specific interaction between PHD3 and actin and identified a new post-translational modification of actin, the hydroxylation of two specific prolyl residues. A number of post-translational modifications of actin were shown previously including methylation, N-terminal acetylation, acylation, arginylation and phosphorylation of several serine, threonine and tyrosine residues but this study is the first one to show proline hydroxylation. The hydroxylation of actin was shown to have an effect on the organisation of the actin cytoskeleton as well as on cell migration.

As shown in chapter 3, a substrate can be trapped on the PHD enzyme under hypoxia suggesting that PHDs function by a similar binding mechanism to the one described for other α -ketoglutarate-dependent oxygenases [30]. In a quantitative proteomic approach actin was identified as a possible substrate of PHDs. The specific interaction of PHD3 and β -actin was confirmed in chapter 4. PHD3 was the only isoform strongly binding to β -actin specifically under hypoxia. Subsequently β -actin was found to be hydroxylated at Pro70 and Pro322. The hydroxylated prolyl residues lie within sequences resembling the LXXLAP binding motif described in the literature for HIF1 α [53], even though one or both leucine residues are replaced by the structurally similar isoleucine. In immunofluorescence experiments, PHD3 did not co-localise with actin stress fibres but rather with more diffuse actin patterns. However a rearrangement of the actin cytoskeleton was observed under hypoxia. In chapter 5 the biological function of the interaction between actin and PHD3 was investigated in more detail. Hypoxia-induced changes in the actin cytoskeleton were found to be dependent on PHD3 activity. Knockdown of PHD3 was sufficient to increase intracellular G-actin levels and decrease intracellular F-actin levels. Hypoxia-induced cell migration and invasion were dependent on the loss of PHD3 activity as well. Both hydroxylated prolyl residues in β -actin (Pro70 and Pro322) appear to be important, however this needs to be investigated further. Mutation of both prolyl residues to alanine led to rearrangement of the actin cytoskeleton as well

as increased cell migration. Single mutations had a lesser effects on actin organisation and cell migration.

Therefore, our current working model is as follows (Figure 6.1): PHD3-dependent hydroxylation of actin is important for the maintenance of the intracellular G- to F-actin ratio as hydroxylated actin is incorporated into actin filaments and stabilises them. Reduction of PHD3 activity leads to an increase in the intracellular G- to F-actin ratio, rearrangement of the actin cytoskeleton and increase in cell migration and invasion.

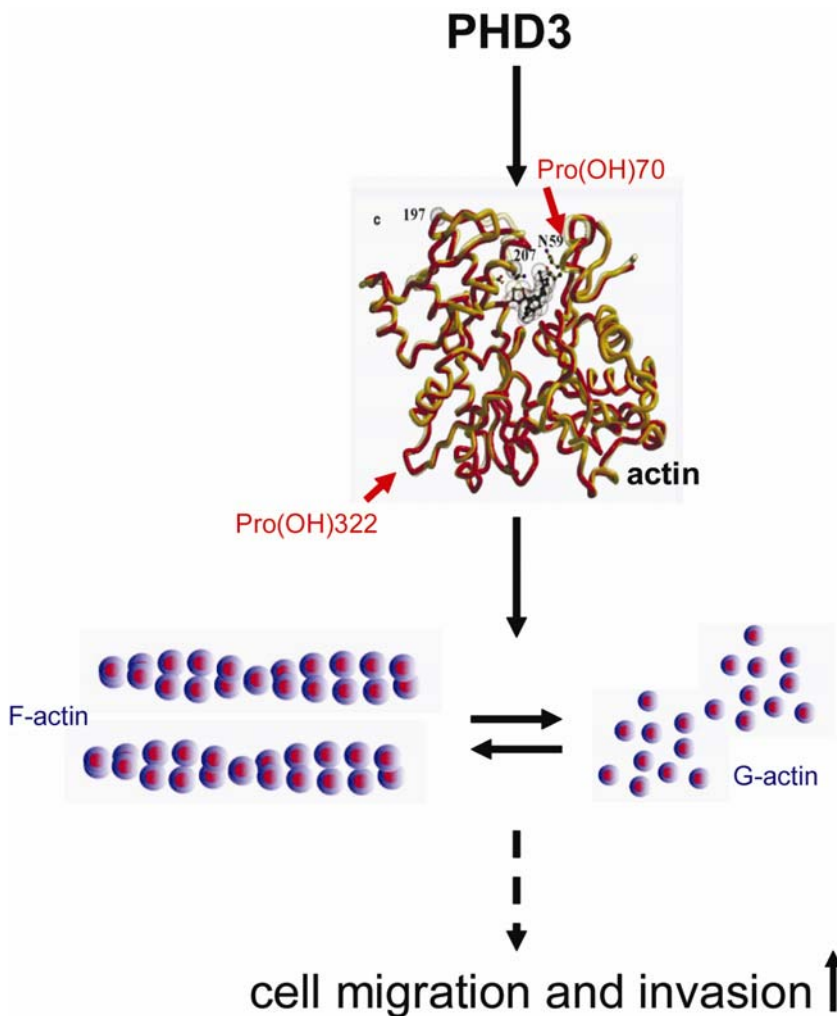


Figure 6.1: Working model of how PHD3 regulates the actin cytoskeleton (as described in the text)

Taken together, our results suggest a new signalling mechanism for actin polymerisation and it is the first study to describe how oxygen-sensing pathways are able to interact directly with the actin cytoskeleton. However, some questions still remain unanswered: Is the hydroxylation of actin solely dependent on PHD3 or are there other prolyl hydroxylases involved as well? How does actin get de-hydroxylated under hypoxia? Do PHD3 and actin directly interact? How does the hydroxylation of actin effect the polymerisation of actin? And what is the mechanism that leads from actin cytoskeleton rearrangement to an increase in cell migration and invasion?

A crucial point to elucidate the mechanism is to prove, that actin is truly hydroxylated by PHD3. It is technically challenging to identify hydroxylation sites and no systematic approach has been developed yet to do so. As there are no hydroxyproline specific antibodies available at the moment, the only method to identify hydroxylation sites is by mass spectrometry. In this study we used a mass spectrometric based method described by Unwin [122] to identify hydroxylation sites. Using this method we are currently trying to find differences in actin hydroxylation in PHD3 knockdown and knockout cells compared to wildtype cells. As about 10% of actin is hydroxylated under normoxia, it suggests a role of hydroxylation in actin signalling. However, the percentage of hydroxylated actin under hypoxia should be analysed. Furthermore, it would be interesting to know how and how quickly actin is de-hydroxylated. So far no de-hydroxylase has been identified and other proteins that are hydroxylated such as HIF1 α are targeted for proteasomal degradation making dehydroxylation unnecessary. In our case we do not have evidence supporting either the dehydroxylation or the degradation of actin, but it would be interesting to find out what happens to hydroxylated actin under hypoxia. Most of the HIF-dependent hypoxic response is due to gene transcription even though HIF1 α accumulates within minutes after exposure to hypoxia and degrades as quickly after reoxygenation. The fact that a short treatment of 1 hour with DMOG has an effect on the actin cytoskeleton, suggests that regulation other than transcription is important in this case.

PHD3 was identified to interact with actin and the results in this study are mostly based on β -actin. However, in the SILAC screen γ -actin was identified as a

potential substrate of PHDs as well. The sequences of β - and γ -actin are 98% identical and the prolyl residues found to be hydroxylated in β -actin are conserved in γ -actin as well as in α -actin. As differences in the functions of actin isoforms have been proposed [109], it would be interesting to investigate these other actin isoforms and their potential to interact with PHD3. Preliminary experiments using Fluorescent Lifetime Imaging Microscopy (FLIM) were performed to investigate the intracellular location and interaction of PHD3 and β -actin in more detail (data not shown). The fluorescent lifetime of a fluorophore is the time an electron remains in the excited state before returning to the ground state while emitting a photon. This time is characteristic for every fluorophore, but can be altered by its local environment. Interaction with another fluorophore leading to energy transfer to the acceptor fluorophore decreases the lifetime of a donor fluorophore, a process called Fluorescence Resonance Energy Transfer (FRET). The efficiency of the energy transfer is dependent on the distance between the two molecules. Detection of FRET between two proteins fused to appropriate fluorophores (a donor and an acceptor) indicates their interaction [129]. In these preliminary experiments a lifetime shift was observed when PHD3 localised to actin bundles under normoxia, but further analyses are needed to identify where in the cell and under which conditions PHD3 and actin interact. Furthermore, it would be important to determine, if PHD3 binds to actin monomers or actin filaments either directly or indirectly using *in vitro* binding studies.

Hydroxylated actin seems to be targeted to the filaments, however many questions remain to be elucidated: how does hydroxylated actin stabilise actin filaments and how does it effect polymerisation? Does hydroxylated actin localise at specific sites within the filaments or lead to binding of specific proteins? Does it influence nucleation or the release of phosphate within the filament? The effect of actin hydroxylation on filament stability and turn-over should be tested with biochemical assays. However, the position of the hydroxylated prolyl residues could give some implications for a signalling mechanism (Figure 6.1): Pro70 is located in subdomain 2 close to the ATP-binding site of actin, possibly influencing nucleotide exchange. Pro322 is located in subdomain 3, which could influence actin polymerisation as subdomain 1 and 3 comprise the (+) end of actin. Binding of a number of actin binding proteins influencing actin signalling

pathways could be affected. As RhoA activity and phosphorylation of myosin light chains are important for the formation of actin stress fibres, it would be interesting to investigate PHD3-dependent changes in this signalling cascade. Recently PHD2 has been described to be able to regulate the RhoA/ROCK/cofilin pathway [130].

The next question is how actin rearrangement is linked to an increase in cell migration and invasion. As discussed in chapter 1, hypoxia has been described to affect several pathways that are important for invasion and metastasis [88, 90-92]. However most of the pathways described seem to be HIF-dependent. A rearrangement of the actin cytoskeleton under hypoxia was reported previously where an increase in central stress fibres was observed using phalloidin-staining [130-132]. However changes in the actin cytoskeleton were not investigated in more detail. For efficient actin based cell migration fine tuning of intracellular G- and F-actin levels is important as was shown in chapter 5, when increasing concentrations of latrunculin A were used and the rate of cell migration was monitored. However, for efficient cell migration not only protrusion but also retraction of the cell body is needed [100, 101]. Retraction is mediated by actomyosin contractility and stress fibres. As discussed in chapter 1, different cell types are able to invade in different modes and are able to switch between mesenchymal or amoeboid invasion depending on the microenvironment [97, 98]. A375 cells tend to invade in an amoeboid fashion but the effect on PHD3 on migration should be tested in cell lines invading in a mesenchymal mode as well.

In our studies migration on a plastic dish appears to be solely dependent on PHD3 and independent of HIF. However, invasion into a 3D environment (as is the situation *in vivo*) is more complex and requires several independent mechanisms some of which are HIF-dependent [88, 90-92]. Our results hint to an involvement of HIF-independent pathways downstream of PHD3 which are less well understood. It could be interesting to look at a combination of PHD knockdowns and their effect on invasion. Furthermore it would be important to investigate the *in vivo* function of the interaction between PHD3 and actin and to investigate the potential anti-metastatic role of PHD3 in PHD3^{-/-} mice. Tumour hypoxia is linked to resistance to radio- and chemotherapies as well as increase in metastatic potential [13, 14]. As HIF is activated in a variety of tumours affecting a number of pathways, a lot of effort has been made to

develop HIF inhibitors or inhibitors for specific HIF target genes such as VEGF which stimulates angiogenesis [7, 12, 133]. However, as shown in this study there are HIF-independent pathways controlling cell migration and metastasis under hypoxia, but few agents are available that directly modulate PHD activity and hence target the oxygen-sensing pathways upstream of HIF [128, 134].

In this study the role of PHD3 activity in actin cytoskeleton rearrangement and its role in regulating hypoxia-induced cell migration were investigated. β -actin was identified as potential substrate of PHD3, and subsequently found to be hydroxylated at two specific prolyl residues needed for regulating actin cytoskeleton and cell migration.

References

1. Evan G. Cancer--a matter of life and cell death. *Int J Cancer*. 1997 May 29;71(5):709-11.
2. Hanahan D, Weinberg RA. The hallmarks of cancer. *Cell*. 2000 Jan 7;100(1):57-70.
3. Kroemer G, Pouyssegur J. Tumor cell metabolism: cancer's Achilles' heel. *Cancer Cell*. 2008 Jun;13(6):472-82.
4. Luo J, Solimini NL, Elledge SJ. Principles of cancer therapy: oncogene and non-oncogene addiction. *Cell*. 2009 Mar 6;136(5):823-37.
5. Ruan K, Song G, Ouyang G. Role of hypoxia in the hallmarks of human cancer. *J Cell Biochem*. 2009 Aug 15;107(6):1053-62.
6. Rankin EB, Giaccia AJ. The role of hypoxia-inducible factors in tumorigenesis. *Cell Death Differ*. 2008 Apr;15(4):678-85.
7. Harris AL. Hypoxia--a key regulatory factor in tumour growth. *Nat Rev Cancer*. 2002 Jan;2(1):38-47.
8. Brahimi-Horn MC, Chiche J, Pouyssegur J. Hypoxia and cancer. *J Mol Med*. 2007 Dec;85(12):1301-7.
9. Bertout JA, Patel SA, Simon MC. The impact of O₂ availability on human cancer. *Nat Rev Cancer*. 2008 Dec;8(12):967-75.
10. Kenneth NS, Rocha S. Regulation of gene expression by hypoxia. *Biochem J*. 2008 Aug 15;414(1):19-29.
11. Cummins EP, Taylor CT. Hypoxia-responsive transcription factors. *Pflugers Arch*. 2005 Sep;450(6):363-71.
12. Semenza GL. Targeting HIF-1 for cancer therapy. *Nat Rev Cancer*. 2003 Oct;3(10):721-32.
13. Hockel M, Vaupel P. Tumor hypoxia: definitions and current clinical, biologic, and molecular aspects. *J Natl Cancer Inst*. 2001 Feb 21;93(4):266-76.
14. Poon E, Harris AL, Ashcroft M. Targeting the hypoxia-inducible factor (HIF) pathway in cancer. *Expert Rev Mol Med*. 2009;11:e26.
15. Jokilehto T, Hogel H, Heikkinen P, Rantanen K, Elenius K, Sundstrom J, et al. Retention of prolyl hydroxylase PHD2 in the cytoplasm prevents PHD2-induced anchorage-independent carcinoma cell growth. *Exp Cell Res*. 2010 Apr 15;316(7):1169-78.
16. Percy MJ, Furlow PW, Beer PA, Lappin TR, McMullin MF, Lee FS. A novel erythrocytosis-associated PHD2 mutation suggests the location of a HIF binding groove. *Blood*. 2007 Sep 15;110(6):2193-6.
17. Ladroue C, Carcenac R, Leporrier M, Gad S, Le Hello C, Galateau-Salle F, et al. PHD2 mutation and congenital erythrocytosis with paraganglioma. *N Engl J Med*. 2008 Dec 18;359(25):2685-92.
18. Ivan M, Haberberger T, Gervasi DC, Michelson KS, Gunzler V, Kondo K, et al. Biochemical purification and pharmacological inhibition of a mammalian prolyl hydroxylase acting on hypoxia-inducible factor. *Proc Natl Acad Sci U S A*. 2002 Oct 15;99(21):13459-64.
19. Myllyharju J. Prolyl 4-hydroxylases, the key enzymes of collagen biosynthesis. *Matrix Biol*. 2003 Mar;22(1):15-24.
20. Gorres KL, Raines RT. Prolyl 4-hydroxylase. *Crit Rev Biochem Mol Biol*. 2010 Apr;45(2):106-24.
21. Taylor MS. Characterization and comparative analysis of the EGLN gene family. *Gene*. 2001 Sep 5;275(1):125-32.

22. Epstein AC, Gleadle JM, McNeill LA, Hewitson KS, O'Rourke J, Mole DR, et al. *C. elegans* EGL-9 and mammalian homologs define a family of dioxygenases that regulate HIF by prolyl hydroxylation. *Cell*. 2001 Oct 5;107(1):43-54.
23. Freeman RS, Hasbani DM, Lipscomb EA, Straub JA, Xie L. SM-20, EGL-9, and the EGLN family of hypoxia-inducible factor prolyl hydroxylases. *Mol Cells*. 2003 Aug 31;16(1):1-12.
24. Bruick RK, McKnight SL. A conserved family of prolyl-4-hydroxylases that modify HIF. *Science*. 2001 Nov 9;294(5545):1337-40.
25. Oehme F, Jonghaus W, Narouz-Ott L, Huetter J, Flamme I. A nonradioactive 96-well plate assay for the detection of hypoxia-inducible factor prolyl hydroxylase activity. *Anal Biochem*. 2004 Jul 1;330(1):74-80.
26. Koivunen P, Tiainen P, Hyvarinen J, Williams KE, Sormunen R, Klaus SJ, et al. An endoplasmic reticulum transmembrane prolyl 4-hydroxylase is induced by hypoxia and acts on hypoxia-inducible factor alpha. *J Biol Chem*. 2007 Oct 19;282(42):30544-52.
27. Schofield CJ, Zhang Z. Structural and mechanistic studies on 2-oxoglutarate-dependent oxygenases and related enzymes. *Curr Opin Struct Biol*. 1999 Dec;9(6):722-31.
28. McDonough MA, Li V, Flashman E, Chowdhury R, Mohr C, Lienard BM, et al. Cellular oxygen sensing: Crystal structure of hypoxia-inducible factor prolyl hydroxylase (PHD2). *Proc Natl Acad Sci U S A*. 2006 Jun 27;103(26):9814-9.
29. Chowdhury R, McDonough MA, Mecinovic J, Loenarz C, Flashman E, Hewitson KS, et al. Structural basis for binding of hypoxia-inducible factor to the oxygen-sensing prolyl hydroxylases. *Structure*. 2009 Jul 15;17(7):981-9.
30. Schofield CJ, Ratcliffe PJ. Oxygen sensing by HIF hydroxylases. *Nat Rev Mol Cell Biol*. 2004 May;5(5):343-54.
31. Bruick RK. Oxygen sensing in the hypoxic response pathway: regulation of the hypoxia-inducible transcription factor. *Genes Dev*. 2003 Nov 1;17(21):2614-23.
32. Hirsila M, Koivunen P, Gunzler V, Kivirikko KI, Myllyharju J. Characterization of the human prolyl 4-hydroxylases that modify the hypoxia-inducible factor. *J Biol Chem*. 2003 Aug 15;278(33):30772-80.
33. Selak MA, Armour SM, MacKenzie ED, Boulahbel H, Watson DG, Mansfield KD, et al. Succinate links TCA cycle dysfunction to oncogenesis by inhibiting HIF-alpha prolyl hydroxylase. *Cancer Cell*. 2005 Jan;7(1):77-85.
34. Isaacs JS, Jung YJ, Mole DR, Lee S, Torres-Cabala C, Chung YL, et al. HIF overexpression correlates with biallelic loss of fumarate hydratase in renal cancer: novel role of fumarate in regulation of HIF stability. *Cancer Cell*. 2005 Aug;8(2):143-53.
35. MacKenzie ED, Selak MA, Tennant DA, Payne LJ, Crosby S, Frederiksen CM, et al. Cell-permeating alpha-ketoglutarate derivatives alleviate pseudohypoxia in succinate dehydrogenase-deficient cells. *Mol Cell Biol*. 2007 May;27(9):3282-9.
36. Tennant DA, Frezza C, MacKenzie ED, Nguyen QD, Zheng L, Selak MA, et al. Reactivating HIF prolyl hydroxylases under hypoxia results in metabolic catastrophe and cell death. *Oncogene*. 2009 Nov 12;28(45):4009-21.
37. Schofield CJ, Ratcliffe PJ. Signalling hypoxia by HIF hydroxylases. *Biochem Biophys Res Commun*. 2005 Dec 9;338(1):617-26.
38. Lieb ME, Menzies K, Moschella MC, Ni R, Taubman MB. Mammalian EGLN genes have distinct patterns of mRNA expression and regulation. *Biochem Cell Biol*. 2002;80(4):421-6.
39. Willam C, Maxwell PH, Nichols L, Lygate C, Tian YM, Bernhardt W, et al. HIF prolyl hydroxylases in the rat; organ distribution and changes in expression

- following hypoxia and coronary artery ligation. *J Mol Cell Cardiol.* 2006 Jul;41(1):68-77.
40. Metzen E, Berchner-Pfannschmidt U, Stengel P, Marxsen JH, Stolze I, Klingler M, et al. Intracellular localisation of human HIF-1 alpha hydroxylases: implications for oxygen sensing. *J Cell Sci.* 2003 Apr 1;116(Pt 7):1319-26.
41. del Peso L, Castellanos MC, Temes E, Martin-Puig S, Cuevas Y, Olmos G, et al. The von Hippel Lindau/hypoxia-inducible factor (HIF) pathway regulates the transcription of the HIF-proline hydroxylase genes in response to low oxygen. *J Biol Chem.* 2003 Dec 5;278(49):48690-5.
42. Metzen E, Stiehl DP, Doege K, Marxsen JH, Hellwig-Burgel T, Jelkmann W. Regulation of the prolyl hydroxylase domain protein 2 (phd2/egln-1) gene: identification of a functional hypoxia-responsive element. *Biochem J.* 2005 May 1;387(Pt 3):711-7.
43. Pescador N, Cuevas Y, Naranjo S, Alcaide M, Villar D, Landazuri MO, et al. Identification of a functional hypoxia-responsive element that regulates the expression of the egl nine homologue 3 (egln3/phd3) gene. *Biochem J.* 2005 Aug 15;390(Pt 1):189-97.
44. Marxsen JH, Stengel P, Doege K, Heikkinen P, Jokilehto T, Wagner T, et al. Hypoxia-inducible factor-1 (HIF-1) promotes its degradation by induction of HIF-alpha-prolyl-4-hydroxylases. *Biochem J.* 2004 Aug 1;381(Pt 3):761-7.
45. Nakayama K, Frew IJ, Hagensen M, Skals M, Habelhah H, Bhoumik A, et al. Siah2 regulates stability of prolyl-hydroxylases, controls HIF1alpha abundance, and modulates physiological responses to hypoxia. *Cell.* 2004 Jun 25;117(7):941-52.
46. Yasumoto K, Kowata Y, Yoshida A, Torii S, Sogawa K. Role of the intracellular localization of HIF-prolyl hydroxylases. *Biochim Biophys Acta.* 2009 May;1793(5):792-7.
47. Steinhoff A, Pientka FK, Mockel S, Kettelhake A, Hartmann E, Kohler M, et al. Cellular oxygen sensing: Importins and exportins are mediators of intracellular localisation of prolyl-4-hydroxylases PHD1 and PHD2. *Biochem Biophys Res Commun.* 2009 Oct 2;387(4):705-11.
48. Masson N, Appelhoff RJ, Tuckerman JR, Tian YM, Demol H, Puype M, et al. The HIF prolyl hydroxylase PHD3 is a potential substrate of the TRiC chaperonin. *FEBS Lett.* 2004 Jul 16;570(1-3):166-70.
49. Hopfer U, Hopfer H, Jablonski K, Stahl RA, Wolf G. The novel WD-repeat protein Morg1 acts as a molecular scaffold for hypoxia-inducible factor prolyl hydroxylase 3 (PHD3). *J Biol Chem.* 2006 Mar 31;281(13):8645-55.
50. Nakayama K, Gazdoui S, Abraham R, Pan ZQ, Ronai Z. Hypoxia-induced assembly of prolyl hydroxylase PHD3 into complexes: implications for its activity and susceptibility for degradation by the E3 ligase Siah2. *Biochem J.* 2007 Jan 1;401(1):217-26.
51. Baek JH, Mahon PC, Oh J, Kelly B, Krishnamachary B, Pearson M, et al. OS-9 interacts with hypoxia-inducible factor 1alpha and prolyl hydroxylases to promote oxygen-dependent degradation of HIF-1alpha. *Mol Cell.* 2005 Feb 18;17(4):503-12.
52. Appelhoff RJ, Tian YM, Raval RR, Turley H, Harris AL, Pugh CW, et al. Differential function of the prolyl hydroxylases PHD1, PHD2, and PHD3 in the regulation of hypoxia-inducible factor. *J Biol Chem.* 2004 Sep 10;279(37):38458-65.
53. Masson N, Willam C, Maxwell PH, Pugh CW, Ratcliffe PJ. Independent function of two destruction domains in hypoxia-inducible factor-alpha chains activated by prolyl hydroxylation. *Embo J.* 2001 Sep 17;20(18):5197-206.

54. Huang J, Zhao Q, Mooney SM, Lee FS. Sequence determinants in hypoxia-inducible factor-1alpha for hydroxylation by the prolyl hydroxylases PHD1, PHD2, and PHD3. *J Biol Chem*. 2002 Oct 18;277(42):39792-800.
55. Huang LE, Pete EA, Schau M, Milligan J, Gu J. Leu-574 of HIF-1alpha is essential for the von Hippel-Lindau (VHL)-mediated degradation pathway. *J Biol Chem*. 2002 Nov 1;277(44):41750-5.
56. Kageyama Y, Koshiji M, To KK, Tian YM, Ratcliffe PJ, Huang LE. Leu-574 of human HIF-1alpha is a molecular determinant of prolyl hydroxylation. *Faseb J*. 2004 Jun;18(9):1028-30.
57. Li D, Hirsila M, Koivunen P, Brenner MC, Xu L, Yang C, et al. Many amino acid substitutions in a hypoxia-inducible transcription factor (HIF)-1alpha-like peptide cause only minor changes in its hydroxylation by the HIF prolyl 4-hydroxylases: substitution of 3,4-dehydroproline or azetidine-2-carboxylic acid for the proline leads to a high rate of uncoupled 2-oxoglutarate decarboxylation. *J Biol Chem*. 2004 Dec 31;279(53):55051-9.
58. Villar D, Vara-Vega A, Landazuri MO, Del Peso L. Identification of a region on hypoxia-inducible-factor prolyl 4-hydroxylases that determines their specificity for the oxygen degradation domains. *Biochem J*. 2007 Dec 1;408(2):231-40.
59. Flashman E, Bagg EA, Chowdhury R, Mecinovic J, Loenarz C, McDonough MA, et al. Kinetic rationale for selectivity toward N- and C-terminal oxygen-dependent degradation domain substrates mediated by a loop region of hypoxia-inducible factor prolyl hydroxylases. *J Biol Chem*. 2008 Feb 15;283(7):3808-15.
60. Wenger RH. Cellular adaptation to hypoxia: O₂-sensing protein hydroxylases, hypoxia-inducible transcription factors, and O₂-regulated gene expression. *Faseb J*. 2002 Aug;16(10):1151-62.
61. Kaelin WG. Proline hydroxylation and gene expression. *Annu Rev Biochem*. 2005;74:115-28.
62. Dann CE, 3rd, Bruick RK. Dioxygenases as O₂-dependent regulators of the hypoxic response pathway. *Biochem Biophys Res Commun*. 2005 Dec 9;338(1):639-47.
63. Ivan M, Kondo K, Yang H, Kim W, Valiando J, Ohh M, et al. HIFalpha targeted for VHL-mediated destruction by proline hydroxylation: implications for O₂ sensing. *Science*. 2001 Apr 20;292(5516):464-8.
64. Jaakkola P, Mole DR, Tian YM, Wilson MI, Gielbert J, Gaskell SJ, et al. Targeting of HIF-alpha to the von Hippel-Lindau ubiquitylation complex by O₂-regulated prolyl hydroxylation. *Science*. 2001 Apr 20;292(5516):468-72.
65. Berra E, Benizri E, Ginouves A, Volmat V, Roux D, Pouyssegur J. HIF prolyl-hydroxylase 2 is the key oxygen sensor setting low steady-state levels of HIF-1alpha in normoxia. *Embo J*. 2003 Aug 15;22(16):4082-90.
66. Chan DA, Kawahara TL, Sutphin PD, Chang HY, Chi JT, Giaccia AJ. Tumor vasculature is regulated by PHD2-mediated angiogenesis and bone marrow-derived cell recruitment. *Cancer Cell*. 2009 Jun 2;15(6):527-38.
67. Ozer A, Wu LC, Bruick RK. The candidate tumor suppressor ING4 represses activation of the hypoxia inducible factor (HIF). *Proc Natl Acad Sci U S A*. 2005 May 24;102(21):7481-6.
68. Barth S, Nesper J, Hasgall PA, Wirthner R, Nytko KJ, Edlich F, et al. The peptidyl prolyl cis/trans isomerase FKBP38 determines hypoxia-inducible transcription factor prolyl-4-hydroxylase PHD2 protein stability. *Mol Cell Biol*. 2007 May;27(10):3758-68.
69. Aprelikova O, Pandolfi S, Tackett S, Ferreira M, Salnikow K, Ward Y, et al. Melanoma antigen-11 inhibits the hypoxia-inducible factor prolyl hydroxylase 2 and activates hypoxic response. *Cancer Res*. 2009 Jan 15;69(2):616-24.

70. Lee S, Nakamura E, Yang H, Wei W, Linggi MS, Sajan MP, et al. Neuronal apoptosis linked to EglN3 prolyl hydroxylase and familial pheochromocytoma genes: developmental culling and cancer. *Cancer Cell*. 2005 Aug;8(2):155-67.
71. Schlisio S, Kenchappa RS, Vredeveld LC, George RE, Stewart R, Greulich H, et al. The kinesin KIF1Bbeta acts downstream from EglN3 to induce apoptosis and is a potential 1p36 tumor suppressor. *Genes Dev*. 2008 Apr 1;22(7):884-93.
72. Fu J, Menzies K, Freeman RS, Taubman MB. EGLN3 prolyl hydroxylase regulates skeletal muscle differentiation and myogenin protein stability. *J Biol Chem*. 2007 Apr 27;282(17):12410-8.
73. Fu J, Taubman MB. Prolyl hydroxylase EGLN3 regulates skeletal myoblast differentiation through an NF-kappaB-dependent pathway. *J Biol Chem*. 2010 Mar 19;285(12):8927-35.
74. Koditz J, Nesper J, Wottawa M, Stiehl DP, Camenisch G, Franke C, et al. Oxygen-dependent ATF-4 stability is mediated by the PHD3 oxygen sensor. *Blood*. 2007 Nov 15;110(10):3610-7.
75. Sato M, Sakota M, Nakayama K. Human PRP19 interacts with prolyl-hydroxylase PHD3 and inhibits cell death in hypoxia. *Exp Cell Res*. 2010 Jun 30.
76. Xie L, Xiao K, Whalen EJ, Forrester MT, Freeman RS, Fong G, et al. Oxygen-regulated beta(2)-adrenergic receptor hydroxylation by EGLN3 and ubiquitylation by pVHL. *Sci Signal*. 2009;2(78):ra33.
77. Cummins EP, Berra E, Comerford KM, Ginouves A, Fitzgerald KT, Seeballuck F, et al. Prolyl hydroxylase-1 negatively regulates IkkappaB kinase-beta, giving insight into hypoxia-induced NFkappaB activity. *Proc Natl Acad Sci U S A*. 2006 Nov 28;103(48):18154-9.
78. Siddiq A, Aminova LR, Troy CM, Suh K, Messer Z, Semenza GL, et al. Selective inhibition of hypoxia-inducible factor (HIF) prolyl-hydroxylase 1 mediates neuroprotection against normoxic oxidative death via HIF- and CREB-independent pathways. *J Neurosci*. 2009 Jul 8;29(27):8828-38.
79. Aragones J, Schneider M, Van Geyte K, Fraisl P, Dresselaers T, Mazzone M, et al. Deficiency or inhibition of oxygen sensor Phd1 induces hypoxia tolerance by reprogramming basal metabolism. *Nat Genet*. 2008 Feb;40(2):170-80.
80. Schneider M, Van Geyte K, Fraisl P, Kiss J, Aragones J, Mazzone M, et al. Loss or silencing of the PHD1 prolyl hydroxylase protects livers of mice against ischemia/reperfusion injury. *Gastroenterology*. 2010 Mar;138(3):1143-54 e1-2.
81. Zhang Q, Gu J, Li L, Liu J, Luo B, Cheung HW, et al. Control of cyclin D1 and breast tumorigenesis by the EglN2 prolyl hydroxylase. *Cancer Cell*. 2009 Nov 6;16(5):413-24.
82. Mikhaylova O, Ignacak ML, Barankiewicz TJ, Harbaugh SV, Yi Y, Maxwell PH, et al. The von Hippel-Lindau tumor suppressor protein and Egl-9-Type proline hydroxylases regulate the large subunit of RNA polymerase II in response to oxidative stress. *Mol Cell Biol*. 2008 Apr;28(8):2701-17.
83. Kuznetsova AV, Meller J, Schnell PO, Nash JA, Ignacak ML, Sanchez Y, et al. von Hippel-Lindau protein binds hyperphosphorylated large subunit of RNA polymerase II through a proline hydroxylation motif and targets it for ubiquitination. *Proc Natl Acad Sci U S A*. 2003 Mar 4;100(5):2706-11.
84. Takeda K, Ho VC, Takeda H, Duan LJ, Nagy A, Fong GH. Placental but not heart defects are associated with elevated hypoxia-inducible factor alpha levels in mice lacking prolyl hydroxylase domain protein 2. *Mol Cell Biol*. 2006 Nov;26(22):8336-46.
85. Bishop T, Gallagher D, Pascual A, Lygate CA, de Bono JP, Nicholls LG, et al. Abnormal sympathoadrenal development and systemic hypotension in PHD3-/- mice. *Mol Cell Biol*. 2008 May;28(10):3386-400.

86. Lomb DJ, Desouza LA, Franklin JL, Freeman RS. Prolyl hydroxylase inhibitors depend on extracellular glucose and hypoxia-inducible factor (HIF)-2alpha to inhibit cell death caused by nerve growth factor (NGF) deprivation: evidence that HIF-2alpha has a role in NGF-promoted survival of sympathetic neurons. *Mol Pharmacol*. 2009 May;75(5):1198-209.
87. Pantel K, Brakenhoff RH. Dissecting the metastatic cascade. *Nat Rev Cancer*. 2004 Jun;4(6):448-56.
88. Chan DA, Giaccia AJ. Hypoxia, gene expression, and metastasis. *Cancer Metastasis Rev*. 2007 Jun;26(2):333-9.
89. Klymkowsky MW, Savagner P. Epithelial-mesenchymal transition: a cancer researcher's conceptual friend and foe. *Am J Pathol*. 2009 May;174(5):1588-93.
90. Pouyssegur J, Dayan F, Mazure NM. Hypoxia signalling in cancer and approaches to enforce tumour regression. *Nature*. 2006 May 25;441(7092):437-43.
91. Sullivan R, Graham CH. Hypoxia-driven selection of the metastatic phenotype. *Cancer Metastasis Rev*. 2007 Jun;26(2):319-31.
92. Erler JT, Giaccia AJ. Lysyl oxidase mediates hypoxic control of metastasis. *Cancer Res*. 2006 Nov 1;66(21):10238-41.
93. Pennacchietti S, Michieli P, Galluzzo M, Mazzone M, Giordano S, Comoglio PM. Hypoxia promotes invasive growth by transcriptional activation of the met protooncogene. *Cancer Cell*. 2003 Apr;3(4):347-61.
94. Esteban MA, Tran MG, Harten SK, Hill P, Castellanos MC, Chandra A, et al. Regulation of E-cadherin expression by VHL and hypoxia-inducible factor. *Cancer Res*. 2006 Apr 1;66(7):3567-75.
95. Keely S, Glover LE, MacManus CF, Campbell EL, Scully MM, Furuta GT, et al. Selective induction of integrin beta1 by hypoxia-inducible factor: implications for wound healing. *FASEB J*. 2009 May;23(5):1338-46.
96. Rohwer N, Welzel M, Daskalow K, Pfander D, Wiedenmann B, Detjen K, et al. Hypoxia-inducible factor 1alpha mediates anoikis resistance via suppression of alpha5 integrin. *Cancer Res*. 2008 Dec 15;68(24):10113-20.
97. Pankova K, Rosel D, Novotny M, Brabek J. The molecular mechanisms of transition between mesenchymal and amoeboid invasiveness in tumor cells. *Cell Mol Life Sci*. 2010 Jan;67(1):63-71.
98. Friedl P. Prespecification and plasticity: shifting mechanisms of cell migration. *Curr Opin Cell Biol*. 2004 Feb;16(1):14-23.
99. Staiger CJ, Blanchoin L. Actin dynamics: old friends with new stories. *Curr Opin Plant Biol*. 2006 Dec;9(6):554-62.
100. Pollard TD, Borisy GG. Cellular motility driven by assembly and disassembly of actin filaments. *Cell*. 2003 Feb 21;112(4):453-65.
101. Alberts B, Johnson, A., Lewis, J., Raff, M., Roberts, K. and Walter, P. *Molecular Biology of the Cell*, 5th edition. Garland Science, Taylor & Francis Group. 2008.
102. Berg JM, Tymoczko, J.L. and Stryer, L. *Biochemistry*, 5th edition. WHFreeman. 2002.
103. Le Clainche C, Carlier MF. Regulation of actin assembly associated with protrusion and adhesion in cell migration. *Physiol Rev*. 2008 Apr;88(2):489-513.
104. Mitchison TJ, Cramer LP. Actin-based cell motility and cell locomotion. *Cell*. 1996 Feb 9;84(3):371-9.
105. Ladwein M, Rottner K. On the Rho'd: the regulation of membrane protrusions by Rho-GTPases. *FEBS Lett*. 2008 Jun 18;582(14):2066-74.
106. Pellegrin S, Mellor H. Actin stress fibres. *J Cell Sci*. 2007 Oct 15;120(Pt 20):3491-9.

107. Naumanen P, Lappalainen P, Hotulainen P. Mechanisms of actin stress fibre assembly. *J Microsc.* 2008 Sep;231(3):446-54.
108. Hall A. Rho GTPases and the actin cytoskeleton. *Science.* 1998 Jan 23;279(5350):509-14.
109. Tondeleir D, Vandamme D, Vandekerckhove J, Ampe C, Lambrechts A. Actin isoform expression patterns during mammalian development and in pathology: insights from mouse models. *Cell Motil Cytoskeleton.* 2009 Oct;66(10):798-815.
110. Castano E, Philimonenko VV, Kahle M, Fukalova J, Kalendova A, Yildirim S, et al. Actin complexes in the cell nucleus: new stones in an old field. *Histochem Cell Biol.* 2010 Jun;133(6):607-26.
111. Skarp KP, Vartiainen MK. Actin on DNA-an ancient and dynamic relationship. *Cytoskeleton (Hoboken).* 2010 Aug;67(8):487-95.
112. Miralles F, Visa N. Actin in transcription and transcription regulation. *Curr Opin Cell Biol.* 2006 Jun;18(3):261-6.
113. Vartiainen MK. Nuclear actin dynamics--from form to function. *FEBS Lett.* 2008 Jun 18;582(14):2033-40.
114. Ong SE, Mann M. Mass spectrometry-based proteomics turns quantitative. *Nat Chem Biol.* 2005 Oct;1(5):252-62.
115. Ong SE, Blagoev B, Kratchmarova I, Kristensen DB, Steen H, Pandey A, et al. Stable isotope labeling by amino acids in cell culture, SILAC, as a simple and accurate approach to expression proteomics. *Mol Cell Proteomics.* 2002 May;1(5):376-86.
116. Mann M. Functional and quantitative proteomics using SILAC. *Nat Rev Mol Cell Biol.* 2006 Dec;7(12):952-8.
117. Maxwell PH, Dachs GU, Gleadle JM, Nicholls LG, Harris AL, Stratford IJ, et al. Hypoxia-inducible factor-1 modulates gene expression in solid tumors and influences both angiogenesis and tumor growth. *Proc Natl Acad Sci U S A.* 1997 Jul 22;94(15):8104-9.
118. Tennant DA, Gottlieb E. HIF prolyl hydroxylase-3 mediates alpha-ketoglutarate-induced apoptosis and tumor suppression. *J Mol Med.* Apr 11.
119. Coue M, Brenner SL, Spector I, Korn ED. Inhibition of actin polymerization by latrunculin A. *FEBS Lett.* 1987 Mar 23;213(2):316-8.
120. Yarmola EG, Somasundaram T, Boring TA, Spector I, Bubb MR. Actin-latrunculin A structure and function. Differential modulation of actin-binding protein function by latrunculin A. *J Biol Chem.* 2000 Sep 8;275(36):28120-7.
121. Cooper JA. Effects of cytochalasin and phalloidin on actin. *J Cell Biol.* 1987 Oct;105(4):1473-8.
122. Unwin RD, Griffiths JR, Leverentz MK, Grallert A, Hagan IM, Whetton AD. Multiple reaction monitoring to identify sites of protein phosphorylation with high sensitivity. *Mol Cell Proteomics.* 2005 Aug;4(8):1134-44.
123. Wulf E, Deboben A, Bautz FA, Faulstich H, Wieland T. Fluorescent phalloxin, a tool for the visualization of cellular actin. *Proc Natl Acad Sci U S A.* 1979 Sep;76(9):4498-502.
124. Cramer LP, Briggs LJ, Dawe HR. Use of fluorescently labelled deoxyribonuclease I to spatially measure G-actin levels in migrating and non-migrating cells. *Cell Motil Cytoskeleton.* 2002 Jan;51(1):27-38.
125. Machesky LM, Hall A. Role of actin polymerization and adhesion to extracellular matrix in Rac- and Rho-induced cytoskeletal reorganization. *J Cell Biol.* 1997 Aug 25;138(4):913-26.
126. Hennigan RF, Hawker KL, Ozanne BW. Fos-transformation activates genes associated with invasion. *Oncogene.* 1994 Dec;9(12):3591-600.

127. Pollard TD, Blanchoin L, Mullins RD. Molecular mechanisms controlling actin filament dynamics in nonmuscle cells. *Annu Rev Biophys Biomol Struct.* 2000;29:545-76.
128. Tennant DA, Gottlieb E. HIF prolyl hydroxylase-3 mediates alpha-ketoglutarate-induced apoptosis and tumor suppression. *J Mol Med.* 2010 Apr 11.
129. Wallrabe H, Periasamy A. Imaging protein molecules using FRET and FLIM microscopy. *Curr Opin Biotechnol.* 2005 Feb;16(1):19-27.
130. Vogel S, Wottawa M, Farhat K, Zieseniss A, Schnelle M, Le-Huu S, et al. Prolyl Hydroxylase Domain (PHD)2 affects cell migration and F-actin formation via RhoA/ROCK-dependent cofilin phosphorylation. *J Biol Chem.* 2010 Aug 27.
131. Yan W, Fu Y, Tian D, Liao J, Liu M, Wang B, et al. PI3 kinase/Akt signaling mediates epithelial-mesenchymal transition in hypoxic hepatocellular carcinoma cells. *Biochem Biophys Res Commun.* 2009 May 8;382(3):631-6.
132. Erler JT, Bennewith KL, Nicolau M, Dornhofer N, Kong C, Le QT, et al. Lysyl oxidase is essential for hypoxia-induced metastasis. *Nature.* 2006 Apr 27;440(7088):1222-6.
133. Semenza GL. Defining the role of hypoxia-inducible factor 1 in cancer biology and therapeutics. *Oncogene.* 2010 Feb 4;29(5):625-34.
134. Choi HJ, Song BJ, Gong YD, Gwak WJ, Soh Y. Rapid degradation of hypoxia-inducible factor-1alpha by KRH102053, a new activator of prolyl hydroxylase 2. *Br J Pharmacol.* 2008 May;154(1):114-25.